MONASH University

Computer-aided Design of Bio-inspired Catalysts for Solar Hydrogen Production
Siyao Qiu
Doctor of Philosophy

A thesis submitted for the degree of *Doctor of Philosophy* at
Monash University in 2018
(*Name of the enrolling academic unit or Institute*)

COPYRIGHT NOTICE

DECLARATION

In accordance with Monash University thesis Regulations 17. Doctor of Philosophy, the following declarations are made:

This thesis contains no material which has been accepted for the award of any other degree or diploma at any university or equivalent institution and that, to the best of my knowledge and belief, this thesis contains no material previously published or written by another person, except where due reference is made in the text of the thesis.

Signature: …█████████………………

Print Name: …Siyao Qiu……………….

Date: …05/06/2018……………………….

PUBLICATIONS DURING ENROLMENT

Qiu, Siyao, Luis Miguel Azofra, Douglas R. MacFarlane, and Chenghua Sun. "Protein Environment Effect or How Amino Acids Affect the Catalytic Performance for the H_2 Production in [NiFe] Hydrogenases" *Phys. Chem. Chem. Phys., 20,* 6735-6743 (2018).

Qiu, Siyao, Luis Miguel Azofra, Douglas R. MacFarlane, and Chenghua Sun. "Unraveling the Role of Ligands in the Hydrogen Evolution Mechanism Followed by [NiFe] Hydrogenases" *ACS Catal., 6,* 5541-5548 (2016)

Qiu, Siyao, Luis Miguel Azofra, Douglas R. MacFarlane, and Chenghua Sun. "Why Proton is transformed into Hydride by [NiFe] Hydrogenases? An Intrinsic Reactivity Analysis based on Conceptual DFT"*Phys. Chem. Chem. Phys.*, *18*, 15360-15374 (2016).

Thesis including published works declaration

I hereby declare that this thesis contains no material which has been accepted for the award of any other degree or diploma at any university or equivalent institution and that, to the best of my knowledge and belief, this thesis contains no material previously published or written by another person, except where due reference is made in the text of the thesis.
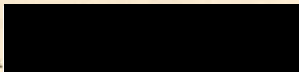
This thesis includes three original papers published in peer reviewed journals and onesubmitted publications. The core theme of the thesis is the computational studies of bio-inspired catalysts for hydrogen production. The ideas, development and writing up of all the papers in the thesis were the principal responsibility of myself, the student, working within the School of Chemistry, Faculty of Science, Monash University, under the supervision ofDr.Chenghua Sun and Prof. Douglas R. MacFarlane.

The inclusion of co-authors reflects the fact that the work came from active collaboration between researchers and acknowledges input into team-based research.In the case of Chapter 2, 3 and 4 my contribution to the work involved the following:

Thesis Chapter	Publication Title	Status	Nature and % of student contribution	Co-author name(s) Nature and % of Co-author's contribution*	Co-author(s), Monash student Y/N*
Chapter 2	Unraveling the Role of Ligands in the Hydrogen Evolution Mechanism Followed by [NiFe] Hydrogenases	Published	80%. Calculations, collecting data and writing first draft	1) Luis Miguel Azofra, manuscript writing and calculation guiding 10%	No
				2) Douglas R. MacFarlane, manuscript revision and concept 5%	No
				3) Chenghua Sun, manuscript revision and concept 5%	No
Chapter 3	Hydrogen-bonding effect between active site and protein environment on catalysis performance in H_2-producing [NiFe] hydrogenases	Published	80%. Calculations, collecting data and writing first draft	1) Luis Miguel Azofra, manuscript writing and calculation guiding 10%	No
				2) Douglas R. MacFarlane, manuscript revision and concept 5%	No
				3) Chenghua Sun, manuscript revision and concept 5%	No

Chapter 4	Why a Proton is transformed into a Hydride by [NiFe] Hydrogenases? An Intrinsic Reactivity Analysis based on Conceptual DFT	Published	60%. Calculations, collecting data and writing first draft	1) Luis Miguel Azofra, manuscript writing, collecting data and calculation guiding30% 2) Douglas R. MacFarlane, manuscript revision and concept 5% 3) Chenghua Sun, manuscript revision and concept 5%	No No No No
	Hydrogen Evolution in [NiFe] Hydrogenases accompanied with Heterolytic Proton-Hydride Approaching	Submitted	80%. Calculations, collecting data and writing first draft	1) Luis Miguel Azofra, manuscript revision and calculation guiding 10% 2) Douglas R. MacFarlane, manuscript revision and concept 5% 3) Chenghua Sun, manuscript revision and concept 5%	No No

I have / have not renumbered sections of submitted or published papers in order to generate a consistent presentation within the thesis.
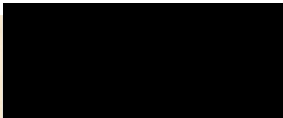
Candidate:
Signature: ███████████
Print Name: ...... Siyao Qiu ....
Date: 05/06/2018

The undersigned hereby certify that the above declaration correctly reflects the nature and extent of the student's and co-authors' contributions to this work. In instances where I am not the responsible author I have consulted with the responsible author to agree on the respective contributions of the authors.

Main Supervisor: ███████████
Signature:
Print Name: ...... Chenghua Sun ......
Date: ...... 05/06/2018 ....

ACKNOWLEDGEMENTS

First and foremost, I would like to sincerely thank my supervisors Dr Chenghua Sun and Prof. Douglas R. MacFarlane for their continuous guide and support in the past three years. Computational chemistry is totally new to me, and Chenghua taught me hand by hand how to build a model, how to calculate and how to analyse the data. As I am not good at writing, Doug would teach me how to revise the paper, discuss sentence by sentence and show me how to express my ideas correctly. Both of them are so patient and encouraging, and spent their time and effort in guiding me and discussing with me.

I would also like to express my gratitude to my supervisor Prof. Annabella Selloni as a visiting student in US. She is very nice, and knowledgeable. From her, I have improved my knowledge about the theoretical chemistry a lot.

I am grateful to Dr. Luis Miguel Azofra and Dr. Seth Olsen for their guiding on the calculations and paper writing. Without their help, I could not be able to study my project so smoothly.

I would also like to thanks my group members Yichun Yin and Chuangwei Liu for their encouragement and help on the research and life during the three years. Also, my friends Honghong, Xiao, Jingrong, Bichen, Weiwei, Mingwei, Chongmin, Shravan and Rupali have brought me so much pleasure and support.

Finally, I am deeply indebted to my parents and grandparents. My families have always been giving me love and courage to overcome any difficulties I met.

TABLE OF CONTENTS

ABSTRACT

In this thesis, DFT calculations have been carried out for the understanding of the hydrogen evolution reaction (HER) on the [NiFe] hydrogenases. From the calculations, the singlet multiplicity pathway was found to be more energetic favoured than the triplet one. Also the two H^+/e^- injection steps were revealed to be the non-spontaneous reaction steps. In contrast, proton transfer towards the NiFe center to form the bridging hydride and the formation of the H_2 molecule are spontaneous processes. Our DFT results investigated the role of the proteic and nonproteic ligands attached to both the Ni and Fe centers.

The protein environment around the active site plays a fundamental role in the HER as well. Our DFT findings show that the reaction Gibbs free energy required for the rate determining step reduces by 7.1 kcal/mol with the surrounding protein environment is taken into account, which is mainly because of energy decreases in the two H^+/e^- addition steps, being the largest thermodynamic impediments of the whole reaction. The hydrogen bonds (H-bonds) between the amino acids and the active site is hypothesised to be the main reason for such stability: H-bonds not only work as electrostatic attractive forces which influence the charge redistribution, but more importantly, they act as an electron 'pull' taking electrons from the active site towards the amino acids.

To closely study the HER mechanism, the DFT calculations of the proton transformation to hydride and the proton-hydride combination suggest that the transformation of proton and proton-hydride approach is motivated by spontaneous rearrangements of the electron density, and stabilisation originates from the decrease of both electronic activity and electrophilicity index of Ni. Moreover, after the approach of the proton and hydride, the two hydrogen atoms terminally bind to Ni and form an H_2 molecule, following the Volmer-Tafel route.

The NiFe bio-inspired molecular catalysts are difficult to synthesis, while large numbers of FeFe molecular catalysts have been synthesized. FeFe bio-inspired molecular catalysts mimicking the [FeFe] hydrogenases have also been widely synthesized. However, HER mechanism taking place on the molecules is poorly understood. Calculations in this work on the FeFe molecular catalysts suggested that the

two hydrogen atoms would terminally bind to one Fe ion on the molecule to form H_2, while the bridging binding hydrogens were not able to generate H_2. Also, the first H^+/e^- injection of the HER on the FeFe molecular catalyst follows the proton transfer followed by electron transfer (PT-ET) mechanism. Moreover, the bridging binding usually requires lower energy than terminal binding for the first proton injection, and the largest thermodynamic impediment is mostly the first proton transfer step. Some terminal ligand modification could obviously change the PT energy, and some other ligand modifications could reduce the largest thermodynamic energy requirement by introducing an intermediate step by providing a proton binding position. By anchoring the FeFe molecular catalysts on the graphene, we found the FeFe molecular maintains its catalytic property. Furthermore, after injection into the graphene the electron is spontaneously delivered to the molecular catalysts when anchored to the surface of an electrode.

LIST OF ABBREVIATIONS

BCP	Bond critical points
CHE	Computational hydrogen electrode
DFT	Density functional theory
EPR	Electron paramagnetic resonance
ET	Electron transfer
FT-IR	Fourier transform infrared
HER	Hydrogen evolution reaction
HOMO	Highest occupied molecular orbital
IRC	Intrinsic reaction coordinate
LUMO	Lowest unoccupied molecular orbital
MM	Molecular mechanics
PCM	Polarizable continuum model
PDB	Protein data bank
PT	Proton transfer
QM	Quantum mechanics
REF	Reaction electronic flux
SCF	Self-consistent field
SHE	Standard hydrogen electrode
TOF	Turnover frequency
TS	Transition state
ZPE	Zero point energy

Chapter 1

Introduction

Dihydrogen (H_2), as one of the eco-friendly energy alternatives to fossil fuel, is attracting growing attention due to its low cost production. However, the existing inorganic catalysts for the hydrogen evolution reaction (HER) are characterised by either low catalytic performance or with high economic cost, like Pt.[1, 2] Hydrogenases, a family of enzymes found in some bacteria and eukarya that carry out HER, exhibit impressive catalytic ability (almost no overpotential and high turnover frequency) and more significantly involve abundant metals only, i.e. Fe and Ni.[3]

The aim of this PhD project is to design a hybrid structure catalyst for HER with low overpotential by anchoring a catalytic cluster, derived from an understanding of the active sites of hydrogenases, onto an inorganic surface with the aid of computational calculation.

1.1 Hydrogenases

Hydrogenases, in regard to the metal ions that constitute the active site, are classified into three kinds, the [NiFe], [FeFe] and [Fe] species (see **Figure 1**).[4, 5] Although all of the hydrogenases could activate the H_2, only the bi-metallic species are able to catalyse the reversible HER.[6] The [FeFe] hydrogenases demonstrate a higher TOF than [NiFe], while the [NiFe] hydrogenases show better O_2 tolerance.[5, 7-11]
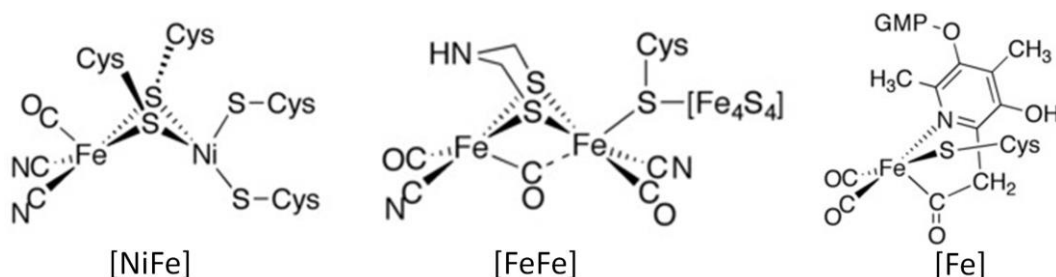

Figure 1. Structures of the active sites of the [NiFe], [FeFe] and [Fe] hydrogenases.

The active site of the two bi-metallic hydrogenases are buried inside a protein matrix, both of them containing cysteine ligands and CO/CN$^-$ inorganic ligands. In [NiFe] hydrogenases, the Ni and Fe metal center is bridged by two cysteine residues, forming a Ni-S-Fe-S four-membered ring.[12, 13] In addition, there are another two cysteines *exo-cyclic* binding on Ni through S atoms, and two cyanide and one carbonyl ligands *exo-cyclic* linked to Fe *via* C atoms.[9] In [FeFe] hydrogenases, the bimetallic Fe centers are bridge ligated by one SCH$_2$NHCN$_2$S ligand and one carbonyl. Moreover, one Fe metal (Fep) is terminally linked with a [Fe4S4] cluster, one carbonyl and one cyanide, while the other Fe (Fed) merely bonds to one carbonyl and one cyanide, leaving a binding position vacant for hydrogen.

Both of the bimetallic hydrogenases are able to catalyse the HER under an H$_2$ abundant atmosphere, where the hydrogenases stay in the active state. When placed in an aerobic environment, the hydrogenases will turn to inactive states, **Ni-A** and **Ni-B**.[12-16] There are three active redox states that could be detected by Electron Paramagnetic Resonance (EPR) and Fourier Transform Infrared (FT-IR) spectroscopy in [NiFe], namely **Ni-SIa**, **Ni-C** and **Ni-R**.[17-21] Accordingly, a reaction pathway has been proposed by Siegbahn et al., as shown in **Scheme 1**.[22-24] **Ni-SIa**, being the most oxidized active state among the reaction path, has no hydrogen atom bound on the active site. The redox state of the Ni and Fe ions are both +2. [25-27] In addition, based on the Mössbauer spectroscopy, the redox state of Fe remains unchanged along the entire reaction pathway. [20, 28] In the **Ni-C** state, a hydride inserts into the four-membered ring after the first H$^+$/e$^-$ gain, bridging between the Ni and Fe ions. [29-31] Correspondingly, the redox state of the Ni becomes +3. An intermediate state **I1** is hypothesized between **Ni-SIa** and **Ni-C**, which has a proton binding to one of the exo-cyclic S atoms and an electron added to the Ni ion leading the charge state of Ni change from +2 to +1. [27] After the second H$^+$/e$^-$ injection, the active site will go to **Ni-R** state. [32] In this state, the proton will be added to the aforementioned exo-cyclic S atom, and the electron will be delivered to the Ni atom, returning the redox state of it to +2. Afterwards, the proton and the hydride tends to move to one metal ion thus forming the H$_2$ molecule, suggesting a second intermediate state **I2** could be

postulated between **Ni-R** and **Ni-SIa** for the whole reaction cycle. Hence, two possible binding position for the $_{H2}$ molecule has been proposed by Wu et al. corresponds to **I2a** (binds to Ni) and **I2b** (Fe), respectively. [33, 34] Previous work on the [NiFe] hydrogenases suggested Ni binding in singlet state while Fe binding in triplet, and the singlet state is more stable than the triplet one.
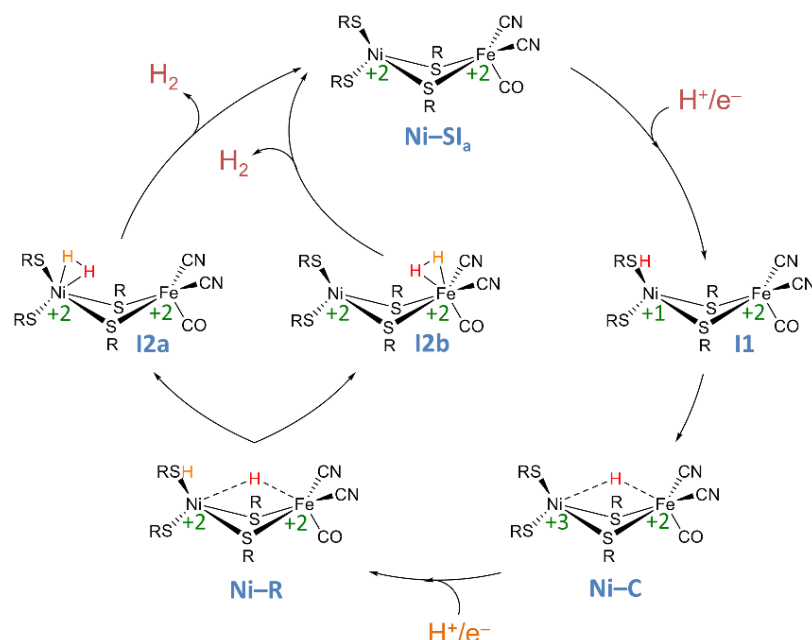
Scheme 1. Hydrogen Evolution Reaction (HER) pathway followed by [NiFe] Hydrogenases.

As for the [FeFe] hydrogenases, previous studies have observed three active states in the whole reaction cycle: **Hox**, **Hred**, **Hsred** (**Scheme 2**).[35, 36] The Hox state is the most oxidized active state, being the initial state among the reaction path. The first H^+/e^- added will lead to the **Hred** state, with the proton binding on the bridging azadithiolate (adt) ligand *via* N and the electron goes to the Fed. Afterwards, the proton transfer occurs from **Hred** to **Hsred** state, however the proton binding position is still unclear.[37] There are two hypothesized intermediate states for the second H^+/e^- injection, which is the **HoxH⁺H⁻** and HoxH2 state. In the **HoxH⁺H⁻** state, the first added proton is proposed to form a hydride binding on Fed, while the second one links to the adt ligand.[38] Subsequently, the second proton will be delivered to Fed, therefore generating H2 with the hydride and then be released. The Fep atom remains +1 charged along the entire reactive process, while Fed experiences a 'charge route' of +2, +1, and +2 along the **Hox/Hred/ HoxH⁺H⁻** steps.

6
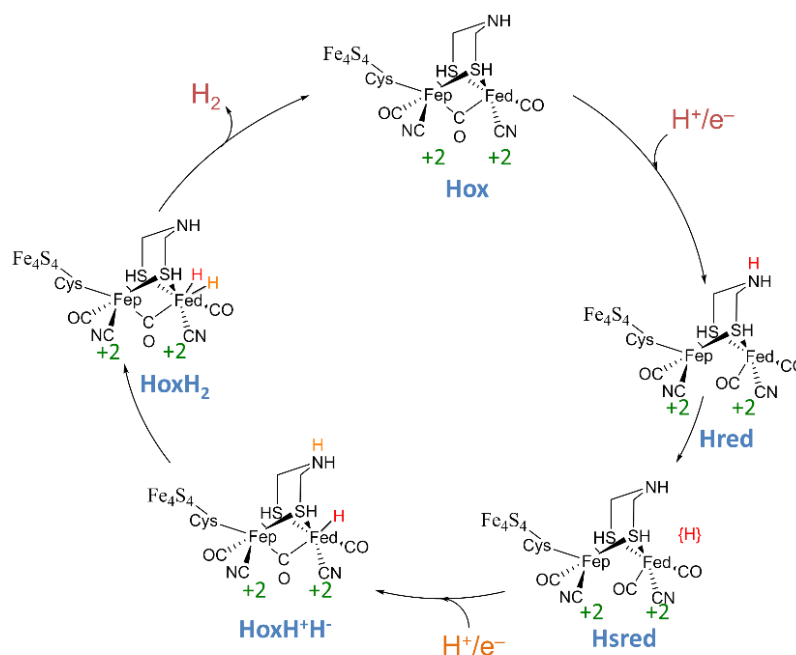
Scheme 2. HER pathway followed by [FeFe] Hydrogenases.

A variety of bio-inspired FeFe molecular catalysts have been synthesized and published.[39-41]However none of the catalysts show as impressive performance as the [FeFe] hydrogenases,[42] underlining the need for advanced investigation of these catalysts. In this PhD work, I focused on the Fe_2S_2 'butterfly' structures to investigate the reason for the different catalytic performance between hydrogenases and molecular catalysts.

1.2 Quantum Chemistry Calculation Background

Computational chemistry calculation has been widely applied in different chemistry aspects as a tool for investigating chemical and physical properties during a chemical reaction, e.g. the geometries, reaction energies and spectra analysis. Quantum chemistry calculation, different to other chemistry calculation methods, are based on the Schrodinger equation (equation 1):

$$\hat{H}\psi(\boldsymbol{r},\boldsymbol{R}) = E\psi(\boldsymbol{r},\boldsymbol{R})$$

in which Hamiltonian operator $\hat{H} = \hat{T} + \hat{V}$.and shows a higher accuracy in predicting the different properties than the other methods.[43]

In our work, Density Functional Theory (DFT) calculations were used for all calculations. This approach simplifies the solution of the wavefunction ψ from Schrodinger equation into the calculation of the electron density ρ (the square of the wavefunction). The solution of the Schrodinger equation can be further simplified by different approximations for a higher computational efficiency as follows.

Firstly, the Born-Oppenheimer approximation suggests the motion of the nuclei could be neglected, as the movement of electrons are much faster than the nuclei.[44]And the Hamiltonian operator could be simplified as $\hat{H} = \hat{T}_e + \hat{V}_{ee} + \hat{V}_{eN} + \hat{V}_{NN}$.

$$\hat{H} = -\frac{1}{2}\sum_{i=1}^{N_e}\nabla_i^2 + \sum_{i>j}\frac{1}{|r_i - r_j|} - \sum_{i=1}^{N_e}\sum_{I=1}^{N}\frac{Z_I}{|r_i - R_I|} + \sum_{I>J}\frac{Z_I Z_J}{|R_I - R_J|}$$

$\hat{T}_e + \hat{V}_{ee}$are similar between two systems which contains same number of electrons. The $\hat{V}_{eN}$ term calculating the electron-electron repulsion still limits the calculation efficiency and could only be calculated for small molecular models. Therefore, the Hohenberg-Kohn Theorem further proposed that the energy could be derived from the electron density, which is the square of the wavefunction.[45]And the $\hat{V}_{eN}$term could be interpreted as the electron energy under an external potential.

$$\langle\hat{V}_{eN}\rangle = \int \rho_0(r)v(r)dr = \int \rho_0(r)\sum_I -\frac{Z_I}{|r_i - R_I|}dr_i = -\sum_I Z_I \int \frac{\rho_0(r_i)}{|r_i - R_I|}dr_i$$

Also, the Hohenberg-Kohn Theorem suggests that any electronic energy derived from the trial electron density is higher than the true energy.[45]

Later, to reduce the error that might be caused during the calculation,the Kohn-Sham approach further introduces the reference systems, which transfer the two terms $\hat{T}_e + \hat{V}_{ee}$ (kinetic and electron-electron repulsion) into a sum of terms with only one small term unknown.[46]Hence, even if

moderately large errors have been introduced to the small term, the final energy would not be largely affected.

$$\Delta\langle T[\rho_0]\rangle = \langle T[\rho_0]\rangle - \langle T_r[\rho_0]\rangle$$

The '$\Delta T[\rho_0]$' is the minor term, and the reference quantity $T_r[\rho_0]$ is the kinetic energy of a system with non-interacting electrons.

$$\langle T_r[\rho_0]\rangle = \langle\psi_r\left|\sum_{i=1}^{2n}-\frac{1}{2}\nabla_i^2\right|\psi_r\rangle$$

As for the electron-electron repulsion term, $\Delta\langle V_{ee}[\rho_0]\rangle$ could be written as

$$\Delta\langle V_{ee}[\rho_0]\rangle = \langle V_{ee}[\rho_0]\rangle - \frac{1}{2}\iint\frac{\rho_0(\boldsymbol{r}_i)\rho_0(\boldsymbol{r}_j)}{|\boldsymbol{r}_i-\boldsymbol{r}_j|}d\boldsymbol{r}_id\boldsymbol{r}_j$$

and the reference term for the electron-electron repulsion is to treat all the electrons as an electron cloud, and individually calculate the single electron interaction with the total electron cloud in a non-quantum coulomb model. Such an electron cloud includes an electron self-interaction part, and should be compensated by an exchange-correlation functional.

$$E_{XC}[\rho_0] = \Delta\langle T[\rho_0]\rangle + \Delta\langle V_{ee}[\rho_0]\rangle$$

The Kohn-Sham energy is calculated under the ideal condition that a system is a non-interacting reference system, which is the same as the reference system during the kinetic calculation. Therefore, in DFT calculation the solution of the Schrodinger equation can be transformed to the Kohn-Sham equation as shown below.

$$\left[-\frac{1}{2}\nabla_i^2-\sum_I\frac{Z_I}{|\boldsymbol{r}_i-\boldsymbol{R}_I|}+\int\frac{\rho(\boldsymbol{r}_j)}{|\boldsymbol{r}_i-\boldsymbol{r}_j|}d\boldsymbol{r}_j+v_{XC}(\text{i})\right]\psi_i^{KS}=\epsilon_i^{KS}\psi_i^{KS}$$

$$v_{XC}[\boldsymbol{r}]=\frac{\delta E_{XC}[\rho(\boldsymbol{r})]}{\delta\rho(\boldsymbol{r})}$$

1.3 Computational details

The calculations on the geometries of the HER pathway followed by bimetallic hydrogenase enzymes have been conducted by DFT using the BP86 functional.[47, 48] Two effective core potential basis sets, Def2TZVPP and Def2SVP, have been applied for all models by the use of the two-layer ONIOM approach, among which the Def2TZVPP is used for the active site (including the metal, sulfur, adt, and inorganic ligands to the Fe ion), and the smaller Def2SVP for the rest of the atoms.[49] The EDIIS/CDIIS procedure has been applied for the self-consistent field (SCF) in all cases. [50] Also, to obtain the free energy and confirm the nature of the stationary points, frequency calculations have been done for all the models. Grimme's D3 damping function has been used for the correction of the dispersion interaction for all models. [51] The same computational parameters are used for the calculations in Chapter 2-4 in this thesis. In Chapter 5, six different DFT functional (PBE, BP86, TPSS, PBE0, B3LYP, M062X) have been applied with Def2TZVPP basis set for the molecular catalysts calculations.

In all cases, the free energy at mild conditions of temperature (T = 298.15 K) and including vibrational zero point energy (ZPE) corrections have been calculated. For the H^+/e^- pair injection steps, the chemical potential of the H^+/e^- pair has been calculated as the half of the chemical potential of H_2, under standard atmosphere and pH = 0 conditions

$$G(H^+ + e^-) = \frac{1}{2}\, G(H_2)$$

This refers to the Standard Hydrogen Electrode (SHE). [52-54] However, since enzymes work at pH = 7 conditions, pH corrections have been carried out, with a value of +9.55 kcal/mol, based on the Nernst equation as:

$$\Delta G_{rxn} = \Delta G_0 + 2.303\ RT\ pH$$

For the calculation under solvent conditions, Polarizable Continuum Model (PCM) was applied in molecular catalysts part programmed by acetonitrile.[55] All the energy calculations were carried out by the facilities provided by the Gaussian09 program package (revision D.01).[56]

The initial calculation models were built based on the X-ray crystallographic data of the hydrogenase from Desulfovibrio vulgaris str. 'Miyazaki F' organism and the Clostridium pasteurianum [FeFe] hydrogenase (PDB accession code 1H2R, 3C8Y) and the molecular catalytsts.[57-58]

A variety of experimental works have been done on the hydrogenase enzyme and the molecular analogues of the active site. However it is difficult to investigate the active site of the hydrogenases by experiment. DFT computational calculations, providing reliable prediction for the properties of a material, are useful for the studies of the active site that are inaccessible by experiment. Moreover, the computational tools could help us study the properties of a newly designed catalyst. Therefore, in this thesis, the DFT calculations were used for the study of the hydrogenases and the bio-inspired molecular catalysts.

1.4 Scope and Goals of this Thesis

The goal of this thesis is to design a catalyst for HER with low overpotential, which is achieved by anchoring a catalytic cluster, inspired from the active sites of hydrogenases, onto an inorganic surface. In doing so, the hydrogen evolution mechanism on the hydrogenases should be understood. In order to meet our final expectation, this thesis included these objectives:

1. Though a majority of works have been done for the research on hydrogenases, the previous calculation research focused more on the comparison of the theoretical data with the experimental result, e.g. X-ray geometry, FTIR spectrum. Only a limited amount of work has emphasised the calculation of the reaction path. The understanding of the hydrogen evolution cycle on the active site of [NiFe] hydrogenases. The goal of this thesis includes an

understanding of the free energy diagram of the HER process, the geometric changes taking place on the active site during HER and the driving force for the proton transfer on the active site.

2. A variety of the bio-inspired molecular catalysts that mimic the active site of hydrogenases have been synthesised, and some catalysts with same metal ions show different catalytic properties as they have different ligands. Hence, the role of the ligands on the active site and how they influence the catalytic performance, including the inorganic (CO and CN) and cysteine ligands at the active site are studied here.

3. Our third objective is to design a bio-mimic molecular catalyst. As molecular catalysts do not have protein environment, it is important to understand how the protein environment around the active site affects the HER catalysis.

1.5 Overview of Thesis

- Chapter 1. This introductory chapter provides an introduction to the hydrogenase enzyme and the theoretical background of the DFT calculations. Motivated by the remarkable catalytic performance of hydrogenases for HER, the previous works proposed the classification of hydrogenases and the geometry of the active site. Also, the metal valence state and multiplicity of the active site, the catalytic states during the catalytic cycle have been studied in the previous papers. In this context, the summary of the previous works related to the study on the hydrogen evolution cycle by hydrogenase enzyme is outlined.

- Chapter 2. The active states invovled in the catalytic cycle of [NiFe] hydrogenases have been studied. The corresponding free energy diagram has been drawn for the understanding on the HER process. The multiplicity of the metal centre of the hydrogenases and the H_2 binding metal are controversial topics, and the results here further support the single multiplicity and Ni binding from the free energy diagram. Also, the influences of the

inorganic and proteic ligands at the active site on the reaction energy diagram have been studied. The paper 'Unraveling the Role of Ligands in the Hydrogen Evolution Mechanism Followed by [NiFe] Hydrogenases' describing this work was published in ACS Catalysis in 2016.

- Chapter 3. The protein environment around the active site of [NiFe] hydrogenase is studied by comparing free energy diagrams of the pure active site model and the model with surrounding amino acids. Also, we have understood which type of amino acids leads to the influence on the catalytic performance and how the amino acids affect the catalysis. The paper 'Protein Environment Effect or How Amino Acids Affect the Catalytic Performance for the H_2 Production in [NiFe] Hydrogenases' describing this wprk was published in Physical Chemistry Chemical Physics on 2018.

- Chapter 4. In order to understand the electronic property changes and the driving force for the proton transfer processes (**I1** to **Ni-C** and **Ni-R** to **I2**) on the active site of [NiFe] hydrogenases, these steps during the HER have been studied by the conceptual DFT calculation. From the intrinsic reaction coordinate calculations, the energy and force change could be directly derived. And by analysing the electronic properties during the reaction, the electronic chemical potential, electronic flux, electrophilicity change on the metal ions and the NBO charge evolution along the process could be derived. The paper 'Why Proton is transformed into Hydride by [NiFe] Hydrogenases? An Intrinsic Reactivity Analysis based on Conceptual DFT' was published in Physical Chemistry Chemical Physics on 2016, and the paper 'Hydrogen Evolution by [NiFe] Hydrogenases: Heterolytic Non-Concerted Mechanism Driven through a Maximum Hardness – Minimum Electrophilicity Scheme' has been submitted.

- Chapter 5. HER on the bio-inspired molecular catalysts has been studied in this chapter. Eight different FeFe molecular catalysts have been calculated. From the free energy calculation along the HER path on the molecular catalysts, the largest thermodynamic

impediment of the HER could be found. By comparing the HER path on the eight different catalysts, we could understand the HER on the [FeFe]-hydrogenases-inspired molecular catalysts. The paper 'DFT studies on the [FeFe]-hydrogenases-inspired molecular catalysts' have been composed.

- Chapter 6. This chapter outlines the main conclusions from this project.

References

1.   B. E. Conway and B. V. Tilak, *Electrochimica Acta*, 2002, **47**, 3571-3594.

2.   J. K. Nørskov, T. Bligaard, A. Logadottir, J. R. Kitchin, J. G. Chen, S. Pandelov and U. Stimming, *Journal of The Electrochemical Society*, 2005, **152**, J23.

3.   C. Madden, M. D. Vaughn, I. Díez-Pérez, K. A. Brown, P. W. King, D. Gust, A. L. Moore and T. A. Moore, *Journal of the American Chemical Society*, 2012, **134**, 1577-1582.

4.   P. M. Vignais and B. Billoud, *Chemical reviews*, 2007, **107**, 4206-4272.

5.   W. Lubitz, H. Ogata, O. Rudiger and E. Reijerse, *Chem. Rev.*, 2014, **114**, 4081-4148.

6.   S. V. Hexter, F. Grey, T. Happe, V. Climent and F. A. Armstrong, *Proceedings of the National Academy of Sciences*, 2012, **109**, 11516-11521.

7.   T. Burgdorf, O. Lenz, T. Buhrke, E. van der Linden, A. K. Jones, S. P. J. Albracht and B. Friedrich, *J. Mol. Microbiol. Biotechnol.*, 2005, **10**, 181-196.

8.   C. Tard and C. J. Pickett, *Chemical reviews*, 2009, **109**, 2245-2274.

9.   J. C. Fontecilla-Camps, A. Volbeda, C. Cavazza and Y. Nicolet, *Chemical reviews*, 2007, **107**, 4273-4303.

10.   J. Fritsch, O. Lenz and B. Friedrich, *Nat Rev Micro*, 2013, **11**, 106-114.

11.   P. Wulff, C. Thomas, F. Sargent and F. A. Armstrong, *J. Biol. Inorg. Chem.*, 2016, **21**, 121-134.

12. A. Pardo, A. De Lacey, V. Fernández, Y. Fan and M. Hall, *J. Biol. Inorg. Chem.*, 2007, **12**, 751-760.

13. P. E. M. Siegbahn, *Comptes Rendus Chimie*, 2007, **10**, 766-774.

14. H. Ogata, S. Hirota, A. Nakahara, H. Komori, N. Shibata, T. Kato, K. Kano and Y. Higuchi, *Structure*, 2005, **13**, 1635-1642.

15. A. Volbeda, L. Martin, C. Cavazza, M. Matho, B. W. Faber, W. Roseboom, S. P. Albracht, E. Garcin, M. Rousset and J. C. Fontecilla-Camps, *Journal of biological inorganic chemistry : JBIC : a publication of the Society of Biological Inorganic Chemistry*, 2005, **10**, 239-249.

16. M. van Gastel, M. Stein, M. Brecht, O. Schröder, F. Lendzian, R. Bittl, H. Ogata, Y. Higuchi and W. Lubitz, *J. Biol. Inorg. Chem.*, 2006, **11**, 41-51.

17. B. Bleijlevens, B. Faber and S. Albracht, *J. Biol. Inorg. Chem.*, 2001, **6**, 763-769.

18. C. Fichtner, C. Laurich, E. Bothe and W. Lubitz, *Biochemistry*, 2006, **45**, 9706-9716.

19. A. L. De Lacey, V. M. Fernández, M. Rousset and R. Cammack, *Chemical reviews*, 2007, **107**, 4304-4330.

20. W. Lubitz, E. Reijerse and M. van Gastel, *Chemical reviews*, 2007, **107**, 4331-4365.

21. M.-E. Pandelia, H. Ogata, L. J. Currell, M. Flores and W. Lubitz, *Biochim. Biophys. Acta*, 2010, **1797**, 304-313.

22. P. E. M. Siegbahn, in *Advances in Inorganic Chemistry*, Academic Press, Editon edn., 2004, vol. Volume 56, pp. 101-125.

23. P. E. M. Siegbahn, J. W. Tye and M. B. Hall, *Chemical reviews*, 2007, **107**, 4414-4435.

24. M. Bruschi, G. Zampella, P. Fantucci and L. De Gioia, *Coord. Chem. Rev.*, 2005, **249**, 1620-1640.

25. H. Wang, C. Y. Ralston, D. S. Patil, R. M. Jones, W. Gu, M. Verhagen, M. Adams, P. Ge, C. Riordan, C. A. Marganian, P. Mascharak, J. Kovacs, C. G. Miller, T. J. Collins, S.

Brooker, P. D. Croucher, K. Wang, E. I. Stiefel and S. P. Cramer, *J. Am. Chem. Soc.*, 2000, **122**, 10544-10552.

26. M. Bruschi, M. Tiberti, A. Guerra and L. De Gioia, *J. Am. Chem. Soc.*, 2014, **136**, 1803-1814.

27. A. Pardo, A. De Lacey, V. Fernández, H.-J. Fan, Y. Fan and M. Hall, *J. Biol. Inorg. Chem.*, 2006, **11**, 286-306.

28. K. K. Surerus, M. Chen, J. W. van der Zwaan, F. M. Rusnak, M. Kolk, E. C. Duin, S. P. J. Albracht and E. Muenck, *Biochemistry*, 1994, **33**, 4980-4993.

29. M. Stein and W. Lubitz, *Physical Chemistry Chemical Physics*, 2001, **3**, 5115-5120.

30. M. Kampa, W. Lubitz, M. van Gastel and F. Neese, *J. Biol. Inorg. Chem.*, 2012, **17**, 1269-1281.

31. S. Foerster, M. Gastel, M. Brecht and W. Lubitz, *J. Biol. Inorg. Chem.*, 2005, **10**, 51-62.

32. H. Ogata, K. Nishikawa and W. Lubitz, *Nature*, 2015, **520**, 571-574.

33. H. Wu and M. B. Hall, *Comptes Rendus Chimie*, 2008, **11**, 790-804.

34. J. M. Keith and M. B. Hall, *Inorg. Chem.*, 2010, **49**, 6378-6380.

35. D. W. Mulder, M. W. Ratzloff, E. M. Shepard, A. S. Byer, S. M. Noone, J. W. Peters, J. B. Broderick and P. W. King, *J. Am. Chem. Soc.*, 2013, **135**, 6921-6929.

36. A. Silakov, C. Kamp, E. Reijerse, T. Happe and W. Lubitz, *Biochemistry*, 2009, **48**, 7780-7786.

37. A. Adamska, A. Silakov, C. Lambertz, O. Rüdiger, T. Happe, E. Reijerse and W. Lubitz, *Angewandte Chemie International Edition*, 2012, **51**, 11458-11462.

38. M. Bruschi, C. Greco, M. Kaukonen, P. Fantucci, U. Ryde and L. De Gioia, *Angewandte Chemie International Edition*, 2009, **48**, 3503-3506.

39. F. Gloaguen and T. B. Rauchfuss, *Chem. Rev. Soc.*, 2009, **38**, 100–108

40. Y. Li and T. B. Rauchfuss, *Chem. Rev.*, **116**, 7043−7077

41. D. Schilter, J. M. Camara, M. T. Huynh, S. Hammes-Schiffer and T. B. Rauchfuss, *Chem. Rev.*, 2016, **116**, 8693−8749

42. G. A. N. Felton, C. A. Mebi, B. J. Petro, A. K. Vannucci, D. H. Evans, R. S. Glass and D. L. Lichtenberger, *Journal of Organometallic Chemistry*, 2009, **694**, 2681-2699.

43. E. Schrodinger, *Ann. Physik.*, 1964, **79**, 361–376

44. M. Born and J. R. Oppenheimer, *Ann. Physik.*, 1927, **84**, 457-484.

45. P. Hohenberg and W. Kohn, *Phys. Rev. B*, 1964, **136**, 864-871.

46. W. Kohn and L. J. Sham, *Phys. Rev. A*, 1965, **140**, 1133-1138.

47. J. P. Perdew, *Phys. Rev. B*, 1986, **33**, 8822-8824.

48. A. D. Becke, *Phys. Rev. A*, 1988, **38**, 3098-3100.

49. F. Weigend and R. Ahlrichs, *Phys. Chem. Chem. Phys.*, 2005, **7**, 3297-3305.

50. K. N. Kudin, G. E. Scuseria and E. Cancès, *J. Chem. Phys.*, 2002, **116**, 8255-8261.

51. S. Grimme, J. Antony, S. Ehrlich and H. Krieg, *J. Chem. Phys.*, 2010, **132**, 154104.

52. J. K. Nørskov, J. Rossmeisl, A. Logadottir, L. Lindqvist, J. R. Kitchin, T. Bligaard and H. Jónsson, *J. Phys. Chem. B*, 2004, **108**, 17886-17892.

53. E. Skulason, G. S. Karlberg, J. Rossmeisl, T. Bligaard, J. Greeley, H. Jonsson and J. K. Norskov, *Phys. Chem. Chem. Phys.*, 2007, **9**, 3241-3250.

54. J. Rossmeisl, Z. W. Qu, H. Zhu, G. J. Kroes and J. K. Nørskov, *Journal of Electroanalytical Chemistry*, 2007, **607**, 83-89.

55. G. Scalmani and M. J. Frisch, *J. Chem. Phys.*, 2010, **132**, 114110.

56. M. J. Frisch, G. W. Trucks, H. B. Schlegel, G. E. Scuseria, M. A. Robb, J. R. Cheeseman, G. Scalmani, V. Barone, B. Mennucci, G. A. Petersson, H. Nakatsuji, M. Caricato, X. Li, H. P. Hratchian, A. F. Izmaylov, J. Bloino, G. Zheng, J. L. Sonnenberg, M. Hada, M. Ehara, K. Toyota, R. Fukuda, J. Hasegawa, M. Ishida, T. Nakajima, Y. Honda, O. Kitao, H. Nakai, T. Vreven, J. A. Montgomery Jr., J. E. Peralta, F. Ogliaro, M. Bearpark, J. J. Heyd, E. Brothers, K. N. Kudin, V. N. Staroverov, R. Kobayashi, J. Normand, K. Raghavachari, A.

Rendell, J. C. Burant, S. S. Iyengar, J. Tomasi, M. Cossi, N. Rega, N. J. Millam, M. Klene, J. E. Knox, J. B. Cross, V. Bakken, C. Adamo, J. Jaramillo, R. Gomperts, R. E. Stratmann, O. Yazyev, A. J. Austin, R. Cammi, C. Pomelli, J. W. Ochterski, R. L. Martin, K. Morokuma, V. G. Zakrzewski, G. A. Voth, P. Salvador, J. J. Dannenberg, S. Dapprich, A. D. Daniels, Ö. Farkas, J. B. Foresman, J. V. Ortiz, J. Cioslowski and D. J. Fox, Gaussian, Inc., Wallingford CT, Editon edn., 2009.

57.   *Protein Data Bank*, http://www.rcsb.org.

58.   A. S. Pandey, T. V. Harris, L. J. Giles, J. W. Peters and R. K. Szilagyi, *J. Am. Chem. Soc.*, 2008, **130**, 4533-4540.

CHAPTER 2

The Role of Ligands in the Hydrogen Evolution Mechanism Catalysed by [NiFe] Hydrogenases

In this chapter, the HER mechanism on the [NiFe] hydrogenases has been studied in detail by DFT methods for the first time. From the study, the conformational changes on the active site of hydrogenases during the HER process could be observed. Also, the Gibbs free energy fluctuations along the HER reaction pathway have been shown. From the energy diagram, the multiplicity of the active site and the rate-determining step of the HER could be derived. Moreover, this chapter has investigated the role of the inorganic and proteic ligands in the HER mechanism.

The work was published in ACS Catalysis 'Unravelling the Role of Ligands in the Hydrogen Evolution Mechanism Followed by [NiFe] Hydrogenases' (*ACS Catal.* 2016, **6**, 5541−5548).

By

Siyao Qiu, Luis Miguel Azofra, Douglas R. MacFarlane, Chenghua Sun.

It can be concluded from the studies in this chapter that:

1. The second H^+/e^- gain (**Ni-C** to **Ni-R**) for the energy pathway along the small model of [NiFe] hydrogenases is the rate-determining step, and the two H^+/e^- gains (**Ni-SI$_a$** to **I1** and **Ni-C** to **Ni-R**) are non-spontaneous while the two proton transfer steps (**I1** to **Ni-C** and **Ni-R** to **I2**) and the H_2 release step (**I2** to **Ni-SI$_a$**) are spontaneous.

2. The energy result of [NiFe] hydrogenases shows a preference to the singlet state than the than the triplet one;

3. H_2 forming position in singlet state is on the Ni ion and in triplet state is on the Fe;

4. The rotation of the S atom in the cysteine residues binding to the active site affect the LUMO energy of the **Ni-SIa** state, thus influence the energy for the first H^+/e^- gain and the H_2 release. And the distortion in the carbon skeleton conformation accompanied with the S rotation will have more significant impact on the energy profile. Such kind of distortion and rotation is on the account of the change on the Ni coordination geometry.

5. The replacing of the CN^- ligands by the neutral CO ligands presents a drastic energy decrease on the two H^+/e^- gains, while the two proton transfer steps become non-spontaneous. The CO ligands replaced by the CN^- tell an opposite story.

Unraveling the Role of Ligands in the Hydrogen Evolution Mechanism Catalyzed by [NiFe] Hydrogenases

Siyao Qiu,[†] Luis Miguel Azofra,[†,‡] Douglas R. MacFarlane,*,[†,‡] and Chenghua Sun*,[†,‡]

[†]School of Chemistry, Faculty of Science, Monash University, Clayton, Victoria 3800, Australia

[‡]ARC Centre of Excellence for Electromaterials Science (ACES), School of Chemistry, Faculty of Science, Monash University, Clayton, Victoria 3800, Australia

S *Supporting Information*

ABSTRACT: DFT investigations have been carried out on the hydrogen evolution reaction (HER) mechanism followed by [NiFe] hydrogenases. Calculations on the active site of the [NiFe] hydrogenase from *Desulfovibrio vulgaris* str. "Miyazaki F" reveal that H_2 is formed as the final product through the "singlet multiplicity" pathway. Nonspontaneous reaction energies can be seen for both H^+/e^- additions to the reactive sulfur atom from the truncated cysteine residues, being the limiting steps of the whole reaction. In contrast, transfers toward the metal environment to produce the bridging hydride and the bonded H_2 molecule at the **Ni-C** and **I2** steps, respectively, are spontaneous processes. Our DFT results highlight the role of the ligands attached to both the Ni and Fe centers. When the protein ligand environment is spatially confined, reaction energies for the HER are lower than those when the ligand carbons are able to freely adjust. In addition, larger changes can be seen on interchanging the $[CN]^-$ and CO ligands on the Fe center; in particular, the energy profile dramatically changes as $[CN]^-$ ligands are replaced by CO. These results may guide materials synthesis efforts toward optimized HER catalysts.

KEYWORDS: H_2 production, spin effect, enzymatic catalysis, bimetallic enzymes, DFT

2H⁺/2e⁻

Hydrogen Evolution Reaction in [NiFe] Hydrogenases

H₂
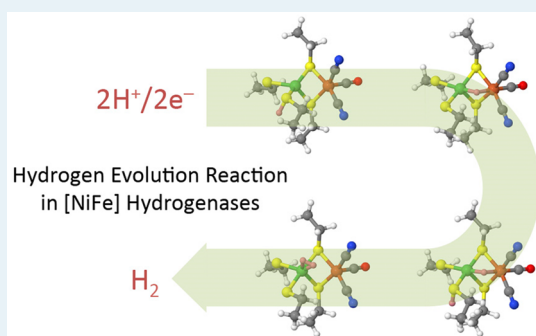
INTRODUCTION

Due to the serious environmental issues stemming from the burning of hydrocarbon compounds based on fossil fuels as energy sources,[1−3] dihydrogen (H_2) is emerging as a promising environmentally friendly alternative. However, the high cost of the most active (usually noble metal) catalysts, such as platinum,[4] creates a real limitation. In this regard, the search for novel catalysts based on only earth-abundant materials is highly desirable. Thus, the challenge lies in finding catalysts that are commercially effective and chemically efficient.[5]

If one candidate attracts much of our attention, undoubtedly, hydrogenase enzymes, representing how Nature produces (or cleaves) H_2, have not only shown impressive catalytic performance for dihydrogen production but also are based on abundant metals.[6]

On the basis of the metal centers composing the active site, hydrogenase enzymes (hereafter simply referred as hydrogenases), can be classified into [NiFe], [FeFe], or [Fe] types.[7,8] Only bimetallic [NiFe] and [FeFe] hydrogenases catalyze the reversible reaction of dihydrogen oxidation into protons and electrons, and [NiFe] hydrogenases have better O_2 tolerance than the [FeFe] species.[9] Thus, the study of [NiFe] hydrogenases is of crucial importance for the development of bioinspired catalysts.

With the exception of the [NiFeSe] subclass, the active sites of the [NiFe] hydrogenases all have a similar atomic composition: a bimetallic four-membered ring connects Ni and Fe metal centers via two sulfur atoms; the latter are part of cysteine residues from the protein environment.[10] Finally, two exocyclic cysteine residues are bound to the Ni through their sulfur atoms and Fe is linked with three inorganic ligands, one neutral carbonyl and two cyanide anions, via the C moiety in all cases (see Scheme 1).[11] In this regard, the structural environment of the Fe ligands has been studied by comparison of quantum chemical calculations of three different configuration models with X-ray and Fourier transform infrared (FT-IR) spectroscopy data.[12]

When they are placed in an aerobic environment, [NiFe] hydrogenases will turn to inactive states. The so-called **Ni-A** and **Ni-B** states have the active site blocked by the presence of the OH^- species acting as bridging moieties between the two metals, as proposed in the literature.[13−19] However, under an H_2 atmosphere, the [NiFe] hydrogenase can be reactivated.
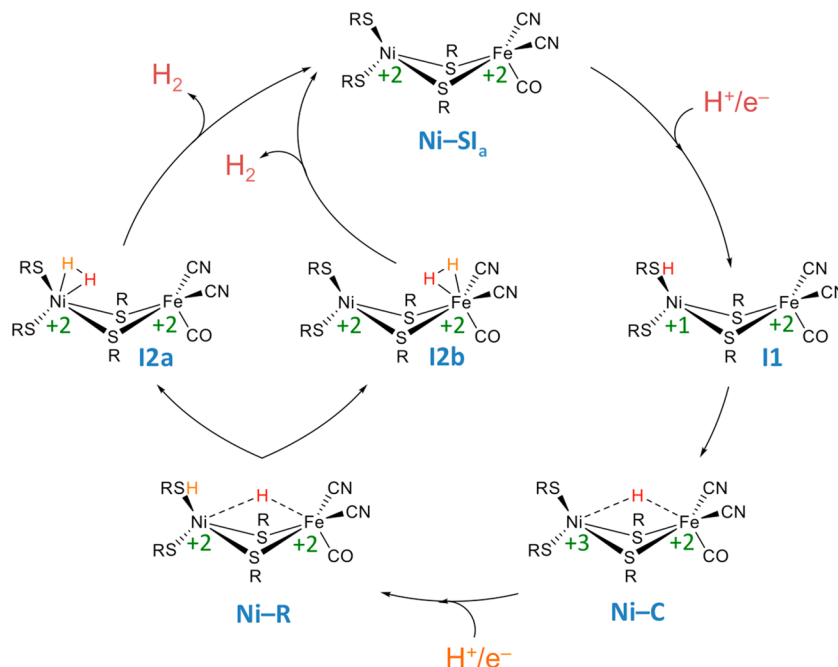
According to FT-IR and electron paramagnetic resonance (EPR) spectroscopy, there are three observed active redox states of the [NiFe] hydrogenases: **Ni-SI$_a$**, **Ni-C**, and **Ni-R**,[20−24] which have been studied by comparison of computational and experimental approaches. According to previous

Scheme 1. Hydrogen Evolution Reaction (HER) Path Followed by [NiFe] Hydrogenases

work presented by Siegbahn et al.,[25] Scheme 1 summarizes the corresponding hydrogen evolution reaction (HER) path followed by [NiFe] hydrogenases; however, a different proposal was previously besought by Niu and co-workers,[26] consisting of postulating an additional proton binding on the exocyclic sulfur in all reaction states.

Following the HER path gathered in Scheme 1, **Ni-SI$_a$** represents the oxidized active state in which a vacant position exists above the four-membered ring. This active site becomes occupied by a hydride in the **Ni-C** state.[15,27−32] **I1** is an intermediate state,[33] during which the first hydrogenation takes place on the sulfur atom of one of the exocyclic cysteine residues directly bonded to Ni, to be finally transferred as a bridging hydride shared between the Ni and Fe metals. After the first hydrogenation, the addition of a second H$^+$/e$^-$ pair leads to the **Ni-R** state. FT-IR spectroscopy indicates the existence of three subforms for this case,[34,35] and recent X-ray crystallography data and computational studies have verified the persistence of the bridging hydride between the two metal ions and the inclusion of the second H$^+$/e$^-$ pair on the previously reacted terminal sulfur ligand in one of the subforms.[36] In addition, another recent work by Ogata and co-workers supported the bridging hydride existence by the vibrational spectroscopy for the first time.[37] As an intermediate state, **I2** links the **Ni-R** and **Ni-SI$_a$** states, involving the migration of the second proton and first hydride toward the metal centers.[29,38] These two hydrogen atoms may bind to the Ni (**I2a**) or to the Fe (**I2b**) atoms and represent the final steps before the release of H$_2$ as the product. In addition, Mössbauer spectroscopy indicates that the Fe atom remains doubly positively charged along the entire reactive process,[39] while Ni experiences a "charge route" of +2, +1, and +3 along the **Ni-SI$_a$/I1/Ni-C** steps.

A variety of studies of the ligand environment of the active sites of the various states discussed above have been published.[14,39−44] The multiplicity of the Ni metal is an important question, as both the high-spin[45] and low-spin[46,47] states are supported by experimental results. In this regard,

DFT investigations indicate that the BP86 functional exhibits an energy preference for the singlet state, while B3LYP suggests the contrary: that triplet states dominate the reaction path for the **Ni-SI$_a$** and **Ni-R** states.[48] According to previous work, BP86 has a smaller mean unsigned error in describing the hydrogenase structures, but more remarkably, accurate ab initio coupled cluster CCSD calculations show an energy preference for the singlet state, being ∼14 kcal/mol more stable than the triplet, for the **Ni-SI$_a$** state.[49] This is significant, as the multiplicity strongly affects the H$_2$ binding position on the active site: while H$_2$ tends to bind at Ni in the singlet state, when the multiplicity is triplet, it tends to bind on Fe.[50]

Finally, while it is widely accepted that the ligand environment affects the reaction pathway, the details and origins of the effects remain unclear. In the present work, models with different truncated cysteine ligands are compared in order to study how the proximal protein environment affects the reaction pathway. We pay special attention to how the confinement of the ligands influences the energy profile. In addition, the effects of neutral CO vs negatively charged [CN]$^-$ ligands are studied.

■ COMPUTATIONAL DETAILS

The geometry and properties of the HER mechanism followed by [NiFe] hydrogenases have been studied through the use of density functional theory (DFT) via the BP86 functional[51,52] in its unrestricted formalism. Two-layer "onion" basis sets have been applied for all models, using the Def2TZVPP effective core potential for the active site (constituted by the metals, sulfurs, and ligands attached to the Fe atom) and the smaller Def2SVP effective core potential for the carbon chains directly bonded to sulfurs.[53] In all cases, the EDIIS/CDIIS procedure was applied for the self-consistent field (SCF) convergence.[54] In addition, frequency calculations were performed in order to confirm the nature of the stationary points and to obtain the zero-point energy (ZPE) as well as the thermal correction terms. Therefore, all the energies reported below are Gibbs free
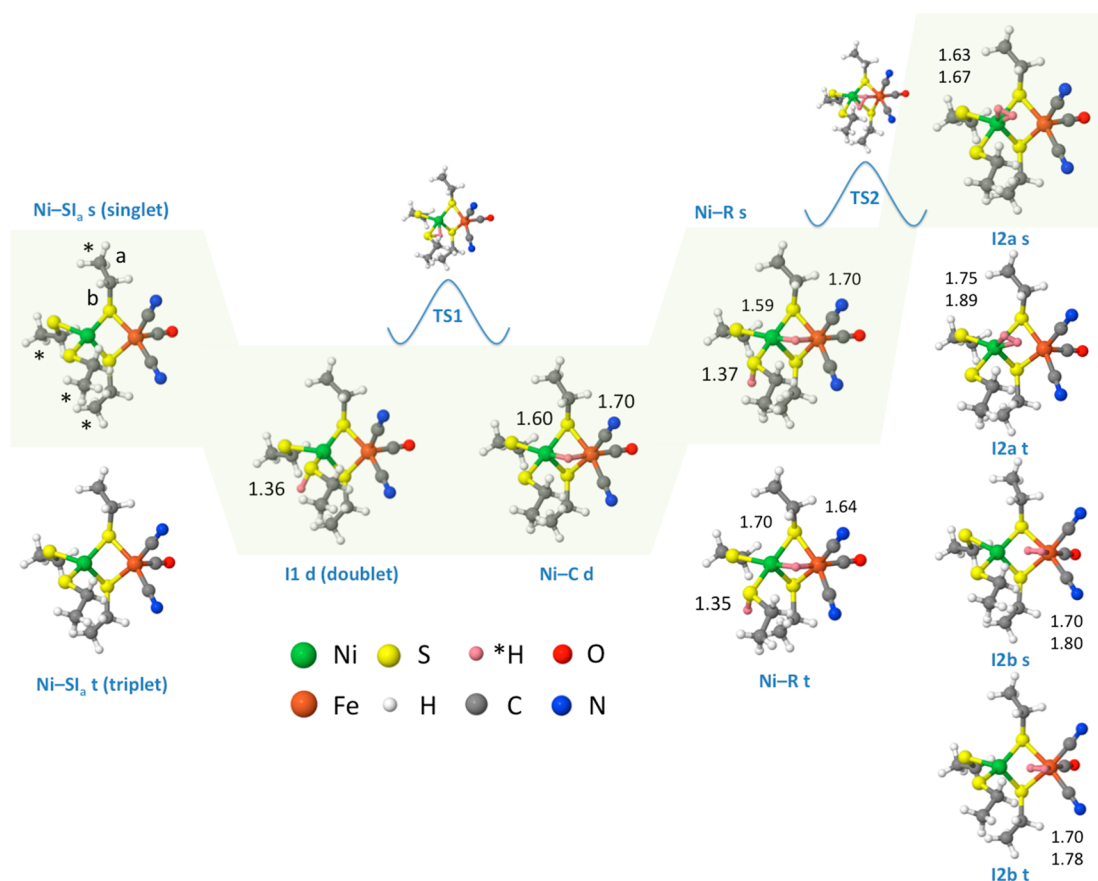
Figure 1. Modeling the HER mechanism steps followed by the [NiFe] active site. Hydrogen atoms participating in the HER pathway are highlighted in pink. Shading indicates the singlet pathway. Frozen carbon atoms are indicated with asterisks at the **Ni-SI$_a$** singlet state; these carbons are frozen throughout the rest of the structures. Selected H−X distances are shown in Å.

energies under mild conditions. In addition, the dispersion interaction correction has been included during geometry optimization by using Grimme's D3 damping function in all models.[55] Under $f(H_2)$ = 101325 Pa and pH 0 conditions, the energy difference for the H$^+$/e$^-$ added step in this work could be approximated as half of the free energy of the H$_2$ molecule referring to the standard hydrogen electrode (SHE): that is, $G(H^+ + e^-) = 1/2[G(H_2)]$ vs SHE.[4,56−58] Since the physiological environment presents pH conditions at around 7, the pH effect for the H$^+$/e$^-$ added steps on the free energy can be corrected as $\Delta G_{rxn} = \Delta G° + 2.303RT \times$ pH according to the Nernst equation, resulting in a factor of +9.55 kcal/mol at pH 7. All calculations were carried out through the facilities provided by the Gaussian09 package (revision D.01).[59]

Models used in the present study have been built on the basis of the X-ray crystallographic structure of the reduced [NiFe] hydrogenase from *Desulfovibrio vulgaris* str. "Miyazaki F" organism (PDB accession code 1H2R)[60] provided by Higuchi et al.[61]

With the aim of studying the effect of the ligands, two strategies have been followed. On the one hand, free, partially frozen, and totally frozen carbon atoms in the protein ligands have been imposed during optimizations.

On the other hand, the nonprotein CO and [CN]$^-$ ligands attached to the Fe moiety have been replaced by each other in the partially frozen model, while considering the possible influence by the interaction between the inorganic ligands and the surrounding amino acids through hydrogen bonding: Pro478, Leu482, Pro501, and Ser502 residues have been also

included in the model. This treatment can discern the key effect played by the ligands, according to their protein or nonprotein nature, showing in some cases important effects in the rate-determining steps of the dihydrogen production mechanism.

■ RESULTS AND DISCUSSION

Reaction Pathway: Spin Preference in the HER Mechanism. In order to understand how H$_2$ is produced on hydrogenases, different paths based on different multiplicity states have been studied (see Figure 1). For this purpose, our truncated model has been built from the X-ray structure of the reduced [NiFe] hydrogenase from *Desulfovibrio vulgaris*,[60,61] retaining the bimetallic [NiFe] active sites as well as the proximal functional groups around them. Finally, with the aim of retaining the enzymatic structure−reactivity pattern, the distal carbon atoms derived from the truncated cysteine residues have been frozen (indicated by asterisks in Figure 1).

In an overall view of the mechanism, while singlet and triplet states can be described for the **Ni-SI$_a$**, **Ni-R**, and **I2** steps, only doublet multiplicity can be seen for the **I1** and **Ni-C** structures, as a result of the odd number of electrons for these radical states. For the singlet and triplet states of **I2**, both the Ni-H$_2$ and Fe-H$_2$ states have been hypothesized as stable states. This is slightly different with respect to the results obtained by Bruschi et al.,[50] who described stable structures for **I2a** in both spin states and showed **I2b** as unstable with singlet multiplicity. Since their and our works are based on a quite similar level of theory (same BP86 functional), this divergence could be caused
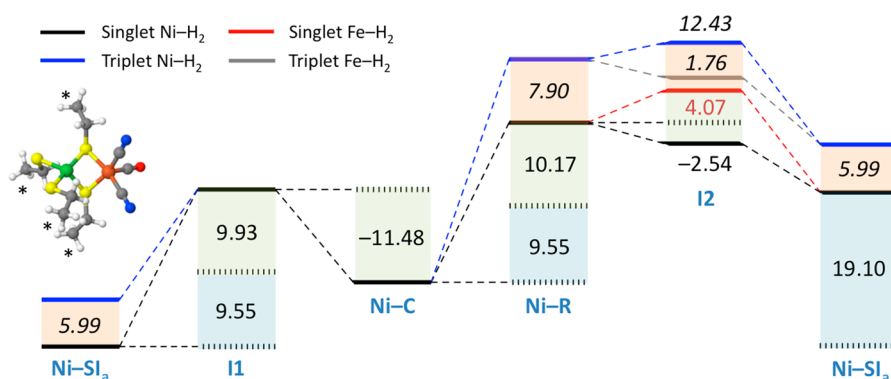
Figure 2. Gibbs free energy profile, in units of kcal/mol, for the HER path analyzing the spin effect. All energies are referred to that of the **Ni-SI$_a$** state. Energy differences between singlet and triplet states are shown in italics and highlighted in orange. Energy data under standard conditions ($f(H_2) = 101325$ Pa and pH 0), under which the H$^+$/e$^-$ injection can be approximated as $G(H^+ + e^-) = 1/2[G(H_2)]$ vs SHE, are presented in green. For the natural environment of hydrogenases (pH 7), pH corrections are also included in the energy profile, highlighted in blue.

by the size of the models; however, recent investigations carried out by us on a large model (similar to Bruschi's model: 180 atoms, including the subsequent protein cell around the active site) demonstrate similar results with respect to the different spin states at **I2**. This leads us to conclude that this divergence might be due to the different protein environment imposed by the kind of [NiFe] hydrogenases studied: in the case of Bruschi's work, *Allochromatium vinosum*; in our case, *Desulfovibrio vulgaris*. Nevertheless, the dihydrogen binding positions at Ni singlet and Fe triplet states are consistent with previous works.[29,50]

An analysis in detail of the mechanism indicates that the first H$^+$ gain is carried out on one of the sulfur atoms from the truncated cysteine residues directly linked to Ni (**I1**). An interatomic S—H distance equal to 1.36 Å is obtained at this computational level. The mechanism shown in Scheme 1 indicates that during this first step the electron injected goes to the Ni metal, modifying its charge state. The second step involves the H transferring from this position to become a bridging hydride shared on the NiFe bimetallic active site (**Ni-C**). It is hypothesized that, during this migration, H$^+$ becomes H:$^-$ by the acquisition of two electrons from Ni, modifying its charge state.[62] Interatomic distances between hydride and the metals are observed to be 1.60 and 1.70 Å for Ni and Fe, respectively. The aforementioned H$^+$/e$^-$ gain during the **I1** and **Ni-C** steps distorts the four-membered-ring structure: e.g., the S—Ni distance is elongated by approximately 0.02 and 0.09 Å, respectively. In addition, dihedral φ_{NiSSFe} angles experience distortions of around 2.1°.

Singlet multiplicity seems to be more stable for the totally reduced **Ni-SI$_a$** structure, i.e. without H adding at the beginning; this trend is also present for the subsequent third and fourth steps, in the **Ni-R** and **I2** structures. In other words, the minimum energy path for the HER mechanism followed by the active site in our [NiFe] hydrogenase model follows a singlet route (highlighted in light green in Figure 1). Previous work by Prabha et al. suggests that the singlet state demonstrated instability between the restricted and unrestricted DFT calculations; however, such a phenomenon could not be seen in this work.[63]

Thus, the **Ni-R** step represents the second H$^+$/e$^-$ gain taking place on the previously protonated S atom. Despite the S—H distance in the triplet state being smaller than that in the singlet (1.35 vs 1.37 Å), this difference seems to be insufficient to modify the singlet minimum energy path identified previously.

Impressively, the multiplicity state strongly affects the coordination environment of the hydride moiety. In the singlet state the proximal hydride—metal distance is to Ni (1.59 Å), and in the case of the triplet this is to Fe (1.64 Å). However, the sum of both Ni—H and Fe—H distances are larger in **Ni-R t** than in **Ni-R s** (**t** and **s** indicating triplet and singlet, respectively).

At this point, it deserves to be mentioned that the possible intermediate stable state between **Ni-R** and **I2**, in which the proton goes to Ni or Fe, has been also calculated.[50] Such a state has been confirmed by both BP86 and B3LYP functionals;[51,52,64] however, while the energy of this state is almost the same as that for the **I2** state (just representing minor structural reordering), it has therefore not been included in the energy profile.

Focusing on the singlet minimum energy path, the addition of both H$^+$/e$^-$ pairs to the reactive sulfur (**Ni-SI$_a$** to **I1** and **Ni-C** to **Ni-R**) practically does not affect the distance between this S and Ni but increases the distance between the nonreactive lower endocyclic sulfur atom and the metals; this is important as the reaction evolves. Increments of 0.09 and 0.23 Å can be seen, in each case. Notwithstanding this, the metal-containing ring is regenerated once the H$_2$ is produced and attached to the metals in the subsequent step (**I2**). In this last case, our DFT calculations corroborate the preference of H$_2$ to interact via the Ni moiety in a singlet state before its final release, as demonstrated by the closer metal—H$_2$ distances on average of 1.65 Å (**I2a s**) vs 1.82 Å (**I2a t**), 1.75 Å (**I2b s**), and 1.74 Å (**I2b t**).

Figure 2 describes the energy profile for the HER pathway at the SHE and under natural environment conditions followed by the active site in our [NiFe] hydrogenase model. As has been previously mentioned, triplet states are less stable than singlet states in all the cases in which both multiplicities can be described, but also the singlet reaction path has a lower energy demand for the thermodynamic rate-determining step than the triplet path. Focusing on the minimum energy path, two important characteristics can be highlighted. On the one hand, the addition of both H$^+$/e$^-$ pairs to the reactive sulfur atom (**Ni-SI$_a$** to **I1** and **Ni-C** to **Ni-R**) indicates positive Gibbs free reaction energies at 298.15 K (hereafter simply referred as reaction energy), and the second addition appears as the highest reaction energy of the whole process (19.48 vs 19.72 kcal/mol including the pH correction). On the other hand, the transfers toward the metal environment to produce the bridging
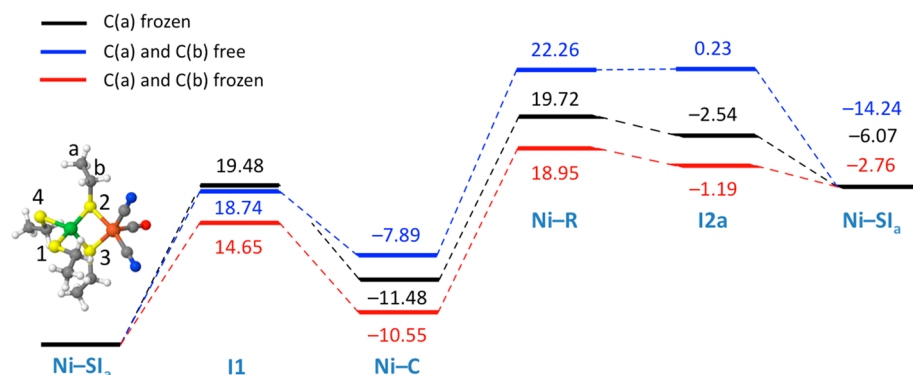
Figure 3. Energy profile, in units of kcal/mol, for the HER singlet pathway attending to three different models on the basis of carbon constraints. Relative energies are referred to the **Ni-SI$_a$** state, in which $\Delta G = 0$ kcal/mol. The pH corrections (pH 7) are also included in the energy profile for the natural environment of hydrogenases.

hydride and the sequestrated H$_2$ molecule at **Ni-C** and **I2**, respectively, are spontaneous processes. However, while for the first of these process 11.48 kcal/mol is released, in the second process the reaction energy only drops 2.54 kcal/mol. Our interpretation for such a reaction energy results is based on the idea that the second H$^+$/e$^-$ gain is more expensive than the first gain, because of the previous hydrogenation existing as a bridging hydride at **Ni-C**. We also suggest that this is the reason the second H transfer from the reactive sulfur to the bimetallic active site is less spontaneous than the first. In addition, the kinetic analysis suggests that the H$_2$ formation is more expensive than the proton to hydride formation. Besides, the activation energy for the **I1** to **Ni-C** step exhibits a barrier of 8.18 kcal/mol (**TS1**), while that for the **Ni-R** to **I2a** step is 12.96 kcal/mol (**TS2**), being smaller than the 19.72 kcal/mol required in the thermodynamic rate-determining step.

Finally, despite the fact that the molecular reactivity can often be explained through consideration of the highest occupied and lowest unoccupied molecular orbitals (HOMO and LUMO), the representation of such frontier orbitals in our case cannot fully explain the 2H$^+$ + 2e$^-$ → H$_2$ transformation route. Nevertheless, the LUMO in the **Ni-SI$_a$** and **Ni-C** states are partially localized on the reactive sulfur atom. In addition, a clearer LUMO is located on the metal environment at **I1**, with a percentage of almost 51%, which explains why the H is transferred into the Ni−H−Fe bridging position (see Figure S1 in the Supporting Information).

Role of the Cysteine Ligands on Ni. It is well-known that the reactivity displayed by enzymes is strongly related to their structure, including the protein environment, displacement/ substitution of inorganic ligands, or conformational fluctuations. Since the bimetallic active site involves exo- and endocyclic cysteines directly bound to it, imposition of structural constraints by freezing of the carbon skeleton can provide clear information about the structure−reactivity patterns.

In the previous section in which the role of multiplicity was explained, the distal carbon atom (C(a)) was frozen during optimization. Comparisons between this and a more constrained model, in which both carbons from the truncated cysteines skeleton are frozen (C(a) and C(b)), reveal that the reaction energy for the first hydrogenation gain, represented by the **Ni-SI$_a$** to **I1** step, decreases by 4.83 kcal/mol (see Figure 3).

This reaction energy diminution is in contrast with the minor structural differences shown between **Ni-SI$_a$** and **I1** in both models; however, an important variation in the stabilization of the LUMO energy explains this fact. In relative terms, the HOMO−LUMO gap decreases by 4.27 kcal/mol (see the Supporting Information) in the totally frozen model. This important observation is in accord with the DFT investigations recently published by Bruschi et al.,[50] who found a similar difference in the frontier orbital behavior when comparing several S−Ni−S geometrical angles for the reverse path of the H$_2$ binding (**I2a** in our model) on the active site of [NiFe] hydrogenases. While for the rest of the steps small structural changes can be seen, no remarkable differences in HOMO−LUMO energy gaps are found. Additionally, reaction energies slightly decrease by 0.77 kcal/mol when both models are compared.

The so-called free model, consisting of unconstrained truncated cysteine moieties during optimization, shows some differences worthy of mention. The first and most important one is on the first hydrogenation from **Ni-SI$_a$** to **I1**. Due to the free movement of the carbon skeleton of the cysteine ligands, $\varphi_{S2S1S3S4}$ dihedral angles vary from −47° in the partially frozen model to −37° in the unconstrained model at **Ni-SI$_a$**. In other words, the sulfur environment attached to Ni evolves from a seesaw conformation into a more planar configuration. Second, at **I1**, the (Ni)-SCH$_2$CH$_3$ ligands experience important rotational distortions, with A_{S1NiS2} and A_{S3NiS4} differences of 48 and 9°. For **Ni-SI$_a$**, A_{S1NiS2} has not experienced any important variation; however, A_{S3NiS4} differs by 23° between both models.

The HOMO−LUMO gap increases by 6.30 kcal/mol in comparison with the partially frozen model, which is larger than the gap disparity between the total and partially frozen models, suggesting a larger difference between the reaction energies. However, a similar reaction energy can be seen for such step, with deviations of merely 0.74 kcal/mol. According to the geometry distortion occurring in the free model, the small reaction energy difference is a result of the electron distribution and the geometric structure. Similarly, we can see an important energy difference when comparing the **I1** and **Ni-C** steps; however, the HOMO−LUMO gap and positions remain quite similar. This indicates that the distortion in the carbon skeleton conformation of the active site, which is caused by a different Ni coordination geometry in the different states, is another important reason for this energy difference in addition to the frontier orbitals. Additionally, for the final H$_2$ release step (**I2**), the HOMO−LUMO gap plays a minor role in comparison with the geometric distortion. On the other hand, the geometries of the protein−metal environment for the intermediate **Ni-C**, **Ni-**
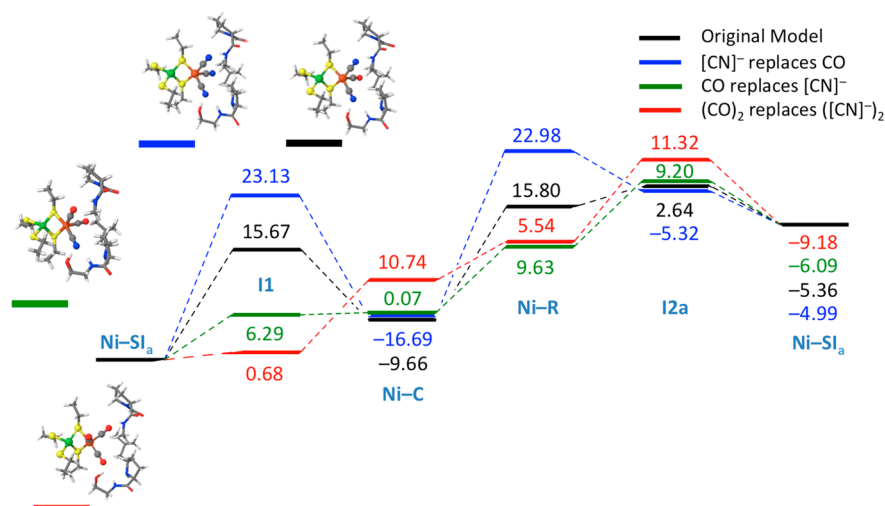
Figure 4. Gibbs free energy profile, in units of kcal/mol, for the HER singlet pathway by replacement of the inorganic ligands attached to Fe. Relative energies are referred to the **Ni-SI$_a$** state, in which $\Delta G = 0$ kcal/mol. The pH corrections (pH 7) are also included in the energy profile for the natural environment of hydrogenases.

R, and **I2** steps surprisingly exhibit high similarity with the constrained models (both one and two carbons frozen), which seems to be a consequence of the hydride/H$_2$ interacting with the metals.

Role of Inorganic Ligands on Fe. CO and [CN]$^-$ ligands have been detected on the active site bonded to the Fe center in both [NiFe] and [FeFe] hydrogenases.[8] Both the CO and [CN]$^-$ species are strong-field ligands that intensely affect the splitting of the d-like orbitals on the metal and therefore contribute to the stabilization of low oxidation states of Fe, indicating the significant role they might play in the catalytic cycle. Although they are very close in the spectrochemical series, they must have different effects on the active site. Previous work on [FeFe] hydrogenases has investigated the energy required for the CO and [CN]$^-$ redisposition and the electronic structure change for the [CN]$^-$ replacement by CO.[65,66] In our work, these two types of ligands have been replaced by each other in order to study their influence on the reaction pathway (see Figure 4). In addition, amino acids around the inorganic ligands are included in our calculation model, which lead to a slight difference in the energy profile, as the energies required for the two thermodynamic rate-determining H$^+$/e$^-$ added steps decrease by ~4 kcal/mol with respect to the initial model without the inclusion of the Pro478, Leu482, Pro501, and Ser502 residues (compare Figures 2 and 4). However, the trends of the profile remain similar. Therefore, the amino acids around could promote the HER, although those steps that presented spontaneous reaction energies are hypothesized to not be strongly affected by the amino acid environment.

The replacement of the two [CN]$^-$ ligands by two neutral CO ligands brings a remarkable change in trend to the reaction energy profile for the whole (highlighted in red at Figure 4). On the one hand, it reduces the energy difference for the first H$^+$/e$^-$ pair gain. While for the original model the energy input for the **Ni-SI$_a$** to **I1** step was 15.67 kcal/mol, the effect of these two CO replacements leads to an almost no-energy-required process with the injection of merely 0.68 kcal/mol. The frontier orbitals show that the HOMO−LUMO gap dramatically decreases by around 8.44 kcal/mol with respect to the original gap, which might be one of the reasons for the change in the

reaction energy. On the other hand, the proton seems to experience some difficulty in transferring toward the bridging position in the bimetallic environment (10.74 kcal/mol), which was spontaneous in the original model. In addition, the second H$^+$/e$^-$ pair injection to this "modified-on-Fe" active site newly displays a significant energy change of 5.54 kcal/mol vs the 15.80 kcal/mol demanded in the original model. The limiting thermodynamic step, located on the **Ni-R** species obtained in the original model, has varied. Notwithstanding, it is transferred to the sequestrated H$_2$ on Ni (**Ni-R** to **I2**) with a nonspontaneous reaction energy equal to 11.32 kcal/mol. In other words, while the two nonspontaneous H addition steps have become easier by the two [CN]$^-$ to two CO replacements, the bridging hydride formation and the production of H$_2$ to be captured on Ni become non-spontaneous and result in the severest reaction energy of the whole reaction.

In this sense, the substitution of just one CO for one of the [CN]$^-$ ligands (indicated in green at Figure 4) newly confirms that the first hydrogenation step (**Ni-SI$_a$** to **I1**) becomes less nonspontaneous with an energy requirement decreasing to 6.29 kcal/mol in comparison with the original model. Very smooth thermodynamics can be analyzed for the subsequent **I1** to **Ni-C** step, with a reaction energy as low as 0.07 kcal/mol. Then, similar to the energy drop for the first hydrogenation, the energy demand for the **Ni-C** to **Ni-R** step drops from 15.80 to 9.63 kcal/mol. Finally, the severest reaction energy is found for the dihydrogen intermediate formation, requiring 9.20 kcal/mol for this. In view of these results, it seems evident that the elimination of [CN]$^-$ moieties in favor of CO ligand substitution supposes dramatic changes for the thermodynamics of the HER catalyzed by [NiFe] hydrogenases. It is worth mentioning that not only the energy required for the thermodynamic rate-limiting step decreases but also this kind of replacement is spontaneous, with 12.95 kcal/mol released under vacuum conditions.

A completely different outcome appears when the only neutral CO ligand in the original model is substituted by another [CN]$^-$ (blue profile at Figure 4). The energy profile exhibits a similar trend with respect to the original model: i.e., H$^+$/e$^-$ injections on the reactive S atom (**Ni-SI$_a$** to **I1** and **Ni-C**

to **Ni-R**) are nonspontaneous, while the transfer of H to become a bridging hydride (**I1** to **Ni-C**) and the production of H$_2$ to be captured on Ni (**Ni-R** to **I2a**) are spontaneous processes. However, both the injection and release of energy show larger reaction energies in both senses: that is, nonspontaneous processes become more "expensive" in terms of energy (23.13 and 22.98 kcal/mol) and spontaneous processes release more energy than in the original model (−16.69 and −5.32 kcal/mol).

Concerning the redox states of Ni and Fe in the original model, the Mulliken spin densities for the **I1** state are 0.6382 and −0.0806, respectively. The substitution of two $[CN]^-$ with two CO leads to spin densities of 0.4766 and 0.0288, while for the case of substitution of just one $[CN]^-$ by one CO, they are 0.5651 and −0.0399. Finally, in the case in which one $[CN]^-$ replaces one CO ligand, such densities are 0.6155 and 0.0004. Hence, we can hypothesize that the metals remain as Ni(I) and Fe(II) after any substitution.

It is surprising to note how changes on the Fe environment produce a major influence on the catalytic path of $[NiFe]$ hydrogenases, despite the fact that Fe has a little-recognized role in comparison with Ni. The latter is the link between the active site and the protein environment through endocyclic cysteine residues, providing the electrons in the transformation of proton into hydride, where H$_2$ prefers to bind until its final release. As the $[CN]^-$ and CO ligands commonly exist in bioinspired catalysts,[67] therefore the replacement of each might be able to tune the energies for the H$^+$/e$^-$ added and the H$_2$ formation.

SUMMARY AND CONCLUSIONS

In summary, DFT investigations of the HER mechanism catalyzed by the active site of $[NiFe]$ hydrogenases indicate that the minimum energy path follows a singlet multiplicity route. The addition of the H$^+$ moieties on the reactive sulfur atom from one of the exocyclic cysteine residues are nonspontaneous processes in terms of the calculated Gibbs free reaction energies at room temperature. The **Ni-C** to **Ni-R** process exhibits the largest thermodynamic impediment of the whole reaction. In contrast, the proton migrations to become a bridging hydride (**I1** to **Ni-C**) and to produce H$_2$ to be captured on Ni (**Ni-R** to **I2a**) are spontaneous processes. We hypothesize that the second step is a less spontaneous step due to a previously existing bridging hydride, which obstructs the second transfer. Even concerning kinetics, the largest and limiting rate-determining step is hypothesized for the **Ni-C** to **Ni-R** step, with 19.72 kcal/mol energy required in a natural environment.

The protein ligand confinement appears to be important in the HER path followed by $[NiFe]$ hydrogenases. Our models, being constrained in different degrees, reveal that the protein environment, as it is in Nature, seems to be more efficient for the catalysis of H$_2$ production (and cleavage). Energy differences between the partially and totally frozen models exhibit a decrease of 4.83 and 0.77 kcal/mol for the **Ni-SI$_a$** to **I1** and **Ni-C** to **Ni-R** steps, respectively.

Remarkable differences can be seen when the inorganic ligands attached to Fe are replaced by each other. This replacement leads to dramatic changes in the reaction energies. While the presence of totally neutral CO ligands on Fe helps the H$^+$/e$^-$ injection and inhibits the H$^+$ to hydride and the H$_2$ sequestration on Ni steps, the removal of CO by another $[CN]^-$ ligand penalizes the classical **Ni-C** to **Ni-R** limiting step. Finally, these dramatic changes could serve as strategies for the design of novel catalysts based on bioinspired molecules for efficient H$_2$ production.

ASSOCIATED CONTENT

Ⓢ Supporting Information

The Supporting Information is available free of charge on the ACS Publications website at DOI: 10.1021/acscatal.6b01359.

Cartesian coordinates for the different structures in all models as well as HOMO/LUMO interpretations (PDF)

AUTHOR INFORMATION

Corresponding Authors

*D.R.M.: tel, ████ fax, ████ e-mail, ████

*C.S.: tel, ████ fax, ████ e-mail, ████

Notes

The authors declare no competing financial interest.

ACKNOWLEDGMENTS

REFERENCES

(1) Karl, T. R.; Trenberth, K. E. *Science* **2003**, *302*, 1719−1723.

(2) Betts, R. A.; Boucher, O.; Collins, M.; Cox, P. M.; Falloon, P. D.; Gedney, N.; Hemming, D. L.; Huntingford, C.; Jones, C. D.; Sexton, D. M. H.; Webb, M. J. *Nature* **2007**, *448*, 1037−1041.

(3) Meyer, J. *Nature* **2008**, *455*, 733−733.

(4) Nørskov, J. K.; Bligaard, T.; Logadottir, A.; Kitchin, J. R.; Chen, J. G.; Pandelov, S.; Stimming, U. *J. Electrochem. Soc.* **2005**, *152*, J23−J26.

(5) Wang, M.; Chen, L.; Sun, L. *Energy Environ. Sci.* **2012**, *5*, 6763−6778.

(6) Madden, C.; Vaughn, M. D.; Díez-Pérez, I.; Brown, K. A.; King, P. W.; Gust, D.; Moore, A. L.; Moore, T. A. *J. Am. Chem. Soc.* **2012**, *134*, 1577−1582.

(7) Vignais, P. M.; Billoud, B. *Chem. Rev.* **2007**, *107*, 4206−4272.

(8) Lubitz, W.; Ogata, H.; Rudiger, O.; Reijerse, E. *Chem. Rev.* **2014**, *114*, 4081−4148.

(9) Burgdorf, T.; Lenz, O.; Buhrke, T.; van der Linden, E.; Jones, A. K.; Albracht, S. P. J.; Friedrich, B. *J. Mol. Microbiol. Biotechnol.* **2006**, *10*, 181−196.

(10) Garcin, E.; Vernede, X.; Hatchikian, E. C.; Volbeda, A.; Frey, M.; Fontecilla-Camps, J. C. *Structure* **1999**, *7*, 557−566.

(11) Fontecilla-Camps, J. C.; Volbeda, A.; Cavazza, C.; Nicolet, Y. *Chem. Rev.* **2007**, *107*, 4273−4303.

(12) Rippers, Y.; Horch, M.; Hildebrandt, P.; Zebger, I.; Mroginski, M. A. *ChemPhysChem* **2012**, *13*, 3852−3856.

(13) Ogata, H.; Hirota, S.; Nakahara, A.; Komori, H.; Shibata, N.; Kato, T.; Kano, K.; Higuchi, Y. *Structure* **2005**, *13*, 1635−1642.

(14) Volbeda, A.; Martin, L.; Cavazza, C.; Matho, M.; Faber, B. W.; Roseboom, W.; Albracht, S. P.; Garcin, E.; Rousset, M.; Fontecilla-Camps, J. C. *JBIC, J. Biol. Inorg. Chem.* **2005**, *10*, 239−249.

(15) van Gastel, M.; Stein, M.; Brecht, M.; Schröder, O.; Lendzian, F.; Bittl, R.; Ogata, H.; Higuchi, Y.; Lubitz, W. *JBIC, J. Biol. Inorg. Chem.* **2006**, *11*, 41–51.

(16) Pardo, A.; De Lacey, A.; Fernández, V.; Fan, Y.; Hall, M. *JBIC, J. Biol. Inorg. Chem.* **2007**, *12*, 751–760.

(17) Siegbahn, P. E. M. *C. R. Chim.* **2007**, *10*, 766–774.

(18) Ogata, H.; Kellers, P.; Lubitz, W. *J. Mol. Biol.* **2010**, *402*, 428–444.

(19) Volbeda, A.; Martin, L.; Barbier, E.; Gutiérrez-Sanz, O.; De Lacey, A. L.; Liebgott, P.-P.; Dementin, S.; Rousset, M.; Fontecilla-Camps, J. C. *JBIC, J. Biol. Inorg. Chem.* **2015**, *20*, 11–22.

(20) Bleijlevens, B.; Faber, B.; Albracht, S. *JBIC, J. Biol. Inorg. Chem.* **2001**, *6*, 763–769.

(21) Fichtner, C.; Laurich, C.; Bothe, E.; Lubitz, W. *Biochemistry* **2006**, *45*, 9706–9716.

(22) De Lacey, A. L.; Fernández, V. M.; Rousset, M.; Cammack, R. *Chem. Rev.* **2007**, *107*, 4304–4330.

(23) Lubitz, W.; Reijerse, E.; van Gastel, M. *Chem. Rev.* **2007**, *107*, 4331–4365.

(24) Pandelia, M.-E.; Ogata, H.; Currell, L. J.; Flores, M.; Lubitz, W. *Biochim. Biophys. Acta, Bioenerg.* **2010**, *1797*, 304–313.

(25) Lill, S. O. N.; Siegbahn, P. E. M. *Biochemistry* **2009**, *48*, 1056–1066.

(26) Niu, S.; Thomson, L. M.; Hall, M. B. *J. Am. Chem. Soc.* **1999**, *121*, 4000–4007.

(27) Li, S.; Hall, M. B. *Inorg. Chem.* **2001**, *40*, 18–24.

(28) Foerster, S.; Stein, M.; Brecht, M.; Ogata, H.; Higuchi, Y.; Lubitz, W. *J. Am. Chem. Soc.* **2003**, *125*, 83–93.

(29) Foerster, S.; Gastel, M.; Brecht, M.; Lubitz, W. *JBIC, J. Biol. Inorg. Chem.* **2005**, *10*, 51–62.

(30) Wu, H.; Hall, M. B. *C. R. Chim.* **2008**, *11*, 790–804.

(31) Pandelia, M. E.; Infossi, P.; Stein, M.; Giudici-Orticoni, M. T.; Lubitz, W. *Chem. Commun.* **2012**, *48*, 823–825.

(32) Kampa, M.; Lubitz, W.; van Gastel, M.; Neese, F. *JBIC, J. Biol. Inorg. Chem.* **2012**, *17*, 1269–1281.

(33) Pardo, A.; De Lacey, A.; Fernández, V.; Fan, H.-J.; Fan, Y.; Hall, M. *JBIC, J. Biol. Inorg. Chem.* **2006**, *11*, 286–306.

(34) De Lacey, A. L.; Pardo, A.; Fernandez, V. M.; Dementin, S.; Adryanczyk-Perrier, G.; Hatchikian, E. C.; Rousset, M. *JBIC, J. Biol. Inorg. Chem.* **2004**, *9*, 636–642.

(35) Kramer, T.; Kampa, M.; Lubitz, W.; van Gastel, M.; Neese, F. *ChemBioChem* **2013**, *14*, 1898–1905.

(36) Ogata, H.; Nishikawa, K.; Lubitz, W. *Nature* **2015**, *520*, 571–574.

(37) Ogata, H.; Kramer, T.; Wang, H.; Schilter, D.; Pelmenschikov, V.; van Gastel, M.; Neese, F.; Rauchfuss, T. B.; Gee, L. B.; Scott, A. D.; Yoda, Y.; Tanaka, Y.; Lubitz, W.; Cramer, S. P. *Nat. Commun.* **2015**, *6*, 7890.

(38) Keith, J. M.; Hall, M. B. *Inorg. Chem.* **2010**, *49*, 6378–6380.

(39) Surerus, K. K.; Chen, M.; van der Zwaan, J. W.; Rusnak, F. M.; Kolk, M.; Duin, E. C.; Albracht, S. P. J.; Muenck, E. *Biochemistry* **1994**, *33*, 4980–4993.

(40) Volbeda, A.; Garcin, E.; Piras, C.; de Lacey, A. L.; Fernandez, V. M.; Hatchikian, E. C.; Frey, M.; Fontecilla-Camps, J. C. *J. Am. Chem. Soc.* **1996**, *118*, 12989–12996.

(41) De Lacey, A.; Stadler, C.; Fernandez, V.; Hatchikian, C.; Fan, H.-J.; Li, S.; Hall, M. *JBIC, J. Biol. Inorg. Chem.* **2002**, *7*, 318–326.

(42) Bleijlevens, B.; van Broekhuizen, F.; De Lacey, A.; Roseboom, W.; Fernandez, V.; Albracht, S. J. *JBIC, J. Biol. Inorg. Chem.* **2004**, *9*, 743–752.

(43) Bruschi, M.; Zampella, G.; Fantucci, P.; De Gioia, L. *Coord. Chem. Rev.* **2005**, *249*, 1620–1640.

(44) Schröder, O.; Bleijlevens, B.; de Jongh, T.; Chen, Z.; Li, T.; Fischer, J.; Förster, J.; Friedrich, C.; Bagley, K.; Albracht, S. J.; Lubitz, W. *JBIC, J. Biol. Inorg. Chem.* **2007**, *12*, 212–233.

(45) Wang, H.; Ralston, C. Y.; Patil, D. S.; Jones, R. M.; Gu, W.; Verhagen, M.; Adams, M.; Ge, P.; Riordan, C.; Marganian, C. A.; Mascharak, P.; Kovacs, J.; Miller, C. G.; Collins, T. J.; Brooker, S.; Croucher, P. D.; Wang, K.; Stiefel, E. I.; Cramer, S. P. *J. Am. Chem. Soc.* **2000**, *122*, 10544–10552.

(46) Wang, C. P.; Franco, R.; Moura, J. J.; Moura, I.; Day, E. P. *J. Biol. Chem.* **1992**, *267*, 7378–7380.

(47) Dole, F.; Fournel, A.; Magro, V.; Hatchikian, E. C.; Bertrand, P.; Guigliarelli, B. *Biochemistry* **1997**, *36*, 7847–7854.

(48) Siegbahn, P. E. M.; Tye, J. W.; Hall, M. B. *Chem. Rev.* **2007**, *107*, 4414–4435.

(49) Delcey, M. G.; Pierloot, K.; Phung, Q. M.; Vancoillie, S.; Lindh, R.; Ryde, U. *Phys. Chem. Chem. Phys.* **2014**, *16*, 7927–7938.

(50) Bruschi, M.; Tiberti, M.; Guerra, A.; De Gioia, L. *J. Am. Chem. Soc.* **2014**, *136*, 1803–1814.

(51) Perdew, J. P. *Phys. Rev. B: Condens. Matter Mater. Phys.* **1986**, *33*, 8822–8824.

(52) Becke, A. D. *Phys. Rev. A: At., Mol., Opt. Phys.* **1988**, *38*, 3098–3100.

(53) Weigend, F.; Ahlrichs, R. *Phys. Chem. Chem. Phys.* **2005**, *7*, 3297–3305.

(54) Kudin, K. N.; Scuseria, G. E.; Cancès, E. *J. Chem. Phys.* **2002**, *116*, 8255–8261.

(55) Grimme, S.; Antony, J.; Ehrlich, S.; Krieg, H. *J. Chem. Phys.* **2010**, *132*, 154104.

(56) Nørskov, J. K.; Rossmeisl, J.; Logadottir, A.; Lindqvist, L.; Kitchin, J. R.; Bligaard, T.; Jónsson, H. *J. Phys. Chem. B* **2004**, *108*, 17886–17892.

(57) Skulason, E.; Karlberg, G. S.; Rossmeisl, J.; Bligaard, T.; Greeley, J.; Jonsson, H.; Norskov, J. K. *Phys. Chem. Chem. Phys.* **2007**, *9*, 3241–3250.

(58) Rossmeisl, J.; Qu, Z. W.; Zhu, H.; Kroes, G. J.; Nørskov, J. K. *J. Electroanal. Chem.* **2007**, *607*, 83–89.

(59) Frisch, M. J.; Trucks, G. W.; Schlegel, H. B.; Scuseria, G. E.; Robb, M. A.; Cheeseman, J. R.; Scalmani, G.; Barone, V.; Mennucci, B.; Petersson, G. A.; Nakatsuji, H.; Caricato, M.; Li, X.; Hratchian, H. P.; Izmaylov, A. F.; Bloino, J.; Zheng, G.; Sonnenberg, J. L.; Hada, M.; Ehara, M.; Toyota, K.; Fukuda, R.; Hasegawa, J.; Ishida, M.; Nakajima, T.; Honda, Y.; Kitao, O.; Nakai, H.; Vreven, T.; Montgomery, J. A., Jr.; Peralta, J. E.; Ogliaro, F.; Bearpark, M.; Heyd, J. J.; Brothers, E.; Kudin, K. N.; Staroverov, V. N.; Kobayashi, R.; Normand, J.; Raghavachari, K.; Rendell, A.; Burant, J. C.; Iyengar, S. S.; Tomasi, J.; Cossi, M.; Rega, N.; Millam, N. J.; Klene, M.; Knox, J. E.; Cross, J. B.; Bakken, V.; Adamo, C.; Jaramillo, J.; Gomperts, R.; Stratmann, R. E.; Yazyev, O.; Austin, A. J.; Cammi, R.; Pomelli, C.; Ochterski, J. W.; Martin, R. L.; Morokuma, K.; Zakrzewski, V. G.; Voth, G. A.; Salvador, P.; Dannenberg, J. J.; Dapprich, S.; Daniels, A. D.; Farkas, Ö.; Foresman, J. B.; Ortiz, J. V.; Cioslowski, J.; Fox, D. J. *Gaussian09 (Revision D.01)*; Gaussian, Inc., Wallingford, CT, 2009.

(60) Protein Data Bank: http://www.rcsb.org.

(61) Higuchi, Y.; Ogata, H.; Miki, K.; Yasuoka, N.; Yagi, T. *Structure* **1999**, *7*, 549–556.

(62) Qiu, S.; Azofra, L. M.; MacFarlane, D. R.; Sun, C. *Phys. Chem. Chem. Phys.* **2016**, *18*, 15369–15374.

(63) Jayapal, P.; Robinson, D.; Sundararajan, M.; Hillier, I. H.; McDouall, J. J. W. *Phys. Chem. Chem. Phys.* **2008**, *10*, 1734–1738.

(64) Becke, A. D. *J. Chem. Phys.* **1993**, *98*, 5648–5652.

(65) Greco, C.; Bruschi, M.; Fantucci, P.; Ryde, U.; De Gioia, L. *Chem. - Eur. J.* **2011**, *17*, 1954–1965.

(66) Bruschi, M.; Greco, C.; Bertini, L.; Fantucci, P.; Ryde, U.; Gioia, L. D. *J. Am. Chem. Soc.* **2010**, *132*, 4992–4993.

(67) Felton, G. A. N.; Mebi, C. A.; Petro, B. J.; Vannucci, A. K.; Evans, D. H.; Glass, R. S.; Lichtenberger, D. L. *J. Organomet. Chem.* **2009**, *694*, 2681–2699.

Unraveling the Role of Ligands in the Hydrogen Evolution Mechanism Catalyzed by [NiFe] Hydrogenases
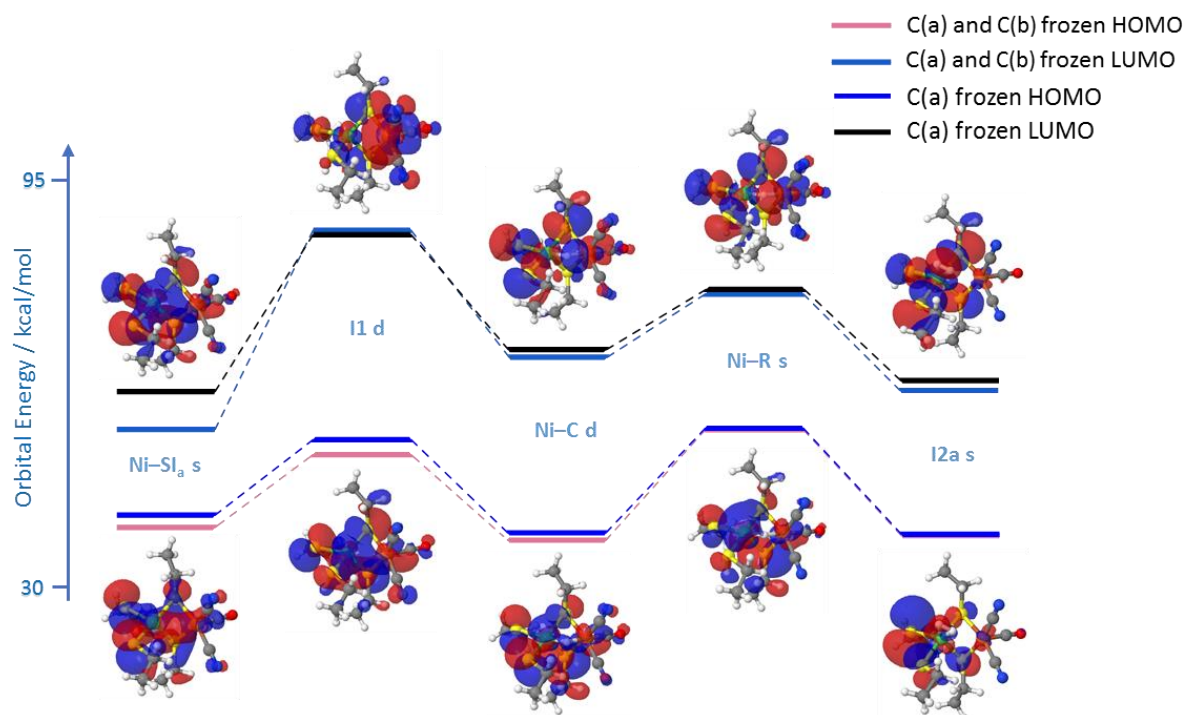

Fig. S1. HOMO and LUMO diagram for the partial and totally frozen models along the HER path. The HOMO and LUMO distributions of the totally frozen models are also shown.

CHAPTER 3

Hydrogen-bonding effect between active site and protein environment on catalysis performance in H2-producing [NiFe] hydrogenases

In this chapter, the effect of the protein environment around the active site on the HER process has been investigated by systematic DFT calculations with varying protein environments explicitly included. This chapter is a follow-up from chapter 2.

The work was published in Physical Chemistry Chemical Physics 'Hydrogen-bonding effect between active site and protein environment on catalysis performance in H2-producing [NiFe] hydrogenases' (*Phys. Chem. Chem. Phys.*, 2018, **20**, 6735—6743).

By

Siyao Qiu, Luis Miguel Azofra, Douglas R. MacFarlane, Chenghua Sun.

The studies on the protein environment found that:

1. The existence of the amino acids around the active site in [NiFe] hydrogenases can reduce the energy required for the H^+/e^- injection steps (**Ni-SIa** to **I1** and **Ni-C** to **Ni-R**), and therefore improve the HER performance.

2. The main contribution of the energy reduction for the two H^+/e^- injection steps comes from the amino acids which have hydrogen-bonding interactions to the active site.

3. The hydrogen bonding between the amino acids and the active site facilitate the HER through charge transfer from the active site to the amino acids via the H-bonds, and a less negative active site is beneficial for the H^+/e^- gain.

Check for updates

Hydrogen bonding effect between active site and protein environment on catalysis performance in H₂-producing [NiFe] hydrogenases†

Siyao Qiu,[a] Luis Miguel Azofra, [ID] [ab] Douglas R. MacFarlane [ID] *[ab] and Chenghua Sun [ID] *[c]

The interaction between the active site and the surrounding protein environment plays a fundamental role in the hydrogen evolution reaction (HER) in [NiFe] hydrogenases. Our density functional theory (DFT) findings demonstrate that the reaction Gibbs free energy required for the rate determining step decreases by 7.1 kcal mol⁻¹ when the surrounding protein environment is taken into account, which is chiefly due to free energy decreases for the two H⁺/e⁻ addition steps (the so-called **Ni-SI$_a$** to **I1**, and **Ni-C** to **Ni-R**), being the largest thermodynamic impediments of the whole reaction. The variety of hydrogen bonds (H-bonds) between the amino acids and the active site is hypothesised to be the main reason for such stability: H-bonds not only work as electrostatic attractive forces that influence the charge redistribution, but more importantly, they act as an electron 'pull' taking electrons from the active site towards the amino acids. Moreover, the electron 'pull' effect through H-bonds *via* the S⁻ in cysteine residues shows a larger influence on the energy profile than that *via* the CN⁻ ligands on Fe.

Introduction

Like many enzymes, hydrogenases, catalysing the reversible hydrogen evolution reaction (HER), exhibit remarkable catalytic properties including low over-potentials and high turnover frequencies.[1–3] Moreover, they typically only contain earth-abundant metals, and may represent an alternative to the expensive noble-metal catalysts, *e.g.*, Pt,[4,5] for large-scale production. A variety of bio-inspired catalysts have been synthesised in previous works in order to mimic the active site of hydrogenases.[6] However, none of the molecular catalysts show performance as impressive as that of the enzyme, making the function of the protein environment around the active site an intriguing and important question.

[NiFe] hydrogenases are one type of hydrogenase enzyme (the others are [FeFe] and [Fe] types).[7,8] However, only bimetallic [NiFe] and [FeFe] hydrogenases catalyse the reversible hydrogen

splitting reaction into protons plus electrons, while the [Fe] hydrogenases merely activate the H₂ under the presence of the substrate methenyltetrahydromet-hanopterin;[9] additionally, [NiFe] hydrogenases show better oxygen tolerance than [FeFe] hydrogenases.[10–12] Against this background, the study of bimetallic [NiFe] hydrogenases is of crucial importance, not only to understand and delve into the question of 'why Nature works in that way', but also to obtain evidence of the specific mechanisms of enzyme activity.

A similar atomic constitution of the active site of [NiFe] hydrogenases can be found, regardless of the source of the enzyme. It consists of a bimetallic four-membered ring linking the Ni and Fe metals with two S atoms;[12,13] the latter are part of cysteine residues from the protein environment. The exocyclic ligands of Ni are another two cysteine residues (*via* their S atoms), while those of Fe are inorganic ligands: two CN⁻ and one CO.[12] In this context, the configuration of the three diatomic inorganic ligands has been studied by computational calculations for the three possible structural conformations. The "best fitted" structure is then derived by comparing such calculations with the experimental Fourier transform infrared (FTIR) spectroscopy measurements of the vibrations of the three diatomic ligands.[14,15]
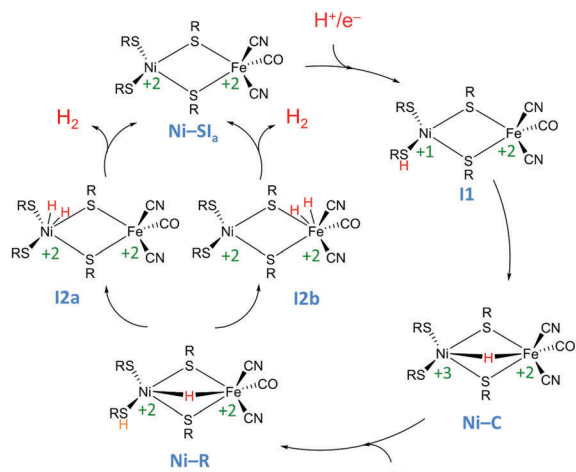
The reversible hydrogen oxidation reaction takes place under an abundant dihydrogen (H₂) atmosphere, where hydrogenases stay in their active states. Hydrogenases become inactive under aerobic environments.[13–18] There are three

[a] School of Chemistry, Faculty of Science, Monash University, Clayton, VIC 3800, Australia. E-mail: Douglas.MacFarlane@monash.edu; Fax: +61 3 9905 4597; Tel: +61 3 9902 9916

[b] ARC Centre of Excellence for Electromaterials Science (ACES), School of Chemistry, Faculty of Science, Monash University, Clayton, VIC 3800, Australia

[c] Department of Chemistry and Biotechnology, Swinburne University of Technology, Hawthorn, VIC 3122, Australia. E-mail: chenghuasun@swin.edu.au

This journal is © the Owner Societies 2018

31

Phys. Chem. Chem. Phys., 2018, **20**, 6735–6743 | 6735

Scheme 1 Hydrogen evolution reaction (HER) path followed by [NiFe] hydrogenases.

active states that have been detected by FTIR and electron paramagnetic resonance (EPR) spectroscopies: the **Ni-SI$_a$**, **Ni-C**, and **Ni-R** states.[18–22] Thus, the reaction cycle shown in Scheme 1, for the specific case of the HER, could be obtained.[23–25] **Ni-SI$_a$**, being the most oxidised active state of the reaction path, has no hydrogen atom bound to the active site.[27,28] The redox states of the Ni and Fe ions are Ni(II) and Fe(II).[26–28] In addition, based on Mössbauer spectroscopy, the redox state of Fe remains unchanged along the entire reaction path.[21,29]

In the **Ni-C** state, a hydride is inserted into the four-membered ring after the first H$^+$/e$^-$ gain, bridging between the Ni and Fe ions.[30–32] Correspondingly, the redox state of the Ni becomes Ni(III). An intermediate state, **I1**, is hypothesised to exist between **Ni-SI$_a$** and **Ni-C**,[25] and it has a proton bound to one of the exocyclic S atoms and an electron added to the Ni centre, leading to a reduced form, Ni(I).[28] Although the so-called 'Ni-L' state has been detected in *E. coli* [NiFe] hydrogenases in the dark, **Ni-L** is only observed under illumination in most other hydrogenases. Therefore, the **I1** state in this scheme is not directly related to **Ni-L**. Our recently published conceptual DFT results on the **I1** to **Ni-C** stage suggest that the forming of the bridging hydride is performed as a non-synchronous two-electron transfer process, which is driven by a decrease in the electronic potential as well as by an important decrease in the electrophilicity index of the Ni.[33] After the second H$^+$/e$^-$ adding, the active site evolves to the **Ni-R** state.[34–36] In this state, the proton will be added to the aforementioned exocyclic S atom, and the electron will be delivered to the Ni atom, returning it to the Ni(II) redox state. The X-ray crystallographic study on the **Ni-R** state in [NiFe] hydrogenases suggests that Cys546 is the site of protonation.[36] Afterwards, the proton and the hydride tend to move to one of the metal ions, thus forming a H$_2$ molecule, suggesting a second intermediate state known as **I2**, which is therefore postulated to exist between **Ni-R** and **Ni-SI$_a$**, closing the reaction cycle. Two possible binding positions for the H$_2$ molecule have been proposed by Wu *et al.*,

corresponding to the so-called **I2a** (H$_2$ binds on Ni) and **I2b** (on Fe), respectively.[37,38] From our previous work on the energy profile of [NiFe] hydrogenases, Ni binding is thermodynamically more favourable than binding to Fe, and the singlet path is preferred over the triplet path.[39]

Though the active site is widely accepted as the origin of enzymatic activity for HER catalysed by [NiFe] hydrogenases, it is well known that the protein matrix plays a key role in the reaction pathway: it transmits the reactants and products throughout the entire reaction, acting as the product channel and the electron/proton pathways; it also tunes the behaviour of the active site.[40–44] Previous work concluded that the protein environment can constrain the geometry of the active site, and consequently affect the reaction.[45] Also, the protein presents a cage effect, that is, the protein around the active site works as a cage to prevent the proton from diffusing away.[46]

Although the protein environment can directly affect the catalysis performance of enzymes, the electrostatic effect of the protein on the active site, and its influence on the reaction, is not yet clearly understood.[47] Previous QM/MM calculations suggest that the protein surrounding the active site affects the energy profile.[48–50] Given that most hydrogenases show almost no over-potential in HER processes,[51,52] further understanding of the effects of the amino acids on the active site could help explain why bio-inspired molecular catalysts rarely achieve the low over-potentials of hydrogenases. It is worth pointing out that the protein has been proposed to act as an electrostatic field, and various electrostatic models have been theoretically studied for decades; these models have been divided by Warshel *et al.* into macroscopic, simplified dipolar, and microscopic all-atom models.[53] Of these, macroscopic models in which the protein is described as a continuum low dielectric medium have been most commonly used.[54,55] However, there is no universal dielectric constant for different protein models. Therefore a microscopic model, containing detailed information about the hydrogenase enzyme, is needed. However, microscopic all-atom models require extensive computational resources. Hence, in the present paper, the electrostatic effect of the protein environment has been studied using a model that contains the active site and the first amino acid shell, focusing on the interaction between the amino acid shell and the active site.[31,36] Also, different types of amino acids have been separately studied to understand their different influences on the catalytic performance of the enzyme in the HER.[31]

Computational details

Calculations of the geometries of the HER pathway followed by [NiFe] hydrogenase enzymes have been conducted by means of density functional theory (DFT) using the BP86 functional.[56,57] Two effective core potential basis sets, Def2TZVPP and Def2SVP, have been applied for all models: Def2TZVPP was used for the active site (including the metals and sulphurs, and three inorganic ligands on the Fe ion), and the smaller Def2SVP for the remaining

6736 | *Phys. Chem. Chem. Phys.*, 2018, **20**, 6735–6743

32

This journal is © the Owner Societies 2018

atoms.[58] The choice of the functional and basis sets is supported by the previous calculations.[28,35,59] The EDIIS/CDIIS procedure has been applied for the self-consistent field (SCF) in all cases.[60] Also, to obtain the free energy and confirm the nature of the stationary points, frequency calculations have been done for all the models. According to the previous paper, considering same atoms are kept frozen during each step and a relatively large model is applied for the calculation, the vibrational frequencies of the frozen atoms are nearly unaffected by the reaction change at the active site, and therefore they could be neglected when calculating the free energy difference between the consecutive steps.[61] Grimme's D3 damping function has been used for the correction of the dispersion interaction for all models in the geometry optimisation.[62] The Synchronous Transit-Guided Quasi-Newton (STQN) method (QST3) has been applied for the location of the transition states (TS).[63]

In all cases, free energies under mild conditions of temperature (T = 298.15 K) include vibrational zero-point energy (ZPE) corrections. For the H^+/e^- pair adding steps, the chemical potential of the H^+/e^- pair has been calculated as half the chemical potential of H_2, under a standard atmosphere and at pH = 0, i.e., at computational hydrogen electrode (CHE) conditions[64–66] [see eqn (1)].

$$\mu(H^+ + e^-) = \frac{1}{2}\mu(H_2) \qquad (1)$$

However, since enzymes work at pH ∼ 7, pH corrections have been carried out, with a value of +9.55 kcal mol^{-1}, based on the Nernst equation [see eqn (2)] as:

$$\Delta G_{rxn} = \Delta G_0 + 2.303\,RT\,pH \qquad (2)$$

For calculations under solvent conditions, the polarizable continuum model (PCM) was applied in this work with different dielectric constants representing pentylamine (ε = 4.20), water (ε = 78.36), and n-methyl-formamide mixture (ε = 181.56) solvents.[67] Also, the PCM correction with pentylamine solvent has been used for the large model calculations, as pentylamine has a static and optical dielectric constant of 4.2 and 2.1, which is similar to the protein environment.[68]

All energy calculations were carried out using the Gaussian09 package (revision D.01).[69] Also, natural bond orbital (NBO) analysis (performed at the same computational level with the NBO 6.0 program)[70] and the atom in molecules (AIM) method (via the AIMALL program)[71] were used to calculate the orbital and electron density parameters for the H-bonds, respectively.

The initial calculation models were built based on the X-ray crystallographic data provided by Higuchi et al. for the reduced [NiFe] hydrogenase from Desulfovibrio vulgaris str. 'Miyazaki F' organism (PDB accession code 1H2R).[72] The model under study in this work includes the active site and the first amino acid shell around it. For comparative purposes in elucidating the protein-environment effect, a model containing only the active site, as studied in one of our recent publications,[39] is also presented and discussed. To distinguish the two models, the one just including the active site is labelled 'Small', while that which also includes the first amino acid shell is named 'Large'.
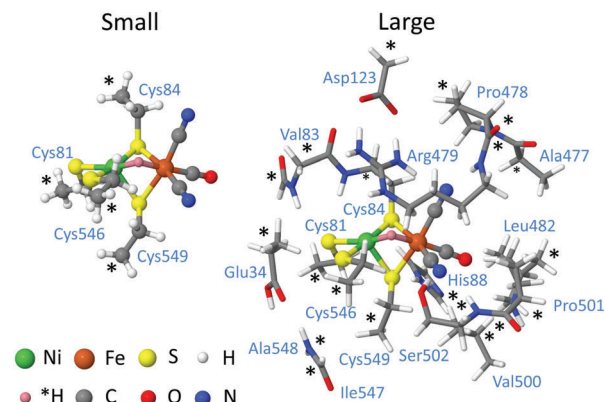

Fig. 1 The 'Small' (left) and 'Large' (right) models (**Ni-SI$_a$** structure) studied in the present work. Asterisks (*) refer to atoms frozen to keep the same structure–reactivity pattern as that in the [NiFe] hydrogenase enzyme from Desulfovibrio vulgaris.

Particular atoms in the models have been fixed during optimization and frequency calculation for imitating the omitted protein matrix. The motion of the frozen atoms is hypothesised to be mostly constrained with the omitted protein matrix existence, therefore the imaginary frequencies coming from the frozen atoms should not be considered during the frequency calculation.[23,32,37,73]

The so-called 'Small' model comprises the four directly ligated Cys81, Cys84, Cys546, and Cys549 residues (40 atoms for the **Ni-SI$_a$** state), while the named 'Large' model comprises the 'Small' model plus the truncated Glu34, Val83, His88, Asp123, Ala477, Pro478, Arg479, Leu482, Val500, Pro501, Ser502, Ala548 and Ile547 residues extracted from the X-ray structure of the [NiFe] hydrogenase from Desulfovibrio vulgaris str. 'Miyazaki F' organism (180 atoms for the **Ni-SI$_a$** state), shown in Fig. 1.[32,72] All these amino acids are neutral, with the exception of Asp123 and Arg479, which are negatively and positively charged, respectively. Due to instabilities in the positively charged His88 during optimisation (the proton on His88 delivers to Cys549), His88 is not protonated in the Large model. Therefore, although Glu34 is negatively charged at pH = 7, it has been modified to be neutral in the Large model so as to retain the same total charge, '−2', as in the Small model.[32] Singlet (**Ni-SI$_a$**, **Ni-C**, and **Ni-R**) and doublet (**I1** and **I2**) multiplicities are studied in this work, supported by our previous calculations.[39]

Results and discussion

Previously, Torrent et al. proposed that the amino acid environment helps tune the geometry of the active site.[45] Recently, Bruschi and co-workers proposed that such geometry tuning improves the H_2 cleavage reaction on the active site of [NiFe] hydrogenases.[27] However, our previous study of the active site of [NiFe] hydrogenases found obvious differences in the energy profiles obtained with and without interaction of amino acids with CN^- ligands at the active site, although the geometries were almost the same.[39] Clearly, as well as constraining the

geometry of active sites, amino acids have additional effects on the reaction. To understand the amino acid effect on the active site of [NiFe] hydrogenases, the so-called Small and Large models have been theoretically studied and compared in the present work. Through detailed comparison of the structural and energy aspects of the HER obtained with the Small and Large models, we will clarify how different types of amino acids (charged, hydrophobic, polar, and H-bonding) affect the catalysis at the active sites. As shown below, charge redistribution through electrostatic interactions and direct electron transfer between the core and the protein surroundings are key effects.

3.1 Catalytic performance

We start with calculations of the five stable states of the HER cycle; the optimised geometries were presented in ref. 39 for the Small model and are in Fig. 2 for the Large model. Initially, the **Ni-SI$_a$** state has no hydrogen atom bound to the active site. The first H$^+$/e$^-$ addition yields the **I1** state, with the proton binding to one of the exocyclic S atoms of the Cys546 residue and the electron going to Ni, modifying its charge state from Ni(II) to Ni(I). Then, the proton and two electrons at the active site will experience a transfer to the bridging position between Ni and Fe (**Ni-C**). It is worth mentioning that the Ni–H distances in both models (1.60 and 1.61 for Small and Large) are close to what has been measured experimentally (1.63 A),[74] indicating that the amino acids around the active site do not have significant influence on the geometry of the active site. After that, the second H$^+$/e$^-$ is added (**Ni-R**) and goes to the same S atom from the Cys546 residue to subsequently form H$_2$ on the
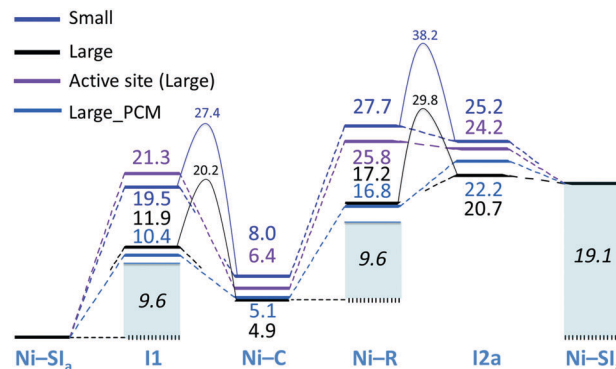
Fig. 3 Reaction Gibbs free energies (kcal mol^{-1}) for the HER in the Small (blue) and Large (black) models of [NiFe] hydrogenase. For comparative purposes, the energy profile for the model just containing the active site of the Large model without the amino acids is indicated in lilac. pH corrections for enzymatic conditions (pH = 7) are highlighted in light blue.

Ni atom (**I2a**) followed by its release to return the original enzyme (**Ni-SI$_a$**).

Upon examining the reaction Gibbs free energy results gathered in Fig. 3, the two profiles corresponding to the Small and Large models exhibit important differences. Firstly, the explicit treatment of the protein environment through the Large model suggests far better performance in catalysing the HER. In the Small case, the reaction energies required for the first and second H$^+$/e$^-$ addition steps (**Ni-SI$_a$** to **I1**, and **Ni-C** to **Ni-R**) are 19.5 and 19.7 kcal mol^{-1}, respectively, giving these steps the largest thermodynamic impediments of the reaction cycle. The other three steps are exergonic, especially **I1** to **Ni-C**, where the proton transfers to the bridging position to form a hydride, with a corresponding energy release of 11.5 kcal mol^{-1}. The transition state searches for the **I1** to **Ni-C** and **Ni-R** to **I2a** state found that the activation energies for the two processes are 7.9 and 10.5 kcal mol^{-1}, respectively. However, the Large model tells a slightly different story, in which the energies required for the two H$^+$/e$^-$ additions notably decrease to 11.9 and 12.3 kcal mol^{-1}; this must be related to the amino acids facilitating the proton attachment to S. Thus, the thermodynamic impediment drops by up to 7.5 kcal mol^{-1} with the surrounding amino acids. The proton transfer (**I1** to **Ni-C**) and the H$_2$ release (**I2a** to **Ni-R**) steps remain exergonic, while the H$_2$ forming step (**Ni-R** to **I2a**) becomes endergonic, with an energy requirement of 3.5 kcal mol^{-1}. Moreover, the energy release decreases, with an energy change of −7.0 kcal mol^{-1} associated with the proton transfer (**I1** to **Ni-C**). This also suggests a smaller energy requirement for the reverse dihydrogen oxidation reaction (H$_2$ cleavage) compared with −11.5 kcal mol^{-1} in the Small model. The activation energies for the **I1** to **Ni-C** and **Ni-R** to **I2a** steps of the Large model are 8.3 and 12.6 kcal mol^{-1}. Thus, the rate-determining step switches from the **Ni-C** to **Ni-R** step in the Small model to the **Ni-R** to **I2a** step in the Large model for HER. The transition state geometries are not shown in Fig. 2, while the geometry coordinates could be found in the ESI.† Also, the energy for the rate-determining step has decreased by 7.1 kcal mol^{-1} when taking into account the amino acid
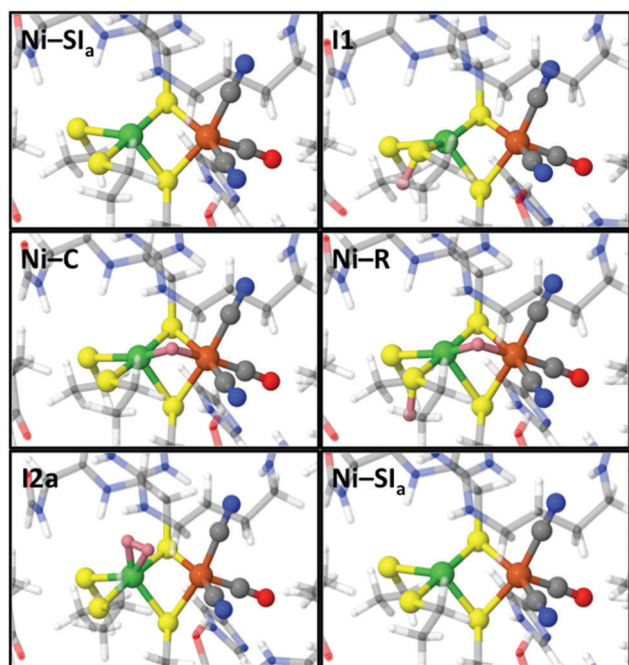

Fig. 2 Structures corresponding to the minimum energy path (singlet multiplicity) for the HER in the Large model of [NiFe] hydrogenase. Reactive H atoms are highlighted in pink.

environment, which is mainly due to the obvious decrease of the H^+/e^- injection step. Assuming that the rest of the protein around the first amino acid shell acts as a solvent with a dielectric constant around 4, such a protein environment slightly changes the energy profile (see Large_PCM profile in Fig. 3).

To further support our hypothesis that the amino acid environment does more than simply stabilise the active-site geometry, a Small model that retains the geometry of the active site in the Large model, [named as Active Site (Large) in Fig. 3] has been also calculated. Results clearly indicate that although the geometry of the active site is retained as it was modelled in the Large model, the energy profile is closer to that of the original Small model than it is to the Large one. This is further evidence that the protein environment affects the reaction occurring at the active site.

From the Mulliken spin analysis on the five active states, the spin of Ni in the **I1** and **Ni-C** states is 0.5884 and 0.4835 in the Small model, and the spin of Fe is 0.0005 and 0.0399. Also, no spin has been found in the **Ni-SI$_a$**, **Ni-R** and **I2a** states in unrestricted BP86 calculations. Thus, the spin changes agree with the charge changes for different states, as suggested in Scheme 1.

3.2 Unravelling the role of amino acids

To better understand the reasons for such energy profile changes, the amino acids in the first amino-acid shell around the active site were divided into 'Charged', 'Hydrophobic', 'Polar', and 'H-bonding' species (see Fig. 4). We then compared these with the Active Site (Large) and Large models to understand which factors have the most effect on transforming the former into the latter. While keeping the geometries of the amino acids and the active site in the Large model, the free energy profiles of the four models were calculated, and they are shown in Fig. 4. We see that charged and hydrophobic amino acids have little influence on the active site. The profile associated with the Charged model (active site plus Asp123 and Arg479 residues) shows a similar trend to that of the Active Site one, with an energy difference of less than 1.9 kcal mol^{-1} (**Ni-SI$_a$** to **I1**) between the two models for each step. As for the Hydrophobic model, it is even more similar to the Active Site profile.

In contrast, the polar amino acids have a far more significant impact on the energy, the Polar model being within 1.4 kcal mol^{-1} of the Large model at all steps. However, in the H-bonding model, which comprises six selected polar amino-acid fragments that also form hydrogen bonds (H-bonds) with the active site, a similar energy profile to that of the Polar model was seen (Fig. 4). The remaining three polar amino acids were also calculated with the active site, but its energy profile almost overlaps with the Active Site (Large) profile (see Fig. S1, ESI†). This clearly implies that hydrogen bonding between the amino acids and the active site is the most important effect of the amino acid environment, especially in reducing the energy needed for the two H^+/e^- addition steps. In this regard, we hypothesise that H-bonds might change the charge distribution, withdrawing charge from the active site to the protein environment, and thus facilitating the two H^+/e^- additions.

3.3 H-Bonds and electrostatic effects

The H-bonds between the amino acids and the active site have been confirmed by calculations of the electron densities using
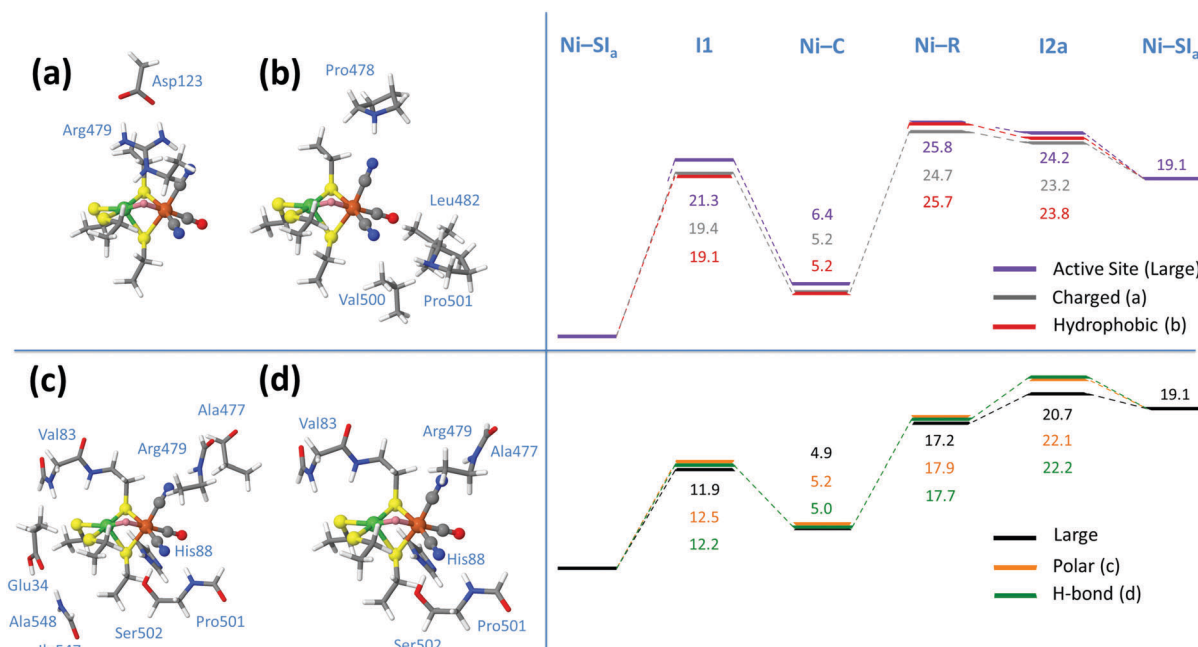

Fig. 4 [NiFe] hydrogenase models (**I1** structures) containing the active site and the: (a) charged; (b) hydrophobic; (c) polar; and (d) H-bonding amino acids. Reaction Gibbs free energy comparisons (in kcal mol^{-1}) between these models and the Active Site (Large) and Large models. The models have been separated vertically into two groups for clarity, note that the energy profiles on the top and bottom have the same initial and final state; a plot of the energy profiles on a common scale is presented in Fig. S7 (ESI†).

the AIM approach. As indicated in Fig. S3 in the ESI,† three main types of H-bonds can be highlighted as the most important non-covalent interactions between the amino-acid shell and the active site: O···H, N···H, and S···H types. O···H acts as the connection between Asp123 and Arg479. Of the other two types of H-bonds, those in which acidic H from the amino acids interacts with the CN^- inorganic ligands on Fe are stronger interactions. Electron densities and corresponding Laplacians of these two types at the bond critical points (BCP) are both approximately reciprocal with the bonding distance (see Fig. S2, ESI†), while under the same distance conditions, the H-bonds *via* sulphur show stronger bonding with the amino acids than those *via* CN^-.

Among the stronger H-bonds found, each CN^- ligand presents two interactions with the protein environment; that with the side-chain of Ser502 shows the strongest interaction of this kind, as indicated by the shortest bonding distance (1.70 Å). The electron densities of the critical points between Ser502 and the active site are around 0.05 a.u., while the rest of the H-bonds between the amino acids and the active site are about 0.02 a.u. According to previous studies on H-bonds, the electron densities that range from 0.02 to 0.05 a.u. belong to the moderate H-bonds.[75–77]

To test the hypothesis that the protein might work through electrostatic attraction to redistribute the charge at the active site, polarizable continuum model (PCM) calculations on the Small model were performed, because the PCM can mimic an electrostatic field around the active site. Under the water solvent conditions, the two H^+/e^- additions were significantly promoted (19.5 and 19.7 in vacuum *vs.* 15.3 and 16.6 kcal mol^{-1} with solvent) while the H_2 forming step was not (-2.5 *vs.* 2.3 kcal mol^{-1}) in terms of the Gibbs free energy (see Fig. S3, ESI†). The natural bond orbital (NBO) analysis on the Small vacuum and PCM models shows an average of about 0.1 e charge difference on the atoms at the active site. Because the PCM works mainly as an electrostatic field, and the calculation yields similar changes in energy to those produced by including the amino-acid environment, it seems as though the main mechanism through which the protein environment affects the energy profiles is *via* changing the charge distribution at the active site. However, such electrostatically induced charge redistribution is not the only reason for the energy change, because when a larger dielectric constant solvent mimicking a higher electrostatic field, like *n*-methyl formamide mixture ($\varepsilon = 181.5$), is applied with the Small model, the energy profile is almost identical to that obtained with the implicit water solvent (see Fig. S3, ESI†). Therefore, it is hypothesised that the charge extraction of electrons by the amino acids from the active site through the H-bonds is of more significance than the effects of pure electrostatic attraction.

NBO calculations were performed for the Small and Large models along the reaction cycle. The charge sums of the active core site (including the two metals, binding hydrogens, the three inorganic ligands and the four sulphur atoms) in the Small model are -1.5509, -1.5586, -1.5463, -1.5443, and -1.5283 e for the **Ni-SI$_a$**, **I1**, **Ni-C**, **Ni-R**, and **I2a** states,

respectively; while in the Large case they are -1.4578, -1.4476, -1.4449, -1.4112, and -1.4218 e. Therefore, a less negative total charge of the active site is produced when the amino acids are included in the calculation; this agrees with the idea that the protein environment acts as an electron 'pull' in [NiFe] hydrogenases. The same trend is observed when comparing the active site including the four cysteine carbon skeletons, in which the total charge is -2 in the Small model, and around -1.5 in the Large model. Also, the charge change between **Ni-SI$_a$** and **I1** is less negative in the Large model (-0.0077 e in Small *vs.* 0.0102 e in Large), as is that for the **Ni-C** to **Ni-R** steps (0.0020 e in Small *vs.* 0.0337 e in Large). From the free energy calculation on the different states of the active site with '-1' and '-3' total charge, the charge switches from '-2' to '-1' are exergonic, while the change from '-2' to '-3' is endergonic (see Table S1, ESI†). Therefore, the less negative charge change is hypothesised to be energetically favourable. The protein environment therefore not only works as an electron 'pull', but also as an electron 'bank' – 'depositing' or 'withdrawing' electrons when needed.

To further support this hypothesis, the Small model with '-1' total charge has been modelled, as shown in Fig. 5. The energy required for the two H^+/e^- additions dramatically decreases from 19.5 and 19.7 kcal mol^{-1} to 5.1 and 5.2 kcal mol^{-1}. Although removing one electron from the active site facilitates the H^+/e^- addition, such a change will impede the transfer of the proton to the hydride and, especially, the forming of the H_2; this H_2 formation then becomes the largest thermodynamic impediment in the reaction cycle, with an energy requirement of 13.2 kcal mol^{-1}. The Mulliken spin densities of the Ni and Fe centres are 0.3588 and 0.0426 in the **Ni-SI$_a$** state, respectively, indicating the redox states of Ni and Fe are +3 and +2 in **Ni-SI$_a$**.

It seems that the energy profile trends for the Small model with -1 total charge follow those of the Large model—removing an electron facilitates H^+/e^- additions but impedes H_2 formation. This may imply that the charge extracted by the protein environment may be optimised to balance the competing effects on H^+/e^- additions and H_2 formation. The fractional charge change of the active site was related to the energy for the first H^+/e^- adding using facilities provided by the Vienna *Ab-Initio* Simulation Package (VASP)[78–81] to reveal that the
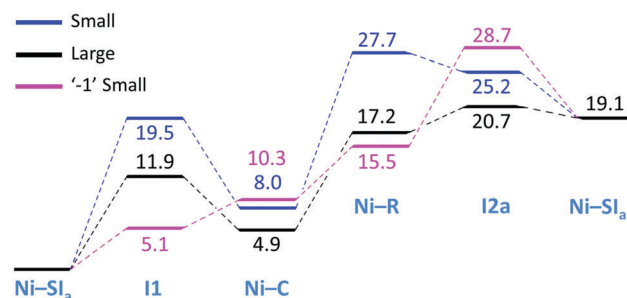

Fig. 5 Gibbs free energy profile (kcal mol^{-1}) for the Small, Large, and -1 Small models.

6740 | *Phys. Chem. Chem. Phys.*, 2018, **20**, 6735–6743

36

This journal is © the Owner Societies 2018

energy changes steadily from endergonic to exergonic regimes as the charge changes from −2 to −1 (see Fig. S4, ESI†), reinforcing our previous idea. This result is also reflected in the analysis of the molecular orbital changes (see Fig. S5, ESI†). Thus, the highest occupied molecular orbital (HOMO) energy in the Large model at the **Ni-SI$_a$** state is about 34 kcal mol^{-1} higher than in the −1 Small model, and 56 kcal mol^{-1} lower than in the classical Small model. In the case of the lowest unoccupied molecular orbital (LUMO), its energy in the Large model is between those of the −1 Small and the classical Small models. It is worth mentioning that the difference in the HOMO–LUMO gap in each state between Large and Small models is much smaller than with the Small −1 model, with an average of 2 vs. 74 kcal mol^{-1}. This could be explained by the very similar locations of the HOMO and LUMO in the Large and Small models. Thus, the protein environment could decrease the energy of the electronic orbitals but will not change the electronic configuration of the orbitals.

The effects of the charge on the active site on the H$^+$/e$^-$ addition can be separated into effects on proton addition and the effects on electron injection. The proton addition under '−1' and '−2' charge conditions has been studied by means of the energy profile for the proton approaching the binding sulphur (see Fig. S6, ESI†). The profile demonstrates that the energy changes induced by the charge variation are less than the 14.4 kcal mol^{-1} energy change found for the first H$^+$/e$^-$ addition; therefore, the change in charge of the active site has a more significant effect on electron injection, that is, the valence state change from Ni(II) to Ni(I), than it does on proton addition.

Calculations on models including the H-bonding amino acids with CN$^-$ or S$^-$ ligands have also been done (see Fig. S1, ESI†). Although a slightly stronger bond is seen between the CN$^-$ ligands and active site than between the active site and the S$^-$ ligands, the hydrogen bonding via S$^-$ atoms is more effective at promoting the two H$^+$/e$^-$ additions (15.4 vs. 15.8 and 15.8 vs. 17.8 kcal mol^{-1}), suggesting that withdrawing some electron density from the S$^-$ atom has a deeper influence on the HER. The S$^-$ ligands are directly bound to the Ni centre, while the CN$^-$ ligands bind to Fe. This could be interpreted as indicating that the ligand environment of Ni is more important for the H$^+$/e$^-$ addition than that of Fe, which agrees with our observation that the redox state of Ni clearly affects the H$^+$/e$^-$ addition.

Conclusions

In summary, the protein environment can dramatically affect the energy profile in [NiFe] hydrogenases via hydrogen bonding. This conclusion comes from the energy profile comparison between the so-called 'Small' (only including the active site) and the 'Large' models, the latter comprising the active site and the first neighbouring amino acid shell. The rate-determining step in the Large model decreases by 7.1 kcal mol^{-1} compared with the Small model, which is mainly due to the free energy decrease of the thermodynamic impeditive steps in the Large

model, being the two H$^+$/e$^-$ addition steps (**Ni-SI$_a$** to **I1**, and **Ni-C** to **Ni-R**), which drop dramatically to 11.9 and 12.3 kcal mol^{-1} in the amino acid environment. By dividing the amino acids into several models, we found that strong hydrogen bonding between the polar amino acids and the active site shows the most significant influence on the energy profile, yielding an energy profile very similar to that of the Large model. Therefore, hydrogen bonding between the active site and the amino acids is the main reason for the energy profile change. Further calculations reveal that geometric distortions caused by the protein environment are not the main reason for the energy profile changes seen in this work. Instead, charge redistribution has been identified as the key reason for the energy profile change.

Charge redistribution could occur because of electrostatic attraction associated with strong H-bonds. PCM calculations reveal that the electrostatic effect has a similar effect to that of the protein environment, reducing the free energies of the two H$^+$/e$^-$ adding steps and inhibiting H$_2$ formation. However, even with an extraordinarily high dielectric constant, we still could not mimic the energy change that comes from the protein environment, suggesting that the electrostatic effect is not the only reason for the charge redistribution.

Another mechanism for charge redistribution is direct charge transfer between the active site and the environment. In contrast with the pure electrostatic interaction, this case results in a net change of charge states for the active site; specifically, the active site in the Large model is less negative than in the Small one. It is proposed that the protein environment may act as an electron 'pull', taking the electron from the active site through hydrogen bonding and leading to a different charge distribution. Using the Small model with the '−1' charge state as a test, it was found that the two H$^+$/e$^-$ adding steps became less endergonic, with energy requirements of 5.1 and 5.2 kcal mol^{-1}, while the H$_2$-forming step became endergonic, with a free energy of 13.2 kcal mol^{-1}. Both results agree with the energy profile changes caused by the protein environment. Therefore, we assume that besides the electrostatic effect, amino acids play a key role through H-bonds in moving the electron outwards from the active site to improve the energy profile.

Conflicts of interest

There are no conflicts to declare.

Acknowledgements

This journal is © the Owner Societies 2018

37

Phys. Chem. Chem. Phys., 2018, **20**, 6735–6743 | **6741**

Notes and references

1 A. Volbeda, M.-H. Charon, C. Piras, E. C. Hatchikian, M. Frey and J. C. Fontecilla-Camps, *Nature*, 1995, **373**, 580–587.

2 A. Volbeda, E. Garcin, C. Piras, A. L. de Lacey, V. M. Fernandez, E. C. Hatchikian, M. Frey and J. C. Fontecilla-Camps, *J. Am. Chem. Soc.*, 1996, **118**, 12989–12996.

3 F. Dole, A. Fournel, V. Magro, E. C. Hatchikian, P. Bertrand and B. Guigliarelli, *Biochemistry*, 1997, **36**, 7847–7854.

4 B. E. Conway and B. V. Tilak, *Electrochim. Acta*, 2002, **47**, 3571–3594.

5 J. K. Nørskov, T. Bligaard, A. Logadottir, J. R. Kitchin, J. G. Chen, S. Pandelov and U. Stimming, *J. Electrochem. Soc.*, 2005, **152**, J23–J26.

6 G. A. N. Felton, C. A. Mebi, B. J. Petro, A. K. Vannucci, D. H. Evans, R. S. Glass and D. L. Lichtenberger, *J. Organomet. Chem.*, 2009, **694**, 2681–2699.

7 P. M. Vignais and B. Billoud, *Chem. Rev.*, 2007, **107**, 4206–4272.

8 W. Lubitz, H. Ogata, O. Rudiger and E. Reijerse, *Chem. Rev.*, 2014, **114**, 4081–4148.

9 S. V. Hexter, F. Grey, T. Happe, V. Climent and F. A. Armstrong, *Proc. Natl. Acad. Sci. U. S. A.*, 2012, **109**, 11516–11521.

10 T. Burgdorf, O. Lenz, T. Buhrke, E. van der Linden, A. K. Jones, S. P. J. Albracht and B. Friedrich, *J. Mol. Microbiol. Biotechnol.*, 2005, **10**, 181–196.

11 C. Tard and C. J. Pickett, *Chem. Rev.*, 2009, **109**, 2245–2274.

12 J. C. Fontecilla-Camps, A. Volbeda, C. Cavazza and Y. Nicolet, *Chem. Rev.*, 2007, **107**, 4273–4303.

13 H. Ogata, S. Hirota, A. Nakahara, H. Komori, N. Shibata, T. Kato, K. Kano and Y. Higuchi, *Structure*, 2005, **13**, 1635–1642.

14 A. Volbeda, L. Martin, C. Cavazza, M. Matho, B. W. Faber, W. Roseboom, S. P. Albracht, E. Garcin, M. Rousset and J. C. Fontecilla-Camps, *J. Biol. Inorg. Chem.*, 2005, **10**, 239–249.

15 M. van Gastel, M. Stein, M. Brecht, O. Schröder, F. Lendzian, R. Bittl, H. Ogata, Y. Higuchi and W. Lubitz, *J. Biol. Inorg. Chem.*, 2006, **11**, 41–51.

16 A. L. De Lacey, V. M. Fernández, M. Rousset and R. Cammack, *Chem. Rev.*, 2007, **107**, 4304–4330.

17 A. Pardo, A. De Lacey, V. Fernández, Y. Fan and M. Hall, *J. Biol. Inorg. Chem.*, 2007, **12**, 751.

18 P. E. M. Siegbahn, *C. R. Chim.*, 2007, **10**, 766–774.

19 B. Bleijlevens, B. Faber and S. Albracht, *J. Biol. Inorg. Chem.*, 2001, **6**, 763–769.

20 C. Fichtner, C. Laurich, E. Bothe and W. Lubitz, *Biochemistry*, 2006, **45**, 9706–9716.

21 W. Lubitz, E. Reijerse and M. van Gastel, *Chem. Rev.*, 2007, **107**, 4331–4365.

22 M.-E. Pandelia, H. Ogata, L. J. Currell, M. Flores and W. Lubitz, *Biochim. Biophys. Acta*, 2010, **1797**, 304–313.

23 P. E. M. Siegbahn, *Adv. Inorg. Chem.*, 2004, **56**, 101–125.

24 M. Bruschi, G. Zampella, P. Fantucci and L. De Gioia, *Coord. Chem. Rev.*, 2005, **249**, 1620–1640.

25 P. E. M. Siegbahn, J. W. Tye and M. B. Hall, *Chem. Rev.*, 2007, **107**, 4414–4435.

26 H. Wang, C. Y. Ralston, D. S. Patil, R. M. Jones, W. Gu, M. Verhagen, M. Adams, P. Ge, C. Riordan, C. A. Marganian, P. Mascharak, J. Kovacs, C. G. Miller, T. J. Collins, S. Brooker, P. D. Croucher, K. Wang, E. I. Stiefel and S. P. Cramer, *J. Am. Chem. Soc.*, 2000, **122**, 10544–10552.

27 A. Pardo, A. De Lacey, V. Fernández, H.-J. Fan, Y. Fan and M. Hall, *J. Biol. Inorg. Chem.*, 2006, **11**, 286–306.

28 M. Bruschi, M. Tiberti, A. Guerra and L. De Gioia, *J. Am. Chem. Soc.*, 2014, **136**, 1803–1814.

29 K. K. Surerus, M. Chen, J. W. van der Zwaan, F. M. Rusnak, M. Kolk, E. C. Duin, S. P. J. Albracht and E. Muenck, *Biochemistry*, 1994, **33**, 4980–4993.

30 M. Stein and W. Lubitz, *Phys. Chem. Chem. Phys.*, 2001, **3**, 5115–5120.

31 S. Foerster, M. Gastel, M. Brecht and W. Lubitz, *J. Biol. Inorg. Chem.*, 2005, **10**, 51–62.

32 M. Kampa, W. Lubitz, M. van Gastel and F. Neese, *J. Biol. Inorg. Chem.*, 2012, **17**, 1269–1281.

33 S. Qiu, L. M. Azofra, D. R. MacFarlane and C. Sun, *Phys. Chem. Chem. Phys.*, 2016, **18**, 15369–15374.

34 A. L. De Lacey, A. Pardo, V. M. Fernandez, S. Dementin, G. Adryanczyk-Perrier, E. C. Hatchikian and M. Rousset, *J. Biol. Inorg. Chem.*, 2004, **9**, 636–642.

35 T. Kramer, M. Kampa, W. Lubitz, M. van Gastel and F. Neese, *ChemBioChem*, 2013, **14**, 1898–1905.

36 H. Ogata, K. Nishikawa and W. Lubitz, *Nature*, 2015, **520**, 571–574.

37 H. Wu and M. B. Hall, *C. R. Chim.*, 2008, **11**, 790–804.

38 J. M. Keith and M. B. Hall, *Inorg. Chem.*, 2010, **49**, 6378–6380.

39 S. Qiu, L. M. Azofra, D. R. MacFarlane and C. Sun, *ACS Catal.*, 2016, **6**, 5541–5548.

40 X. Li, L. W. Chung, P. Paneth and K. Morokuma, *J. Am. Chem. Soc.*, 2009, **131**, 5115–5125.

41 Y. Higuchi, H. Ogata, K. Miki, N. Yasuoka and T. Yagi, *Structure*, 1999, **7**, 549–556.

42 I. Fdez. Galván, A. Volbeda, J. C. Fontecilla-Camps and M. J. Field, *Proteins: Struct., Funct., Bioinf.*, 2008, **73**, 195–203.

43 I. Sumner and G. A. Voth, *J. Phys. Chem. B*, 2012, **116**, 2917–2926.

44 M. McCullagh and G. A. Voth, *J. Phys. Chem. B*, 2013, **117**, 4062–4071.

45 M. Torrent, T. Vreven, D. G. Musaev, K. Morokuma, Ö. Far-kas and H. B. Schlegel, *J. Am. Chem. Soc.*, 2002, **124**, 192–193.

6742 | *Phys. Chem. Chem. Phys.*, 2018, **20**, 6735–6743

38

This journal is © the Owner Societies 2018

46 O. Gutiérrez-Sanz, M. C. Marques, C. S. A. Baltazar, V. M. Fer-nández, C. M. Soares, I. A. C. Pereira and A. L. De Lacey, *J. Biol. Inorg. Chem.*, 2013, **18**, 419–427.

47 D. M. A. Smith, S. Raugei and T. C. Squier, *Phys. Chem. Chem. Phys.*, 2014, **16**, 24026–24033.

48 M. Torrent, T. Vreven, D. G. Musaev, K. Morokuma, O. Farkas and H. B. Schlegel, *J. Am. Chem. Soc.*, 2002, **124**, 192–193.

49 L. Tian and R. A. Friesner, *J. Chem. Theory Comput.*, 2009, **5**, 1421–1431.

50 R. Prabhakar, T. Vreven, M. J. Frisch, K. Morokuma and D. G. Musaev, *J. Phys. Chem. B*, 2006, **110**, 13608–13613.

51 H. S. Shafaat, O. Rüdiger, H. Ogata and W. Lubitz, *Biochim. Biophys. Acta*, 2013, **1827**, 986–1002.

52 P. Rodriguez-Maciá, A. Dutta, W. Lubitz, W. J. Shaw and O. Rüdiger, *Angew. Chem., Int. Ed.*, 2015, **54**, 12303–12307.

53 A. Warshel, P. K. Sharma, M. Kato and W. W. Parson, *Biochim. Biophys. Acta, Proteins Proteomics*, 2006, **1764**, 1647–1786.

54 A. J. Russell, P. G. Thomas and A. R. Fersht, *J. Mol. Biol.*, 1987, **193**, 803–813.

55 L. Li, C. Li, Z. Zhang and E. Alexov, *J. Chem. Theory Comput.*, 2013, **9**, 2126–2136.

56 J. P. Perdew, *Phys. Rev. B: Condens. Matter Mater. Phys.*, 1986, **33**, 8822–8824.

57 A. D. Becke, *Phys. Rev. A: At., Mol., Opt. Phys.*, 1988, **38**, 3098–3100.

58 F. Weigend and R. Ahlrichs, *Phys. Chem. Chem. Phys.*, 2005, **7**, 3297–3305.

59 M. G. Delcey, K. Pierloot, Q. M. Phung, S. Vancoillie, R. Lindhac and U. Ryde, *Phys. Chem. Chem. Phys.*, 2014, **16**, 7927–7938.

60 K. N. Kudin, G. E. Scuseria and E. Cancès, *J. Chem. Phys.*, 2002, **116**, 8255–8261.

61 A. Kubas, C. Orain, D. De Sancho, L. Saujet, M. Sensi, C. Gauquelin, I. Meynial-Salles, P. Soucaille, H. Bottin, C. Baffert, V. Fourmond, R. B. Best, J. Blumberger and C. Léger, *Nat. Chem.*, 2017, **9**, 88–95.

62 S. Grimme, J. Antony, S. Ehrlich and H. Krieg, *J. Chem. Phys.*, 2010, **132**, 154104.

63 C. Peng, P. Y. Ayala, H. B. Schlegel and M. J. Frisch, *J. Comput. Chem.*, 1996, **17**, 49–56.

64 J. K. Nørskov, J. Rossmeisl, A. Logadottir, L. Lindqvist, J. R. Kitchin, T. Bligaard and H. Jónsson, *J. Phys. Chem. B*, 2004, **108**, 17886–17892.

65 J. Rossmeisl, Z. W. Qu, H. Zhu, G. J. Kroes and J. K. Nørskov, *J. Electroanal. Chem.*, 2007, **607**, 83–89.

66 E. Skulason, G. S. Karlberg, J. Rossmeisl, T. Bligaard, J. Greeley, H. Jonsson and J. K. Norskov, *Phys. Chem. Chem. Phys.*, 2007, **9**, 3241–3250.

67 G. Scalmani and M. J. Frisch, *J. Chem. Phys.*, 2010, **132**, 114110.

68 L. I. Krishtalik, A. M. Kuznetsov and E. L. Mertz, *Protein*, 1997, **28**, 174.

69 M. J. Frisch, G. W. Trucks, H. B. Schlegel, G. E. Scuseria, M. A. Robb, J. R. Cheeseman, G. Scalmani, V. Barone, B. Mennucci, G. A. Petersson, H. Nakatsuji, M. Caricato, X. Li, H. P. Hratchian, A. F. Izmaylov, J. Bloino, G. Zheng, J. L. Sonnenberg, M. Hada, M. Ehara, K. Toyota, R. Fukuda, J. Hasegawa, M. Ishida, T. Nakajima, Y. Honda, O. Kitao, H. Nakai, T. Vreven, J. A. Montgomery Jr., J. E. Peralta, F. Ogliaro, M. Bearpark, J. J. Heyd, E. Brothers, K. N. Kudin, V. N. Staroverov, R. Kobayashi, J. Normand, K. Raghavachari, A. Rendell, J. C. Burant, S. S. Iyengar, J. Tomasi, M. Cossi, N. Rega, N. J. Millam, M. Klene, J. E. Knox, J. B. Cross, V. Bakken, C. Adamo, J. Jaramillo, R. Gomperts, R. E. Stratmann, O. Yazyev, A. J. Austin, R. Cammi, C. Pomelli, J. W. Ochterski, R. L. Martin, K. Morokuma, V. G. Zakrzewski, G. A. Voth, P. Salvador, J. J. Dannenberg, S. Dapprich, A. D. Daniels, Ö. Farkas, J. B. Foresman, J. V. Ortiz, J. Cioslowski and D. J. Fox, *Gaussian09 (revision D.01)*, Gaussian, Inc., Wallingford CT, 2009.

70 E. D. Glendening, J. K. Badenhoop, A. E. Reed, J. E. Carpenter, J. A. Bohmann, C. M. Morales, C. R. Landis and F. Weinhold, *NBO6.0, Theoretical Chemistry Institute*, University of Wisconsin, Madison, USA, 2013.

71 AIMAll, 14.11.23, TK Gristmill Software, Overland Park KS, USA, 2014.

72 Protein Data Bank, http://www.rcsb.org.

73 J. W. Ochterski, *Thermochemistry in Gaussian*, Gaussian, Inc., Wallingford, CT, 2000, pp. 1–19.

74 M. Brecht, M. van Gastel, T. Buhrke, B. Friedrich and W. Lubitz, *J. Am. Chem. Soc.*, 2003, **125**, 13075–13083.

75 R. Parthasarathi, V. Subramanian and N. Sathyamurthy, *J. Phys. Chem. A*, 2006, **110**, 3349.

76 H. M. Lee, A. Kumar, M. Kolaski, D. Y. Kim, E. C. Lee, S. K. Min, M. Park, Y. C. Choi and K. S. Kim, *Phys. Chem. Chem. Phys.*, 2010, **12**, 6278–6287.

77 C. Pak, H. M. Lee, J. C. Kim, D. Kim and K. S. Kim, *Struct. Chem.*, 2005, **16**, 187–202.

78 G. Kresse and J. Hafner, *Phys. Rev. B: Condens. Matter Mater. Phys.*, 1993, **47**, 558–561.

79 G. Kresse and J. Hafner, *Phys. Rev. B: Condens. Matter Mater. Phys.*, 1994, **49**, 14251–14269.

80 G. Kresse and J. Furthmüller, *Comput. Mater. Sci.*, 1996, **6**, 15–50.

81 G. Kresse and J. Furthmüller, *Phys. Rev. B: Condens. Matter Mater. Phys.*, 1996, **54**, 11169–11186.

Hydrogen-bonding effect between active site and protein environment on catalysis performance in H2-producing [NiFe] hydrogenases

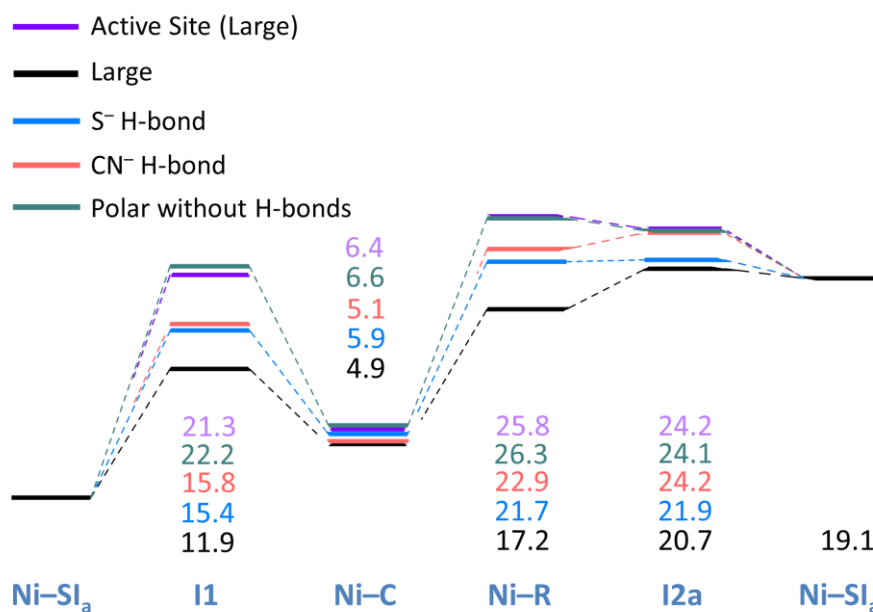## H-BONDING ENERGY PROFILES FOR CN⁻ AND S⁻ LIGANDS

Fig. S1. Gibbs free energy profile, in units of kcal/mol, for the HER referring to different protein environment models. Relative energies referred to the **Ni-SI$_a$** state, in which $\Delta G = 0$ kcal/mol. The pH corrections (pH = 7) are also included in the energy profile for the natural environment of hydrogenases.
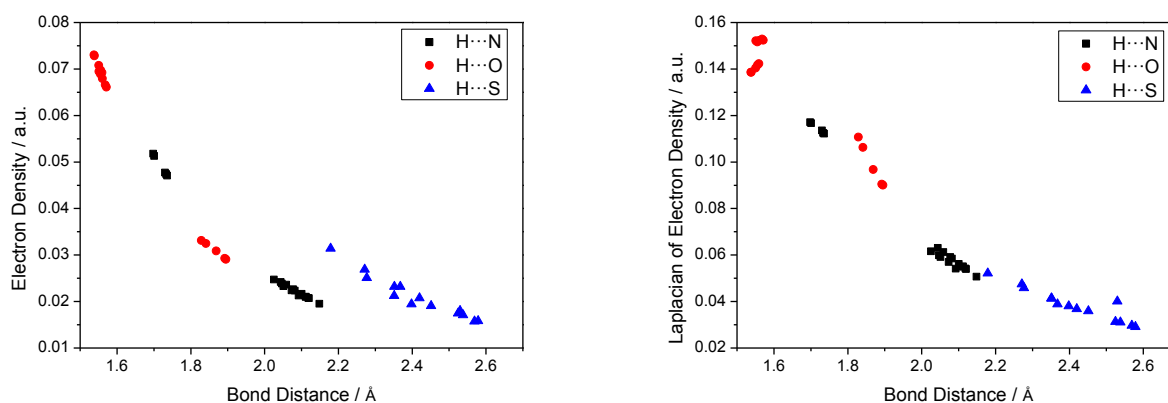
ELECTRONIC DENSITY ANALYSIS

Fig. S2. Electron densities and Laplacian, in a.u., of electron density of the H–N, H–O, and H–S hydrogen bonds *vs.* bond distances, in Å, in the different reaction states of [NiFe] hydrogenases.
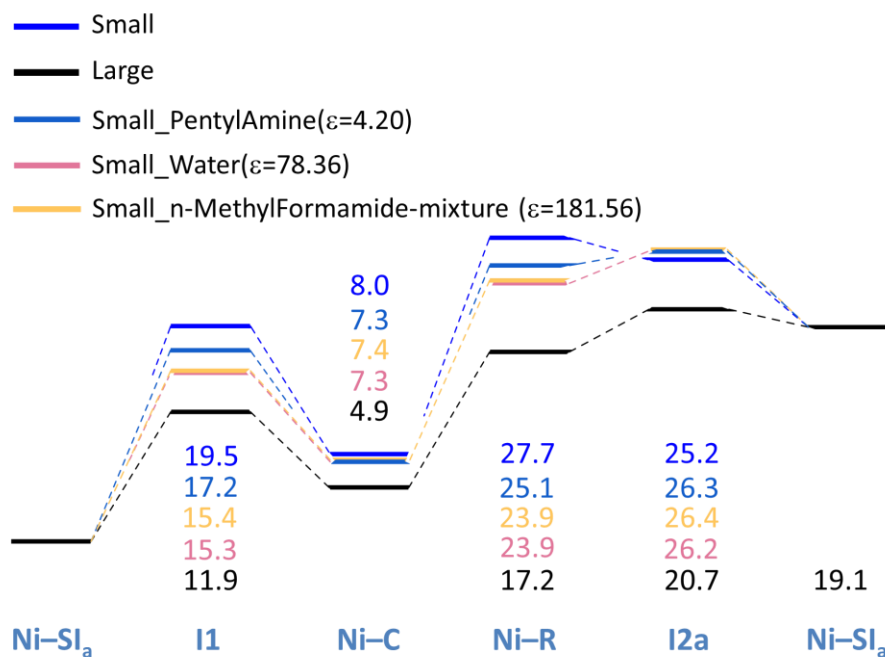
PCM CALCULATIONS

Fig. S3. Gibbs free energy profile, in units of kcal/mol, for the HER attending to different solvent effects through the Polarizable Continuum Model (PCM) in the so-called 'Small' model. Relative energies referred to the **Ni-SI$_a$** state, which ΔG = 0 kcal/mol. The pH corrections (pH = 7) are also included in the energy profile for the natural environment of hydrogenases.
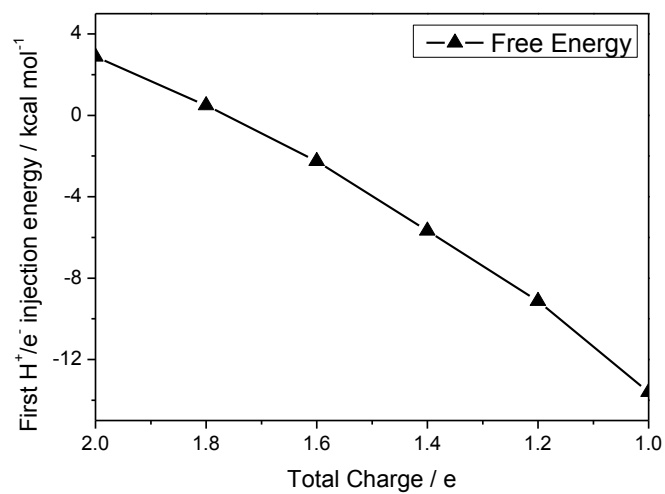
FRACTIONAL CHARGE CALCULATIONS

Fig. S4. First H^+/e^- injection free energy change, in units of kcal/mol, *vs*. the fractional charge changes, in e, on the active site conducted by VASP calculations.
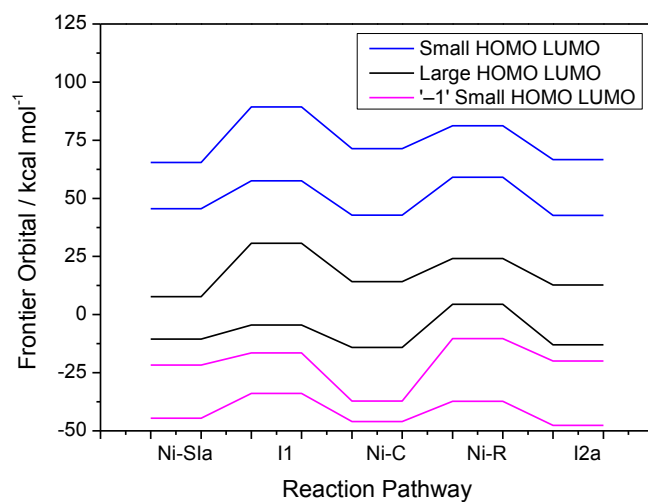
HOMO-LUMO DIAGRAMS

Fig. S5. HOMO and LUMO diagrams, in units of kcal/mol, for the so-called 'Small', 'Large', and '−1 Small' models along the HER path.
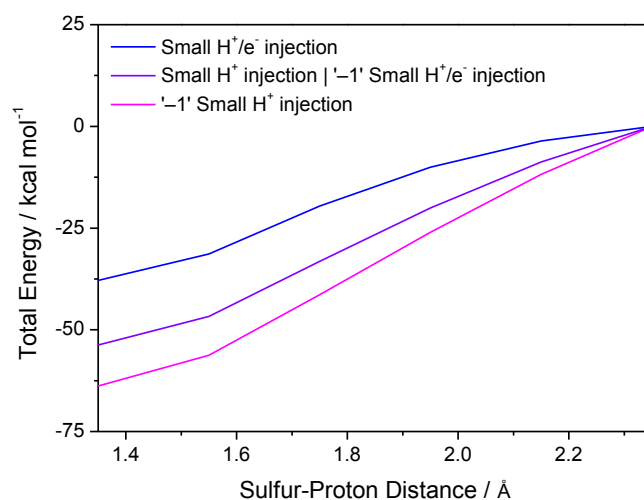
PROTON INJECTION

Fig. S6. Binding energy change, in units of kcal/mol, related to the distance, in Å, between the binding sulfur and proton in the H$^+$/e$^-$ injection for the 'Small', H$^+$ injection in the 'Small', and H$^+$/e$^-$ injection in the '−1 Small' models.

ENERGY PROFILES OF DIFFERENT MODELS ON A COMMON SCALE

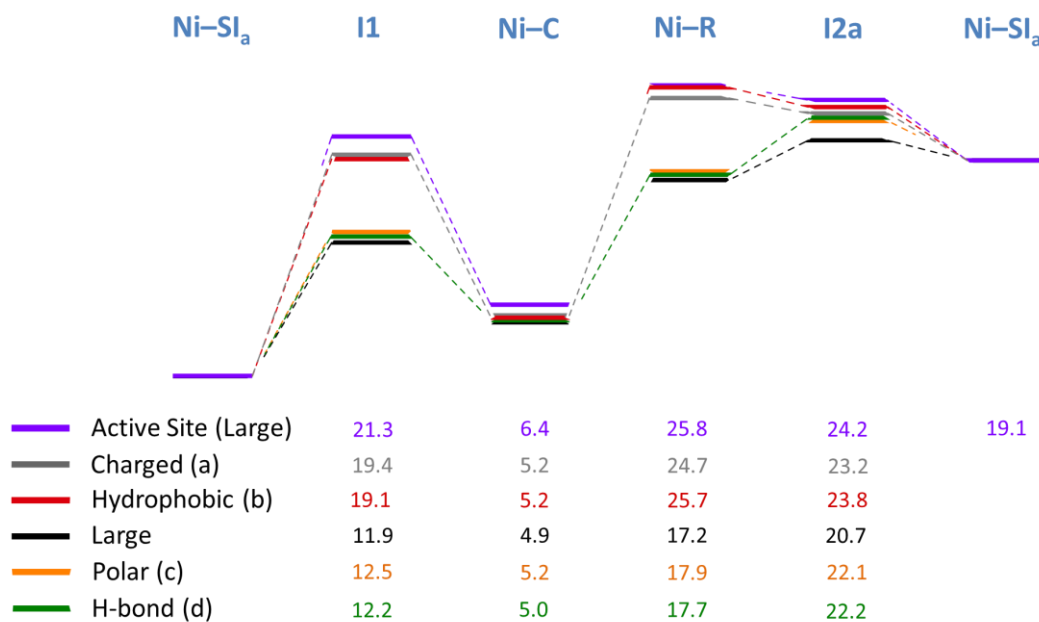|	Ni–SI$_a$	I1	Ni–C	Ni–R	I2a	Ni–SI$_a$
Active Site (Large)		21.3	6.4	25.8	24.2	19.1
Charged (a)		19.4	5.2	24.7	23.2	
Hydrophobic (b)		19.1	5.2	25.7	23.8	
Large		11.9	4.9	17.2	20.7	
Polar (c)		12.5	5.2	17.9	22.1	
H-bond (d)		12.2	5.0	17.7	22.2	

Fig. S7. Gibbs free energy profile, in units of kcal/mol, for the HER reaction on different models. Relative energies referred to the **Ni-SI$_a$** state, in which $\Delta G = 0$ kcal/mol.

ENERGY DIFFERENCE BETWEEN DIFFERENT CHARGED ACTIVE SITE

Tabel S1: Energy difference between '-1', '-3' and '-2' charged active site.[a]

Free energy / kcal*mol^{-1}	Small	'-1' Small	Δ ('-1'-'-2')	'-3' Small	Δ ('-3'-'-2')
Ni-SIa	-3125938.9	-3125943.4	-112.1	-3125839.8	206.8
I1	-3126299.1	-3126317.9	-126.5	-3126188.6	218.2
Ni-C	-3126310.6	-3126312.7	-109.9	-3126214.5	203.7
Ni-R	-3126670.5	-3126687.2	-124.4	-3126556.8	221.3
I2a	-3126673.0	-3126674.0	-108.6	-3126572.1	208.6

[a]Free energy of the electron has been approximated by $G(e^-) = G(1/2H_2) - G(H^+)$, the free energy of the proton is 262.4 kcal/mol (J. Phys. Chem. A, *2001*, **105**, *11534*).

CHAPTER 4

Proton Transformation and Dihydrogen Formation Process on the [NiFe] Hydrogenases

This chapter addresses the understanding of how proton transforms to hydride and how dihydrogen forms on the [NiFe] hydrogenases. By applying the intrinsic reactivity analysis,the energy, orbital and charge changes during the two processes could be seen at a high level of detail.

4.1   Proton to Hydride Transformation

The work was published in Physical Chemistry Chemical Physics 'Why a Proton is transformed into a Hydride by [NiFe] Hydrogenases? An Intrinsic Reactivity Analysis based on Conceptual DFT' (*Phys. Chem. Chem. Phys.*, 2016, **18**, 15369—15374).

By

Siyao Qiu, Luis Miguel Azofra, Douglas R. MacFarlane, Chenghua Sun.

From the study in section 4.1, it could be understood that:

1. The intrinsic reaction analysis shows the motivations for the first proton transfer to forming the bridging hydride (**I1** to **Ni-C**) and the second proton approaching the hydride (**Ni-R** to **I2**) are the decrease of the electronic activity and the electrophilicity of the Ni ion in [NiFe] hydrogenases.

2. The transformation of the proton to hydride is accompanied by two electron transfers from Ni, changing Ni(I) to Ni(III), and the transfer of these two electrons does not occur simultaneously, but in two non-synchronous stages.

Why is a proton transformed into a hydride by [NiFe] hydrogenases? An intrinsic reactivity analysis based on conceptual DFT†

Siyao Qiu,‡[a] Luis Miguel Azofra,‡[ab] Douglas R. MacFarlane*[ab] and Chenghua Sun*[ab]

The hydrogen evolution reaction (HER) catalysed by [NiFe] hydrogenases entails a series of chemical events involving great mechanistic interest. In an attempt to understand and delve into the question about 'Why does nature work in that way?', an in-depth intrinsic reactivity analysis based on conceptual DFT has been carried out focusing on the so-called **I1** to **Ni-C** step, *i.e.* our work tries to answer how and why the proton attached to the reactive sulphur atom from one of the *exo*-cyclic cysteine residues is transformed into a bridging hydride to be shared between the Ni/Fe metals in the active site of [NiFe] hydrogenases, which involves not only H migration, but also a change of the charge state on Ni from Ni(I) to Ni(III). Our DFT results suggest that the transformation is motivated by spontaneous rearrangements of the electron density, and stabilisation comes from the decrease of both electronic activity and electrophilicity index from Ni.

Introduction

Hydrogenases[1,2] are an extraordinary group of metal-containing enzymes specialised towards the reversible catalytic conversion of protons plus electrons into dihydrogen (H_2). The performance of catalysts in this simplest chemical reaction (eqn (1)) attracts much attention, not only due to its crucial importance in the understanding of the biochemistry of hydrogenases, but also because it can serve as the basis of the bio-inspired design of high-performance catalysts based on earth-abundant metals[3,4] for the efficient production of H_2—a promising environmentally friendly alternative to energy sources based on hydrocarbon compounds.[5,6]

$$2H^+ + 2e^- \rightarrow H_2 \qquad (1)$$
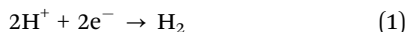
Focusing on the metal ions in the active site, hydrogenase enzymes can be classified into three main kinds: [NiFe], [FeFe], and [Fe]. However, only bimetallic [NiFe] and [FeFe] hydrogenases can catalyse the reversible H_2 oxidation into protons plus electrons. [NiFe] hydrogenases also have better O_2 tolerance

than the [FeFe] ones.[7] The active site of the [NiFe] hydrogenases is constituted by a bimetallic four-membered ring connecting the Ni and Fe metals through two sulphur atoms as part of two cysteine residues from the protein environment.[8] Also, as *exo*-cyclic ligands, two cysteine residues are attached on the Ni metal, and three inorganic ligands are linked to Fe composing the $[Fe(CN)_2(CO)]$ moiety.

Several studies, both theoretical and experimental, have been carried out in the recent decades with the aim to deepen the understanding of the hydrogen evolution reaction (HER) mechanism followed by [NiFe] hydrogenases. Those involving structural characterisation[9–30] and investigations of the metal multiplicities[31–35] deserve special mention, having generated extensive and rich literature. The study of the enzymatic activity of [NiFe] hydrogenases which turn to inactive states when placed under aerobic conditions deserves special mention: by the presence of the OOH^- and OH^- species interacting at the active site, a blocking of the bi-metallic site prevents the HER, the [NiFe] hydrogenases being reactivated once under a H_2 atmosphere.[14,15,18,22]

From an overall point of view, the active site of [NiFe] hydrogenases in their oxidised active state, **Ni-SI$_a$** (see Scheme 1), acts as the site for the injection of one H^+/e^- pair. The so-called **I1** state is postulated as an intermediate structure[17] during which the H^+ ion is placed on the reactive sulphur atom from one of the *exo*-cyclic cysteine residues; the electron goes to Ni, modifying its charge state by a reduction from Ni(II) to Ni(I). Subsequently, Ni(I) is re-oxidised, losing $2e^-$ to transform H^+ into hydride forming Ni(III) in the **Ni-C** state, as suggested by
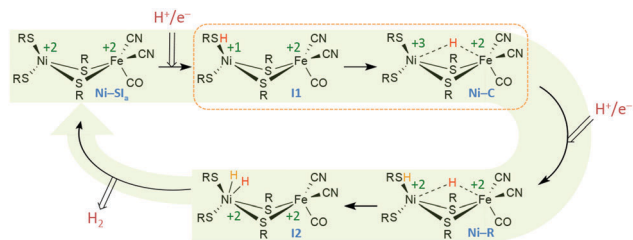
[a] *School of Chemistry, Faculty of Science, Monash University, Clayton, VIC 3800, Australia. E-mail: Douglas.MacFarlane@monash.edu, Chenghua.Sun@monash.edu; Fax: +61 3 9905 4597; Tel: +61 3 9902 9916*

[b] *ARC Centre of Excellence for Electromaterials Science (ACES), School of Chemistry, Faculty of Science, Monash University, Clayton, VIC 3800, Australia*

† Electronic supplementary information (ESI) available: Theoretical framework, analysis of other conceptual DFT properties, and Cartesian coordinates for the TS. See DOI: 10.1039/c6cp00948d

‡ These authors have equally contributed to the development of this work.

This journal is © the Owner Societies 2016

46

Phys. Chem. Chem. Phys., 2016, **18**, 15369–15374 | **15369**

Scheme 1 Hydrogen evolution reaction (HER) path followed by [NiFe] hydrogenases.

Siegbahn in 2004.[36] The objective of the present work is to provide further insights into this crucial step.

As a second step along the HER path, another H^+/e^- pair is collected by the **Ni-R** species. In similarity with **I1**, **I2** is postulated as an intermediate structure in which H_2 is produced and sequestrated by the Ni centre, to be finally released. The active site is thereby returned to the original **Ni-SI$_a$** configuration. Recent investigations by our group corroborate that the minimum energy path for the HER in [NiFe] hydrogenases follows a singlet multiplicity route.[37]

Computational details

Thus the geometries of the minima and the transition state (TS) for the proton transformation into hydride catalysed by the active site of [NiFe] hydrogenases (the so-called **I1** to **Ni-C** step) have been fully optimised through the use of density functional theory (DFT) *via* the spin-unrestricted Kohn–Sham (UKS) formalism and the BP86 functional.[38,39] Two-layered-integrated basis sets through the ONIOM approach[40] have been applied, using the Def2TZVPP effective core potential for the active site (constituted by the metal, sulphur, and ligands attached to the Fe atoms), and the smaller Def2SVP effective core potential for the carbon chains directly bound to sulphur atoms.[41] In all cases, the EDIIS/CDIIS procedure was applied for the self-consistent field (SCF) convergence.[42] The synchronous transit-guided quasi-Newton (STQN)[43] method (QST3) has been used to locate the TS, having checked that no spin contamination occurs during the breaking and formation of bond events in the TS. With the aim to confirm that the located TS connects reactants and products and in order to describe the intermediate structures along the minimum energy path, the intrinsic reaction coordinate (IRC) procedure, in which the reaction coordinate, ξ, is expressed in mass-weighted internal coordinates,[44] has been employed using a step-size equal to 0.05 bohr. During the IRC calculation, a tight criterion was imposed for convergence and the force constants were computed through the improved CalcFC algorithm. In all cases, frequency calculations were performed in order to confirm the nature of the stationary points (minima or first-order TS with one imaginary frequency). All calculations were carried out using the facilities provided by the Gaussian09 package (revision D.01).[45]

According to previous studies, the DFT modelling of [NiFe] hydrogenases exhibits a smaller unsigned error in describing the enzymatic structure when using the BP86 functional. Also, the effect of the basis set has only a minor role. Thus, the selection of the level of theory in the present work is not only justified by this, but also offers results comparable with *ab initio* coupled-cluster CCSD calculations that, contrary to what is observed when using B3LYP, show an energy preference for the singlet state in both the **Ni-SI$_a$** oxidised form and along the entire path for the HER.[35]

The model used in the present study has been built on the basis of the X-ray crystallographic structure of the reduced [NiFe] hydrogenase from *Desulfovibrio vulgaris* str. 'Miyazaki F' organism (PDB accession code 1H2R)[46] provided by Higuchi *et al.*[47] In this regard, in order to keep the same structure–reactivity pattern as in the original enzyme, the distal carbon atoms were frozen during optimisation and IRC calculations.

Finally, since natural bond orbital (NBO)[48] methodology provides reliable estimations of the electronic population, the NBO6.0 program[49] has been employed for such a purpose on the atomic centres.

Results and discussion

Conceptual DFT[50] (CDFT) offers a range of useful theoretical tools allowing an analysis of the intrinsic reactivity for the chemical events occurring at the electronic level, which are directly associated with the physicochemical properties of both global and local nature. When the energy of the process is represented along the intrinsic reaction coordinate (IRC = ξ),[51] three main points can be located: reactants (ξ_R, most negative value of ξ), transition state ($\xi_{TS} = 0$ amu$^{1/2}$ bohr, by definition), and products (ξ_P, most positive value of ξ). In the case at hand, the activation energy for the reaction involving the proton transformation into hydride catalysed by [NiFe] hydrogenases, $E^{\ddagger} = E(\xi_{TS}) - E(\xi_R)$, shows a value of 7.6 kcal mol^{-1} (see Fig. 1, left), while the reaction energy, $E_R = E(\xi_P) - E(\xi_R)$, is equal to -13.2 kcal mol^{-1}. Calculations at the same computational level indicate a value of Gibbs free reaction energy at room temperature equal to -12.0 kcal mol^{-1}, as proof of the spontaneity of this process under mild conditions.[37]

Similarly, the representation of the reaction force F *vs.* the IRC (F is defined as the negative first derivative of the energy with respect to ξ, eqn (2)) pinpoints the existence of one minimum between $[\xi_R, \xi_{TS}]$ and one maximum between $[\xi_{TS}, \xi_P]$, corresponding to the so-called ξ_1 and ξ_2 values on the reaction coordinate.

$$F(\xi) = -dE/d\xi \qquad (2)$$

This simple tool has a great significance from a mechanistic point of view, since the areas between the $[\xi_R, \xi_1]$, $[\xi_1, \xi_2]$, and $[\xi_2, \xi_P]$ ranges are considered as the regions associated with reactants (R), transition state (TS), and products (P), respectively.

As indicated in the theoretical framework (see ESI†), the activation energy of a reaction can be split into two quantities, W_1 and W_2 (eqn (3)):
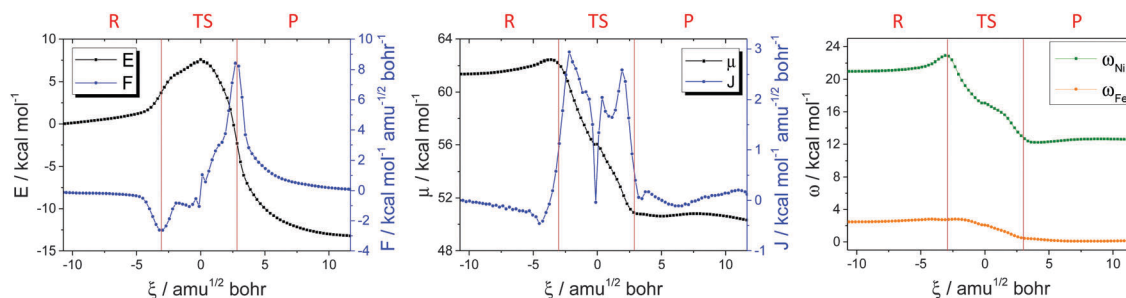
$$E^{\ddagger} = W_1 + W_2 \qquad (3)$$

15370 | *Phys. Chem. Chem. Phys.*, 2016, **18**, 15369–15374

47

This journal is © the Owner Societies 2016

Fig. 1 Left, energy (in kcal mol^{-1}, black) and reaction force (in kcal mol^{-1} amu$^{-1/2}$ bohr^{-1}, blue) profiles; centre, electronic chemical potential (in kcal mol^{-1}, black) and reaction electronic flux (in kcal mol^{-1} amu$^{-1/2}$ bohr^{-1}, blue) profiles; and right, local electrophilicity index profiles (in kcal mol^{-1}) for Ni (green) and Fe (orange) atoms vs. the IRC (in amu$^{1/2}$ bohr). Note: $\Delta\xi = 0.26$ amu$^{1/2}$ bohr has been selected for clarity in the chart representations.

As stated by Politzer and co-workers,[52] and nestled between the ξ_1 and ξ_R IRC positions (initial stage of the reaction at the R area and up to reach the TS zone), $W_1 = E(\xi_1) - E(\xi_R)$ can be related to the amount of energy required for the system to be reorganised geometrically, i.e. mainly due to structural reordering as a consequence of, for example, bond elongation/shortening, angle bending, or rotational events. Such structural modifications prepare the system to start with the formal reactive process in this early stage of the reaction, and once entering the TS area, bond breaking and formation starts to occur. In this regard, $W_2 = E(\xi_{TS}) - E(\xi_1)$ can be related to the amount of energy demanded for the system for an electronic reorganisation in order to reach the TS, i.e. mainly electronic rearrangement along the aforementioned bond breaking/formation events.

In contradistinction to ideal-behaviour reaction force profiles,[53] for the proton transformation into hydride catalysed by [NiFe] hydrogenases (see Fig. 1, left) it can be seen that once the system passes beyond the reactant zone ($\xi_1 = -2.97$ amu$^{1/2}$ bohr), the slope of F increases. The expected behaviour establishes that this trend should be constant along the TS area and up to the product region; however in the range $\xi \in [-1.80, -0.89]$ amu$^{1/2}$ bohr, the slope of F returns to negative.

Precisely based on the above concepts, this information can reveal that after the geometrical reorganisation up to ξ_1, a certain amount of energy is spent on the first electron transfer from Ni(I) to H$^+$, to form Ni(II) and H$^\bullet$. Subsequently, the system is required to be structurally reorganised along the range $\xi \in [-1.80, -0.89]$ amu$^{1/2}$ bohr, to be prepared for the second electron transfer to form Ni(III) and hydride (H:$^-$). According to the reaction force profile, this second transfer is produced before the TS is reached. Otherwise, a change in the slope of F should occur between ξ_{TS} and ξ_2. Similar trends in the reaction force have been recently described by Toro-Labbé and co-workers in the study of the carbocationic triple shift rearrangement,[54] in which elementary reactions constituted by the classical R, TS, and P stationary points display atypical F profiles with the appearance of more than two critical points. According to their interpretations, this results in the co-existence of primary (bond breaking and forming processes) and secondary (weakening and strengthening processes) events that occur asynchronously although in a concerted way.

Quantitatively of the 7.6 kcal mol^{-1} demanded as the activation barrier, the first geometrical reorganisation requires 53% of this, followed by 26% associated with the first electron transfer, and 11% and 10% are used for the second geo-metrical reorganisation and second electron transfer, respectively.

The mechanistic information derived from the energy and the reaction force profiles is supplemented with the analysis of the electronic chemical potential, μ, and its negative first derivative with respect to ξ, the so-called reaction electronic flux (REF), J. (eqn (4) and (5)). In this regard, the application of finite differences and Koopmans' theorem[55] by extension of the Hartree–Fock theory can approximate μ as the semi-sum of the energy for the lowest-unoccupied and highest-occupied frontier orbitals, LUMO (ε_L) and HOMO (ε_H), respectively, corresponding to the β and α lowest-unoccupied and highest-occupied electrons in the case of the paramagnetic (spin doublet state) **I1** and **Ni-C** forms of our [NiFe] hydrogenase model, in each case.

$$\mu = (\varepsilon_L + \varepsilon_H)/2 \qquad (4)$$

$$J(\xi) = -d\mu/d\xi \qquad (5)$$

Fig. 1 (centre) shows that the electronic activity measured by μ remains practically unchanged during the reactant and product stages. Thus, the main change in electronic activity takes place in the TS region with an important decrease by almost 11.5 kcal mol^{-1}. On the basis that the larger the electronic activity the higher the reactivity, we can conclude that a decrease in former leads to a more stable state of such a system.

While from ξ_R to ξ_1 the proton attached on S simply experiences a rotation in order to be physically close to the Ni (see Fig. 2), from ξ_1 to reach the TS, the proton undergoes reduction by two electron transfers provided by Ni. This process, which involves the formation of an angularly stressed three-membered Ni–*H–S ring in the TS, is characterised by spontaneous rearrangements of the electron density, indicated by positive values of REF. The REF profile also exhibits some fluctuations coinciding with the changes previously observed in the reaction force profile, despite both properties having a different nature. This supports our hypothesis for the two electron transfers, which do not occur simultaneously but rather in two distinct and non-synchronous stages. Ultimately, the REF displays a small activity slightly displaced from the zero-flux regime at
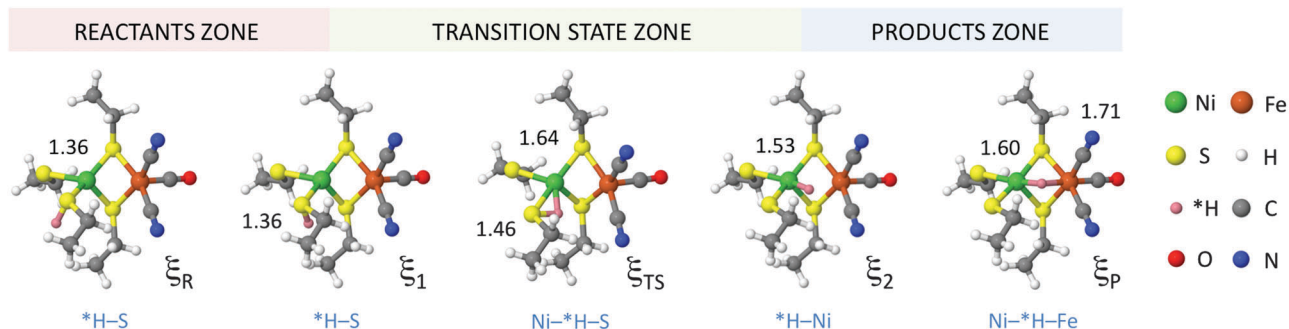
Fig. 2 Stationary points for the energy (reactants, TS, and products at ξ_R, ξ_{TS}, and ξ_P IRC positions, respectively) and for the reaction force (at ξ_1 and ξ_2 IRC positions, in each case). Dark pink colour is used to represent the H atom suspected to be transformed from a proton into a hydride (*H) during the reaction path. Selected *H–X (X = S, Ni, Fe) distances are shown in Å.

the beginning of the product area, which may be due to the incipient hydride–Fe bond formation.

While the analysis of the global properties provides a more general but enlightening insight into the chemical events taking place along the IRC, it is in the estimation of the local properties where a fully conclusive evaluation can be made. Here, the electrophilicity index (see Theoretical framework at ESI†) is profiled as an approach to analysis in the attempt to explain 'what happens' with the added H along the **I1** to **Ni–C** states on [NiFe] hydrogenases.

As indicated in Fig. 1 (right), the electrophilicity index of Ni (ω_{Ni}) increases from 21.0 kcal mol^{-1} at **I1** (ξ_R) to 22.7 kcal mol^{-1} at ξ_1, which is consistent with the idea that one electrophile (positively charged Ni) increases its electrophilic behaviour as another electrophile (H$^+$) comes closer. Previously, it was demonstrated that ξ_1 represents the moment from which the proton starts its transformation into hydride, turning the Ni into a more electrophilic centre, Ni(III), and converting H$^+$ into hydride prior to passing from the H$^\bullet$, a highly nucleophilic species. The consequence of this process is the stabilisation of the system by the occurrence of a Lewis acid–base neutralisation, or from a kinetic perspective, by the occurrence of an electrophile–nucleophile neutralisation, leading to a decrease of ω_{Ni} to 11.4 kcal mol^{-1}.

As additional and fully conclusive evidence about the double-electron cession from Ni to H, NBO contributions for the Ni–*H and Fe–*H bonds in the **Ni-C** state reveal the existence of strongly binding interactions such as covalent forces. Specifically, the converted hydride establishes strong H$_{lp}$ → σ*(NiS) and H$_{lp}$ → σ*(FeC) interactions with $E^{(2)}$ values of 68.8 and 66.1 kcal mol^{-1}, that is, the hydride moiety has a similar behaviour as the H atoms connecting diborane *via* dihydrogen bonds. Finally and more importantly, very high occupancies of 0.53 e (H$_{lp}$) with respective cessions of 0.29 and 0.23 e for the σ*(NiS) and σ*(FeC) orbitals can be seen (see Fig. 3).

However, what we can expect for the electrophilicity index of other 'protagonist' centres like Fe? The evolution of ω_{Fe} along the IRC illustrates the minor role of this atom as an electrophilic centre. A small value of around 2.4 kcal mol^{-1} at **I1** (ξ_R) can be seen, which is in accordance with the negative NBO

$$H_{lp} \rightarrow \sigma^*(NiS)$$
$$E^{(2)} = 68.8 \text{ kcal mol}^{-1}$$

$$H_{lp} \rightarrow \sigma^*(FeC)$$
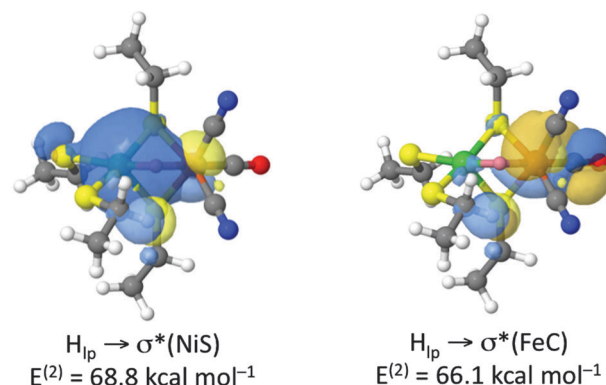$$E^{(2)} = 66.1 \text{ kcal mol}^{-1}$$

Fig. 3 Main NBO contributions to the Ni–*H and Fe–*H bonds for the **Ni-C** state.

atomic charge of Fe (see Fig. 4) due to the strong CN$^-$ donor ligands attached to it. How can the change in q(Fe) to more negative values along the IRC path be interpreted? To answer this, it should be taken into account that the Fe centre acts as
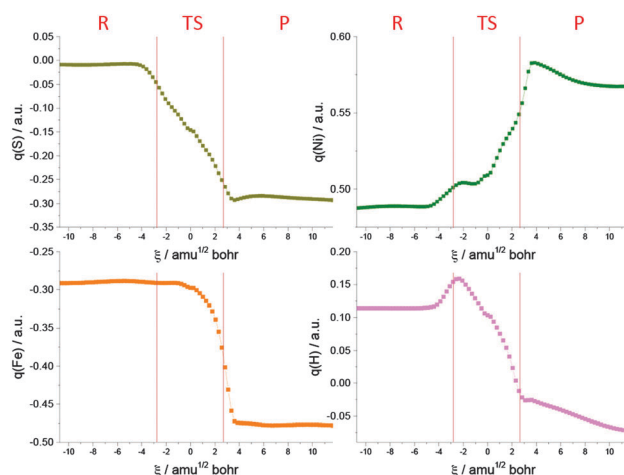

Fig. 4 NBO atomic charge evolution (in a.u.) for the reactive S (olive), Ni (green), Fe (orange), and reactive H (lilac) atoms along the IRC (in amu$^{1/2}$ bohr). Note: for clarity, chart representations only contain a few representative IRC points; however, the q analysis has been done using the full data.

15372 | *Phys. Chem. Chem. Phys.*, 2016, **18**, 15369–15374

49

This journal is © the Owner Societies 2016

an acceptor moiety that also retains the H atom once converted into hydride. This is especially evident just before ξ_2, *i.e.* once the converted hydride starts to interact with Fe.

Monitoring the NBO atomic charge, q, along the IRC also indicates that the main changes are located in the TS area (see Fig. 4). On the one hand, q(Ni) increases to more positive values as a result of loss/transfer of electrons. The opposite is exhibited by q(S), in which the loss of the proton leads to a more negative atomic charge. The NBO charge associated with the H moiety shows a similar behaviour to ω_{Ni}. Whilst at the beginning of the reaction q(H) has a value close to 0.10 a.u., at the end of the reaction, *i.e.* once hydride is formed, the charge is negative (-0.08 a.u.), corroborating the hydride character of this species.

Conclusions

In summary, the **I1** to **Ni-C** step for the HER mechanism in [NiFe] hydrogenases is characterised by the transformation of H^+ into a bridging hydride between the Ni and Fe centres. Two electrons are needed for such a transformation, provided by oxidation of Ni(I) to Ni(III). The transfer of these two electrons does not occur simultaneously but occurs in two non-synchronous stages, as hypothesised by the reaction force along the IRC, among other properties. Our conceptual DFT results suggest that such a transformation is motivated by spontaneous rearrangements of the electron density. Also, stabilisation from the decrease of electronic activity and electrophilicity index from Ni results in the occurrence of a Lewis acid–base neutralisation, or from a kinetic perspective, in the occurrence of an electrophile–nucleophile neutralisation. Finally, the transformation of the proton into hydride exhibits a spontaneous value of the reaction Gibbs free energy at room temperature. Finally, the information provided here may also be of help for the design of bio-inspired catalysts for hydrogen production.

Acknowledgements

Notes and references

1 P. M. Vignais and B. Billoud, *Chem. Rev.*, 2007, **107**, 4206–4272.

2 W. Lubitz, H. Ogata, O. Rüdiger and E. Reijerse, *Chem. Rev.*, 2014, **114**, 4081–4148.

3 J. K. Nørskov, T. Bligaard, A. Logadottir, J. R. Kitchin, J. G. Chen, S. Pandelov and U. Stimming, *J. Electrochem. Soc.*, 2005, **152**, J23–J26.

4 M. Wang, L. Chen and L. Sun, *Energy Environ. Sci.*, 2012, **5**, 6763.

5 N. Armaroli and V. Balzani, *Angew. Chem., Int. Ed.*, 2007, **46**, 52–66.

6 T. R. Cook, D. K. Dogutan, S. Y. Reece, Y. Surendranath, T. S. Teets and D. G. Nocera, *Chem. Rev.*, 2010, **110**, 6474–6502.

7 T. Burgdorf, O. Lenz, T. Buhrke, E. van der Linden, A. K. Jones, S. P. J. Albracht and B. Friedrich, *J. Mol. Microbiol. Biotechnol.*, 2005, **10**, 181–196.

8 E. Garcin, X. Vernede, E. C. Hatchikian, A. Volbeda, M. Frey and J. C. Fontecilla-Camps, *Structure*, 1999, **7**, 557–566.

9 B. Bleijlevens, B. Faber and S. Albracht, *JBIC, J. Biol. Inorg. Chem.*, 2001, **6**, 763–769.

10 S. Li and M. B. Hall, *Inorg. Chem.*, 2001, **40**, 18–24.

11 S. Foerster, M. Stein, M. Brecht, H. Ogata, Y. Higuchi and W. Lubitz, *J. Am. Chem. Soc.*, 2003, **125**, 83–93.

12 A. De Lacey, A. Pardo, V. Fernández, S. Dementin, G. Adryanczyk-Perrier, E. C. Hatchikian and M. Rousset, *JBIC, J. Biol. Inorg. Chem.*, 2004, **9**, 636–642.

13 S. Foerster, M. Gastel, M. Brecht and W. Lubitz, *JBIC, J. Biol. Inorg. Chem.*, 2005, **10**, 51–62.

14 H. Ogata, S. Hirota, A. Nakahara, H. Komori, N. Shibata, T. Kato, K. Kano and Y. Higuchi, *Structure*, 2005, **13**, 1635–1642.

15 A. Volbeda, L. Martin, C. Cavazza, M. Matho, B. Faber, W. Roseboom, S. J. Albracht, E. Garcin, M. Rousset and J. Fontecilla-Camps, *JBIC, J. Biol. Inorg. Chem.*, 2005, **10**, 239–249.

16 C. Fichtner, C. Laurich, E. Bothe and W. Lubitz, *Biochemistry*, 2006, **45**, 9706–9716.

17 A. Pardo, A. De Lacey, V. Fernández, H.-J. Fan, Y. Fan and M. Hall, *JBIC, J. Biol. Inorg. Chem.*, 2006, **11**, 286–306.

18 M. van Gastel, M. Stein, M. Brecht, O. Schröder, F. Lendzian, R. Bittl, H. Ogata, Y. Higuchi and W. Lubitz, *JBIC, J. Biol. Inorg. Chem.*, 2006, **11**, 41–51.

19 A. L. De Lacey, V. M. Fernández, M. Rousset and R. Cammack, *Chem. Rev.*, 2007, **107**, 4304–4330.

20 J. C. Fontecilla-Camps, A. Volbeda, C. Cavazza and Y. Nicolet, *Chem. Rev.*, 2007, **107**, 4273–4303.

21 W. Lubitz, E. Reijerse and M. van Gastel, *Chem. Rev.*, 2007, **107**, 4331–4365.

22 A. Pardo, A. De Lacey, V. Fernández, Y. Fan and M. Hall, *JBIC, J. Biol. Inorg. Chem.*, 2007, **12**, 751–760.

23 P. E. M. Siegbahn, *C. R. Chim.*, 2007, **10**, 766–774.

24 H. Wu and M. B. Hall, *C. R. Chim.*, 2008, **11**, 790–804.

25 M.-E. Pandelia, H. Ogata, L. J. Currell, M. Flores and W. Lubitz, *Biochim. Biophys. Acta*, 2010, **1797**, 304–313.

26 M. Kampa, W. Lubitz, M. van Gastel and F. Neese, *JBIC, J. Biol. Inorg. Chem.*, 2012, **17**, 1269–1281.

27 M. E. Pandelia, P. Infossi, M. Stein, M. T. Giudici-Orticoni and W. Lubitz, *Chem. Commun.*, 2012, **48**, 823–825.

28 Y. Rippers, M. Horch, P. Hildebrandt, I. Zebger and M. A. Mroginski, *ChemPhysChem*, 2012, **13**, 3852–3856.

50

29 T. Krämer, M. Kampa, W. Lubitz, M. van Gastel and F. Neese, *ChemBioChem*, 2013, **14**, 1898–1905.

30 H. Ogata, K. Nishikawa and W. Lubitz, *Nature*, 2015, **520**, 571–574.

31 C. P. Wang, R. Franco, J. J. Moura, I. Moura and E. P. Day, *J. Biol. Chem.*, 1992, **267**, 7378–7380.

32 F. Dole, A. Fournel, V. Magro, E. C. Hatchikian, P. Bertrand and B. Guigliarelli, *Biochemistry*, 1997, **36**, 7847–7854.

33 H. Wang, C. Y. Ralston, D. S. Patil, R. M. Jones, W. Gu, M. Verhagen, M. Adams, P. Ge, C. Riordan, C. A. Marganian, P. Mascharak, J. Kovacs, C. G. Miller, T. J. Collins, S. Brooker, P. D. Croucher, K. Wang, E. I. Stiefel and S. P. Cramer, *J. Am. Chem. Soc.*, 2000, **122**, 10544–10552.

34 P. E. M. Siegbahn, J. W. Tye and M. B. Hall, *Chem. Rev.*, 2007, **107**, 4414–4435.

35 M. G. Delcey, K. Pierloot, Q. M. Phung, S. Vancoillie, R. Lindh and U. Ryde, *Phys. Chem. Chem. Phys.*, 2014, **16**, 7927–7938.

36 P. E. M. Siegbahn, *Adv. Inorg. Chem.*, 2004, **56**, 101–125.

37 S. Qiu, L. M. Azofra, D. R. MacFarlane and C. Sun, *ACS Catal.*, 2016, in revision.

38 J. P. Perdew, *Phys. Rev. B: Condens. Matter Mater. Phys.*, 1986, **33**, 8822–8824.

39 A. D. Becke, *Phys. Rev. A: At., Mol., Opt. Phys.*, 1988, **38**, 3098–3100.

40 M. Svensson, S. Humbel, R. D. J. Froese, T. Matsubara, S. Sieber and K. Morokuma, *J. Phys. Chem.*, 1996, **100**, 19357–19363.

41 F. Weigend and R. Ahlrichs, *Phys. Chem. Chem. Phys.*, 2005, **7**, 3297–3305.

42 K. N. Kudin, G. E. Scuseria and E. Cancès, *J. Chem. Phys.*, 2002, **116**, 8255–8261.

43 C. Peng, P. Y. Ayala, H. B. Schlegel and M. J. Frisch, *J. Comput. Chem.*, 1996, **17**, 49–56.

44 C. Gonzalez and H. B. Schlegel, *J. Phys. Chem.*, 1990, **94**, 5523–5527.

45 M. J. Frisch, G. W. Trucks, H. B. Schlegel, G. E. Scuseria, M. A. Robb, J. R. Cheeseman, G. Scalmani, V. Barone, B. Mennucci, G. A. Petersson, H. Nakatsuji, M. Caricato, X. Li, H. P. Hratchian, A. F. Izmaylov, J. Bloino, G. Zheng, J. L. Sonnenberg, M. Hada, M. Ehara, K. Toyota, R. Fukuda, J. Hasegawa, M. Ishida, T. Nakajima, Y. Honda, O. Kitao, H. Nakai, T. Vreven, J. A. Montgomery Jr., J. E. Peralta, F. Ogliaro, M. Bearpark, J. J. Heyd, E. Brothers, K. N. Kudin, V. N. Staroverov, R. Kobayashi, J. Normand, K. Raghavachari, A. Rendell, J. C. Burant, S. S. Iyengar, J. Tomasi, M. Cossi, N. Rega, N. J. Millam, M. Klene, J. E. Knox, J. B. Cross, V. Bakken, C. Adamo, J. Jaramillo, R. Gomperts, R. E. Stratmann, O. Yazyev, A. J. Austin, R. Cammi, C. Pomelli, J. W. Ochterski, R. L. Martin, K. Morokuma, V. G. Zakrzewski, G. A. Voth, P. Salvador, J. J. Dannenberg, S. Dapprich, A. D. Daniels, Ö. Farkas, J. B. Foresman, J. V. Ortiz, J. Cioslowski and D. J. Fox, *Gaussian09 (revision D.01)*, Gaussian, Inc., Wallingford CT, 2009.

46 I. Alkorta, J. Elguero and C. FocesFoces, *Chem. Commun.*, 1996, 1633–1634.

47 Y. Higuchi, H. Ogata, K. Miki, N. Yasuoka and T. Yagi, *Structure*, 1999, **7**, 549–556.

48 F. Weinhold and C. R. Landis, *Valency and Bonding. A Natural Bond Orbital Donor-Aceptor Perspective*, Cambridge Press, Cambridge, UK, 2005.

49 E. D. Glendening, J. K. Badenhoop, A. E. Reed, J. E. Carpenter, J. A. Bohmann, C. M. Morales, C. R. Landis and F. Weinhold, *NBO6.0*, Theoretical Chemistry Institute, University of Wisconsin, Madison, USA, 2013.

50 P. Geerlings, F. De Proft and W. Langenaeker, *Chem. Rev.*, 2003, **103**, 1793–1874.

51 K. Fukui, *Acc. Chem. Res.*, 1981, **14**, 363–368.

52 A. Toro-Labbé, S. Gutiérrez-Oliva, J. S. Murray and P. Politzer, *Mol. Phys.*, 2007, **105**, 2619–2625.

53 See some references concerning classical reaction force profiles: L. M. Azofra, I. Alkorta, J. Elguero and A. Toro-Labbé, *J. Phys. Chem. A*, 2012, **116**, 8250–8259; L. M. Azofra, I. Alkorta, A. Toro-Labbé and J. Elguero, *Phys. Chem. Chem. Phys.*, 2013, **15**, 14026–14036.

54 D. E. Ortega, S. Gutiérrez-Oliva, D. J. Tantillo and A. Toro-Labbé, *Phys. Chem. Chem. Phys.*, 2015, **17**, 9771–9779.

55 T. Koopmans, *Physica*, 1934, **1**, 104–113.

15374 | *Phys. Chem. Chem. Phys.*, 2016, **18**, 15369–15374

51

This journal is © the Owner Societies 2016

Why a Proton is transformed into a Hydride by [NiFe] Hydrogenases? An Intrinsic Reactivity Analysis based on Conceptual DFT

Theoretical Framework

Energy and Reaction Force: A transition state (TS) is a chemical entity that exhibits one imaginary frequency and is a maximum along the intrinsic reaction coordinate (IRC = ξ).[1, 2] It connects reactants and products through the minimum potential energy surface (PES) in a one-step chemical reaction.

The reaction force, F, is defined as the negative first derivative of the total energy, E, with respect the IRC (Eqn .1):

$$F(\xi) = -\frac{dE}{d\xi}$$

(1)

According to the Transition State Theory[3] (TST), the energy profile of an elementary step presents three critical points: two minima, one for reactants (ξ_R) and another for products (ξ_P), and one maximum for the TS (ξ_{TS}) (see Scheme below). In addition, F exhibits two critical points: a minimum at ξ_1 and a maximum at ξ_2. Thus, three regions can be defined along the IRC: i) in the [ξ_R, ξ_1] range, region associated to reactants and mainly driven by structural rearrangements; ii) in the (ξ_1, ξ_2) range, region associated to the TS and where most electron rearrangements by formation and breaking of bonds take place; and iii) in the [ξ_2, ξ_P] range, region associated to products where mainly occurs structural relaxations.[4-10] Note that $\xi_R < \xi_1 < \xi_{TS} < \xi_2 < \xi_P$.

The reaction force analysis provides an energy partition of the activation barrier, $E^{\neq}$. Thus, W_1 represents the energy required for the system to be reorganized geometrically, i.e. purely structural

reordering; and W_2 represents the energy demanded for the system for an electronic reorganization in order to reach the TS, i.e. purely electronic rearrangement (Eqns. 2 to 4):

$$E^{\neq} = W_1 + W_2 \tag{2}$$

$$W_1 = -\int_{\xi_R}^{\xi_1} F(\xi)d\xi > 0 = E(\xi_1) - E(\xi_R) \tag{3}$$

$$W_2 = -\int_{\xi_1}^{\xi_{TS}} F(\xi)d\xi > 0 = E(\xi_{TS}) - E(\xi_1) \tag{4}$$

Scheme 1. The solid and black line represents a generic energy profile, *E*, *vs*. the IRC. The dotted and blue line represents the reaction of force, *F*, *vs*. the IRC. The location of the stationary points of the energy and reaction force are indicated as $\xi_R/\xi_{TS}/\xi_P$ and ξ_1/ξ_2, respectively. Two vertical lines separate the reactants region (left), the TS region (center), and the products region (right).
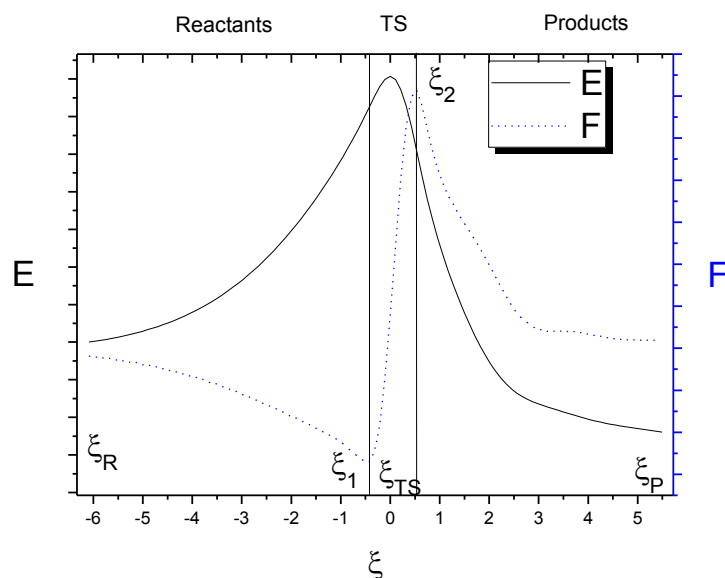
Global Chemical Properties based on Conceptual DFT: Conceptual DFT[11, 12] offers a range of useful theoretical tools allowing an analysis of the intrinsic reactivity for the chemical events occurring at electronic level, which are directly associated within physicochemical properties from both global and local nature.

Concerning the global properties, the electronic chemical potential, μ, for a system containing N electrons is defined as the derivative of the total energy, E, with respect N when the external potential, $v(r)$, remains constant (Eqn. 5). Considering that the number of electrons, N, is a discontinuous variable, the electronic chemical potential can be approximated, through the application of finite differences and the Koopmans' theorem[13] by extension of the Hartree-Fock theory, as the negative semi-sum of the first ionization potential, I, and the electron affinity, A. Also, these two parameters, A and I, can be approximated to the energy values of the highest occupied and lowest unoccupied molecular orbitals, ε_H (HOMO) and ε_H (LUMO)☐ respectively. The electronegativity,[14] χ, is defined as the opposite of μ:

$$\mu = -\chi = \left(\frac{\partial E}{\partial N}\right)_{v(r)} \approx -\left(\frac{I+A}{2}\right) = \frac{\varepsilon_L + \varepsilon_H}{2}$$

(5)

By analogy between E and F, the reaction electronic flux (REF), J, can be defined as the negative first derivative of the electronic chemical potential, μ, with respect the IRC (Eqn .6):

$$J(\xi) = -\frac{d\mu}{d\xi}$$

(6)

While the electronic chemical potential measures the electronic activity, the interpretation of the REF results from the analogy with classical thermodynamics: positive values of J should be associated with spontaneous rearrangements of the electron density driven by bond strengthening or forming processes, and negative values of J are indicating non-spontaneous rearrangements of the electron density that are mainly driven by bond weakening or breaking processes.[15]

Furthermore, the chemical hardness,[16, 17] η, is defined as the second derivative of the total energy, E, with respect N when $v(r)$ is constant (Eqn. 7). Also, applying the finite differences

approximation and the Koopmans' theorem, it can be approximated as the difference between the energy of the LUMO and HOMO. The chemical softness, S, is defined as the inverse of η:

$$\eta = S^{-1} = \left(\frac{\partial^2 E}{\partial N^2}\right)_{v(r)} \approx -(I - A) \approx \varepsilon_L - \varepsilon_H \tag{7}$$

Finally, the electrophilic power, ω, which was introduced by Parr *et al.*[18] by analogy with the power in classical electricity, is defined as (Eqn. 8):

$$\omega \approx \frac{\mu^2}{2\eta} \approx \frac{(I+A)^2}{8(I-A)} \approx \frac{(\varepsilon_L + \varepsilon_H)^2}{8(\varepsilon_L - \varepsilon_H)} \tag{8}$$

Local Properties. The Fukui Function: The global properties defined, so far, are useful in monitoring intrinsic changes in the molecules. However, the reactivity of such molecules resides on the atomic centers, and consequently, the evaluation of local properties are desirable. They can be calculated from the Fukui function,[19] *f(r)*, which is defined as the second derivative of the total energy with respect N and *v(r)* (Eqn. 9). This function complies an important property: its integration over all the space gives the unit value (Eqn. 10):

$$f(r) = \left| \frac{\partial^2 E}{\partial N \delta v(r)} \right| \tag{9}$$

$$\int_\Omega f(r) dr = 1 \tag{10}$$

Due to the discrete nature of N, two Fukui functions can be derived: the nucleophilic, $f^+(r)$, and the electrophilic, $f^-(r)$, functions. They can be approximated through the electron density of the

LUMO and HOMO frontier orbitals, respectively. Both, nucleophilic and electrophilic Fukui functions can be evaluated for each atom as indicated in Eqns. 11 and 12:

$$f^+(r)=\left|\phi^L(r)\right|^2=\rho^L(r)\rightarrow f_k^+=p_k(N+1)-p_k(N)$$

(11)

$$f^-(r)=\left|\phi^H(r)\right|^2=\rho^H(r)\rightarrow f_k^-=p_k(N)-p_k(N-1)$$

(12)

where the subscript k refers to a particular atom k. Then, $p_k(N)$ is the electronic population on an atom k in the neutral molecule, $p_k(N+1)$ is the electronic population on an atom k in the radical anion molecule, and $p_k(N-1)$ is the electronic population on an atom k in the radical cation molecule.

Using the nucleophilic Fukui function and the global electrophilicity, the local electrophilicity index, $\square_k$ for an atom k, is defined as (Eqn. 13):[20]

$$\omega_k=f_k^+\omega$$

(13)

References

1.   K. Fukui, *J. Phys. Chem.*, 1970, **74**, 4161-4163.

2.   K. Fukui, *Acc. Chem. Res.*, 1981, **14**, 363-368.

3.   K. J. Laidler and M. C. King, *J. Phys. Chem.*, 1983, **87**, 2657-2664.

4.   A. Toro-Labbé, *J. Phys. Chem. A*, 1999, **103**, 4398-4403.

5.   P. Jaque and A. Toro-Labbé, *J. Phys. Chem. A*, 2000, **104**, 995-1003.

6.   A. Toro-Labbé, S. Gutiérrez-Oliva, M. C. Concha, J. S. Murray and P. Politzer, *J. Chem. Phys.*, 2004, **121**, 4570-4576.

7.   J. Martínez and A. Toro-Labbé, *Chem. Phys. Lett.*, 2004, **392**, 132-139.

8. S. Gutiérrez-Oliva, B. Herrera, A. Toro-Labbé and H. Chermette, *J. Phys. Chem. A*, 2005, **109**, 1748-1751.

9. P. Politzer, A. Toro-Labbé, S. Gutiérrez-Oliva, B. Herrera, P. Jaque, M. Concha and J. Murray, *J. Chem. Sci.*, 2005, **117**, 467-472.

10. E. Rincón and A. Toro-Labbé, *Chem. Phys. Lett.*, 2007, **438**, 93-98.

11. R. G. Parr and W. Yang, *Density-Functional Theory of Atoms and Molecules*, Oxford University Press, Oxford, 1994.

12. P. Geerlings, F. De Proft and W. Langenaeker, *Chem. Rev.*, 2003, **103**, 1793-1874.

13. T. Koopmans, *Physica*, 1934.

14. R. G. Parr, R. A. Donnelly, M. Levy and W. E. Palke, *J. Chem. Phys.*, 1978, **68**, 3801-3807.

15. M. L. Cerón, E. Echegaray, S. Gutiérrez-Oliva, B. Herrera and A. Toro-Labbé, *Scien. Chin. Chem.*, 2011, **54**, 1982-1988.

16. R. G. Parr and R. G. Pearson, *J. Am. Chem. Soc.*, 1983, **105**, 7512-7516.

17. R. Pearson, *J. Chem. Sci.*, 2005, **117**, 369-377.

18. R. G. Parr, L. v. Szentpály and S. Liu, *J. Am. Chem. Soc.*, 1999, **121**, 1922-1924.

19. P. Hohenberg and W. Kohn, *Phys. Rev.*, 1964, **136**, B864-B871.

20. A. Toro-Labbé, *Theoretical Aspects of Chemical Reactivity*, Elsevier, Amsterdam, 2007.

4.2   Dihydrogen formation

The work includes a paper 'Hydrogen Evolution in [NiFe] Hydrogenases accompanied with Heterolytic Proton-Hydride Approaching' has been submitted.

By

Siyao Qiu, Luis Miguel Azofra, Douglas R. MacFarlane, Chenghua Sun.

From the study in section 4.2, it could be understood that:

1. The formation of dihydrogen on the active site in [NiFe] hydrogenases could be divided into three steps, i) the conformational change of the proton position on the S atom of the cysteine ligand, ii) the heterolytic proton and hydride approaching along with the electron transfer between proton and hydride, and iii) the two hydrogen atoms combination following the Volmer-Tafel mechanism.

From chapter 2 to 4, the three chapters illustrate the HER on the active site of the [NiFe] hydrogenases, and the ligand and protein influences on the HER. The understanding of the HER in hydrogenases could further provide some strategies for the design of the bio-inspired HER catalysts

PCCP

COMMUNICATION

Hydrogen Evolution in [NiFe] Hydrogenases accompanied with Heterolytic Proton-Hydride Approaching

Siyao Qiu,[a] Luis Miguel Azofra,[a, b] Douglas R. MacFarlane*[a] and Chenghua Sun*[c]

The mechanism for the Hydrogen Evolution Reaction (HER) in [NiFe] hydrogenase enzymes distinguishes from the inorganic catalysts. The first H^+/e^- pair injected to the active site of the hydrogenases transforms into hydride, while the second H^+/e^- pair injection leads to the existence of the H^-/H^+ pair both binding on the active site. The two opposite charged hydrogens heterolytically approach to each other in order to form dihydrogen (H_2), which is enhanced by the Coulomb force. Our DFT calculations suggest that the approach and the charge transfer between the two hydrogens are spontaneous, being motivated by the stabilization of the electronic activity and the electrophilicity of Ni. After the electron transfer and proton-hydride approaching, the two hydrogen atoms attach to the Ni ion and combine homolytically.

Dihydrogen (H_2), as a carbon-free energy carrier, is emerging as a promising future energy alternative.[1] However, the large-scale production of H_2 is limited by the lack of low-cost and highly efficient catalysts, as the existing high-performance catalysts for H_2-production usually involve some noble metal, like platinum.[2] In Nature, hydrogenase enzymes are found in particular organisms, and exhibit impressive catalytic properties; more importantly they are based on earth-abundant elements.[3] Therefore, the understanding of the low overpotential and kinetics barrier of hydrogenases is of special significance.

Hydrogenases can be classified, considering the different metal ions at the active site, into [NiFe], [FeFe] and [Fe] species.[4, 5] The [NiFe] hydrogenases catalyze the hydrogen evolution reaction (HER) and the reverse hydrogen cleavage into protons (H^+) and electrons (e^-), but also some particular [NiFe] hydrogenases demonstrate better oxygen tolerance than [FeFe] kind.[6-8] The active site of [NiFe] hydrogenases consists of a four-membered ring involving nickel, iron and two bridging sulphur from cysteine residues. In addition, two terminal cysteine residues connect with Ni via S, while one carbonyl and two cyanides groups ligate with Fe through C.[9]

In the HER, most of the inorganic catalysts mechanistically follow the Volmer-Tafel route (**Scheme 1**).[1, 10] In this, two protons combine with two electrons separately on the surface of the catalyst to finally form H_2 homolytically from two adsorbed H atoms (adatoms). Alternatively, in the Volmer-Heyrovsky mechanism, a second proton directly approaches to the first H adatom to be subsequently reduced. For the [NiFe] hydrogenases, it is accepted that the enzyme catalyzes the H_2 evolution/cleavage heterolytically.[11, 12] However, the difference between the H_2 combination mechanism on the [NiFe] hydrogenases and the V-H mechanism on inorganic catalysts is still not quite clear. In our study, we delve into the mechanistic aspects about how and why the H^- and H^+ moieties, both binding on the active site, heterolytically approach to each other in order to form H_2.
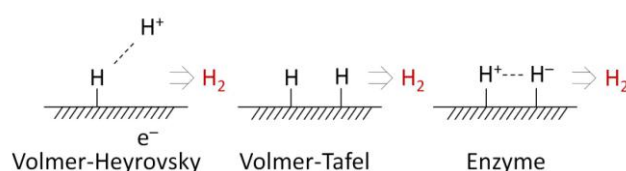
Scheme 1. Mechanisms of HER following the Volmer–Tafel and Volmer–Heyrovsky Routes.
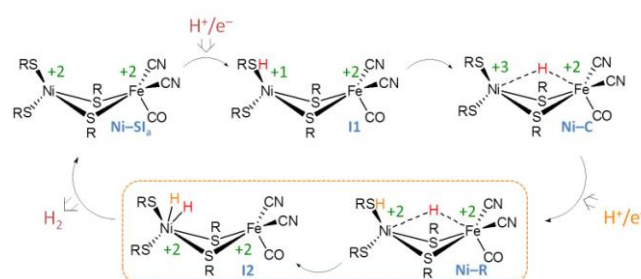
Scheme 2. HER Path followed by [NiFe] Hydrogenases.

a. School of Chemistry, Faculty of Science, Monash University, Clayton, VIC 3800, Australia. E-mail: Douglas.MacFarlane@monash.edu
b. KAUST Catalysis Center (KCC), King Abdullah University of Science and Technology (KAUST), Thuwal 23955-6900 (Saudi Arabia)
c. Department of Chemistry and Biotechnology, Faculty of Science, Engineering and Technology, Swinburne University of Technology, Hawthorn, VIC 3122, Australia. E-mail: chenghuasun@swin.edu.au
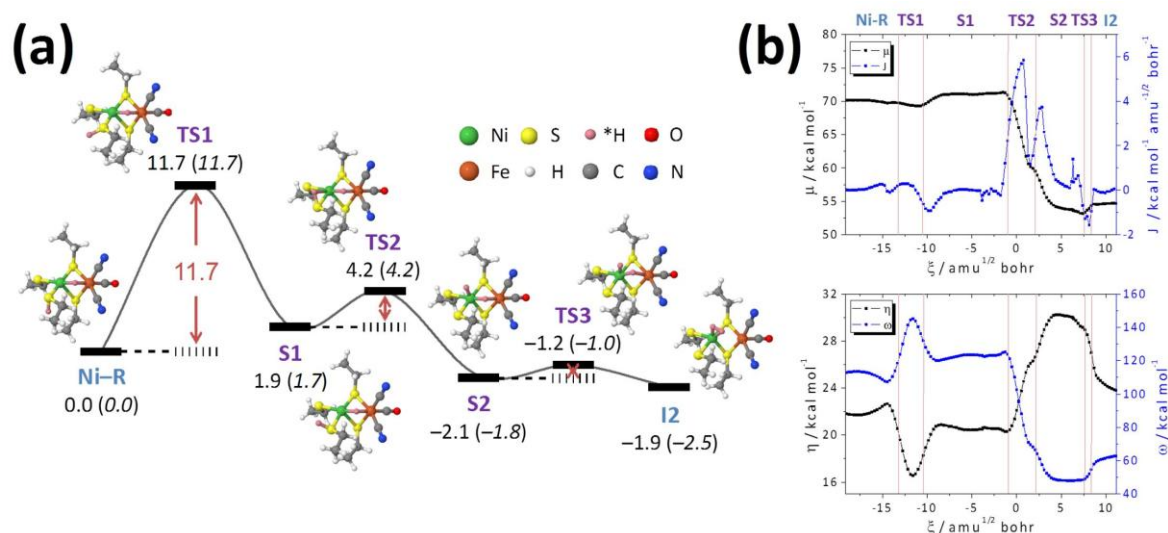
PCCP

COMMUNICATION

Figure 1. (a) Enthalpy diagram (Gibbs free energies, rt, in parenthesis), kcal mol^{-1}, and optimised structures for the **Ni-R** to **I2** path of HER by [NiFe] hydrogenase. Note: reactive H atoms are highlighted in pink. (b) Top, electronic chemical potential, in kcal mol^{-1}, and reaction electronic flux, in kcal mol^{-1} amu$^{-\frac{1}{2}}$ bohr^{-1}, profiles along the reaction pathway; bottom, total hardness and electrophilicity, in kcal mol^{-1}, profiles. Note: red lines separate the different regions through the intrinsic reaction coordinate.

To understand the whole HER path in [NiFe] hydrogenases, a general view of the reaction is shown in **Scheme 2**.[12, 13] The injection of the first H$^+$/e$^-$ pair to the initial state, **Ni-SI$_a$**,[14-19] leads to the **Ni-C** state. In this, the negative hydride is formed between Ni and Fe centre which leads to (or is promoted by) the conversion of the Ni redox state to Ni^{III}.[21-26] I1 state is postulated to connect the **Ni-SI$_a$** and **Ni-C** state, in which the proton that is delivered to the active site firstly binds to the terminal S atom at the active site, while the electron goes to Ni, altering the redox state of Ni from Ni^{II} to Ni^{I}.[20] Recent DFT investigations carried out by us has proven the two electron transfer occur asynchronously, being motivated by spontaneous rearrangements of the electron density and being stabilised by decrease of both the electronic activity and the electrophilicity index of Ni.[27] (The use of these parameters is discussed further below). Then, the **Ni-R** state is generated with the second H$^+$/e$^-$ pair injection. Similar to what happened with the first H$^+$/e$^-$ pair, the second proton is added to the terminal S and the electron is injected into Ni, changing the Ni redox state from Ni^{III} to the original Ni^{II}.[28-32] In support of this, three **Ni-R** sub-states have been detected by FTIR spectroscopy,[33] and previous calculation work have proposed the possible structures for the sub-states.[30] The X-ray crystallography work by Ogata *et al.* has confirmed that the **Ni-R1** state has a proton binding on the terminal S and a bridging

hydride placed between the Ni and Fe moieties.[34] Besides, in the **Ni-R1** state, the proton binds at the same side with the bridging hydride (similar with the **S1** state in **Figure 1a**). The proton that binds to the terminal S in the **Ni-R1** state is transferred from Glu34 in *Desulfovibrio vulgaris* [NiFe] hydrogenases, which is part of the proton transfer chain. The position of Glu34 suggests the proton initially binds reversely to the hydride on the active site (**Ni-R** state in **Figure 1a**) and then rotate to the same side. Finally, this proton is proposed to transfer to the metal centre, generating chemisorbed H$_2$ by combination with the hydride on the Ni ion in the so-called **I2** state.[15, 35, 36]

In the present work, our efforts are focused on unravelling the mechanistic aspects involving the hydride-proton combination (**Ni-R** to **I2** steps) leading to H$_2$ in [NiFe] hydrogenases. In consonance with previous mechanistic studies carried out by us,[27] the pure functional BP86 has been applied for the analysis of the reaction path on a constrained active site model (see ESI). Our findings demonstrate that the **Ni-R** to **I2** step: i) the reaction occurs through a non-concerted mechanism with the location of two intermediate states;[11] ii) the reaction is enhanced by Coulombic interactions and motivated by the stabilisation of the electronic activity and the electrophilicity of Ni; iii) such process goes through a heterolytic approaching of the H$^-$/H$^+$ pair.

Phys. Chem. Chem. Phys., 2018, **00**, 1-6 | **2**

60

Please do not adjust margins

As indicated in **Figure 1(a)**, the reaction mechanism for the hydride-proton evolution into H_2 by [NiFe] hydrogenase presents three steps in our DFT calculations (full details can be found in the Supplementary Information). In the first, the proton attached to the reactive S atom in the **Ni-R** state experiences a rotation of 122°. This conformational change prepares the proton to be available for its further reduction, leading to the **S1** intermediate state. As indicated by the energy profile, this appears as the limiting step of the whole reaction, since it presents an activation enthalpy of 11.7 kcal mol^{-1} (Gibbs free energy barrier, ΔG_{act} = 11.7 kcal mol^{-1} at room temperature, *rt*). Additional calculations carried out by us for the counter-clockwise mechanism exhibit an activation enthalpy of 13.9 kcal mol^{-1} (ΔG_{act} = 12.8 kcal mol^{-1}), demonstrating that the proton clockwise rotation along the **Ni-R** to **S1** early step is established as the minimum energy path as imposed by the kinetic control. It is worth mentioning that the **S1** state has similar structural with **Ni-R1** state detected by X-ray crystallography. In the second step, **S1** to **S2**, the proton migrates from the reactive S atom to the Ni^{II} moiety in an exothermic (ΔH_R = −4.0 kcal mol^{-1}), exergonic (ΔG_R = −3.5 kcal mol^{-1}) process, only demanding 2.3 kcal mol^{-1} as activation enthalpy (ΔG_{act} = 2.5 kcal mol^{-1}).

As shown in **Figure 1(b)**, top, during the **Ni-R** to **S1** step there is no change in the electronic activity, establishing this as a mere conformational change process. On the other hand, the important decrease in the electronic chemical potential, as well as the reaction electronic flux (REF) becoming significantly positive, suggest that the electron transfer in the hydride-proton approaching can take place in the **S1** to **S2** step. This is also supported by a higher percentage of the activation energy being due to electronic rearrangement as compared to the energy cost of the geometry reorganisation, ca. 55:45% (around 1.9 kcal/mol electronic rearrangement and 1.6 kcal/mol geometry reorganization).

As third and final step, the enthalpy change between the **S2** and **I2** states is slightly endothermic, 0.2 kcal mol^{-1} (although slightly spontaneous, ΔG_R = −0.7 kcal mol^{-1}) with a small enthalpy barrier of 0.9 kcal mol^{-1} (ΔG_{act} = 0.8 kcal mol^{-1}). This final stage of the mechanistic path exhibits further electronic activity changes and can be ascribed as the one in which the two already transformed hydrogens combine with each other in order to form H_2.

Contrary to what was recently described by us concerning the proton to hydride conversion in the **I1** to **Ni-C** step by [NiFe] hydrogenase (an asynchronous, but concerted process),[27] the **Ni-R** to **I2** hydride-proton evolution into H_2 is characterised to follow a non-concerted mechanism, as shown at **Figure 1a**. The analysis of the total hardness and electrophilicity profiles (**Figure 1b**, bottom) offers an interesting perspective in understanding how these reactivity descriptors are related to the chemical events taking place. Pearson stated his maximum hardness principle (MHP), noting that "*a chemical system at a given temperature will evolve to a configuration of maximum absolute hardness, η*".[37] This general behaviour is directly related to the minimum electrophilicity principle (MEP), since a chemical system will therefore evolve to a configuration of

minimum absolute electrophilicity, ω. Thus, the larger η the smaller ω, and vice versa.

Analysing them by steps, it is observed that during the **Ni-R** to S1 stage, *i.e.*, rotation of the proton attached to the reactive S atom, a decrease of η and an increase of ω can be seen, demonstrating its non-spontaneity as well as being the kinetic limiting step. However, the system rapidly evolves through a maximum hardness − minimum electrophilicity pathway once inserted along the **TS2** intrinsic reaction coordinate region. Although a decrease and an increase of η and ω respectively are observed once **I2** minimum is reached, compliance of the MH and ME principles is seen, *i.e.* this process is driven by a positive and negative balances of η and ω equal to 2.0 and −50.2 kcal mol^{-1}, respectively.

We have also searched for other evidence of this. Until this moment, our analysis has been focused on the interpretation of the information provided by global Conceptual DFT (CDFT) descriptors. Notwithstanding, chemical reactivity resides in local moieties/atoms exhibiting specific functionalities. In this sense, **Figure 2** shows the evolution of the local electrophilicity indexes and the NBO charges of the S, Ni, and Fe atoms that are involved in the hydride-proton → H_2 process. Results show differentiated behaviours not only amongst them, but also along the reaction coordinate as follows:

(i) With the exception of small variations in the **TS1** region for ω(S) and ω(Ni), local electrophilicity indexes remain practically unchanged until the system reaches **TS2**. This is in consonance with the mere conformational change that proton experiences in order to be close to the NiFe active site. This is also supported by the NBO charge profiles of q(S) and q(Ni), which are practically constant during this step. In other words, the change in the proton conformation does not modify the electronic nature and reactivity of the species, especially the already formed hydride as well as the metal centres.

(ii) During the **TS2** region, ω(Ni) rapidly decreases, suggesting that Ni starts to "feel" the presence of an electron-rich entity. Thus, if Ni electrophilicity is stabilised, this proves that the proton is converted into hydrogen since an electron transfer from hydride to proton is the only way in which the latter becomes a nucleophile, meanwhile the proton jumps from the S to the Ni centre (**S1** to **S2**).

(iii) The two hydrogen combination process (**TS3** region) is completed immediately, and the former hydride migrates from the bridge position between the NiFe bi-metallic active site to the Ni centre (**S2** to **I2**). Despite this last step involves a breaking of the H−Fe bond, ω(Fe) remains practically constant during the process. This is in accord with what we have previously observed in the proton conversion into hydride (**I1** to **Ni-C** stage): "*the evolution of ω(Fe) along the reaction coordinate illustrates the minor role of this atom as an electrophilic centre*".[27]

This journal is © The Royal Society of Chemistry 2018

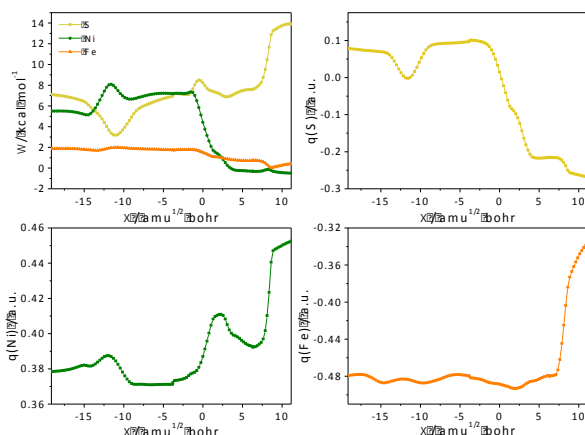*Phys. Chem. Chem. Phys.*, 2017, **00**, 1-6 | **3**

Figure 2. Local electrophilicity index, kcal mol^{-1}, and NBO charge, a.u., profiles for S, Ni, and Fe reactive atoms.

More importantly, NBO charge evolution of the H1 (hydride) and H2 (proton) atoms demonstrate that from **Ni-R** up to **S1** stage (proton conformational change), no charge changes in these species can be seen. However, once **TS2** is reached, an increase of q(H1) (losing electrons) is directly complemented by a decrease of q(H2) (gaining electrons), *i.e.*, the heterolytic proton hydride approaching is demonstrated to be catalysed by [NiFe] hydrogenase through hydride oxidation – proton reduction being motivated by Coulomb forces. Finally, during **TS3** and up to **I2**, the approach of the two hydrogens leads to charges being q(H1) ≈ q(H2) ≈ 0, as indication of the H$_2$ formation.
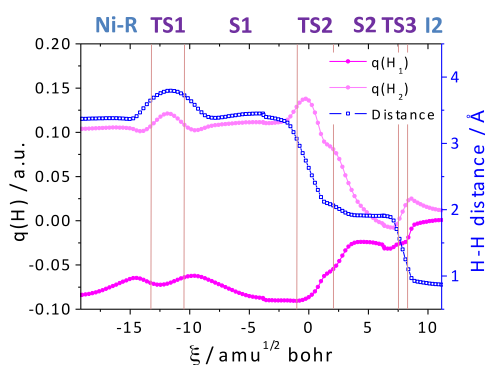

Figure 3. NBO charge, a.u., profile for hydride/H1 (bold pink) and proton/H2 (soft pink), and H1–H2 distance profile, Å. Note: red lines separate the different regions through the intrinsic reaction coordinate.

In the V-H mechanism, the second proton binds directly to the existing hydrogen atom on the catalyst, while in the [NiFe] hydrogenases system, the second proton binds to Ni atom before combining with the hydride and the electron transfer between proton and hydride leads to the homolytic hydrogen combination from **S2** to **I2**. Therefore, the **S2** to **I2** stage shows a hydrogen combination mechanism more close to the V-T

route. However, the **S1** to **S2** process is a heterolytic proton-hydride approaching. Thus the overall proton-hydride combination in the [NiFe] hydrogenases has a different mechanism with both the V-T and V-H routes. Besides, the hybrid functional, M06, was also used for the proton-hydride combination calculation (see ESI). It is worth mentioning that the V-T mechanism HER is energetic favourable in most of the inorganic materials than the V-H mechanism. And the Coulombic interaction between the two hydrogen atoms in the heterolytic V-H mechanism could reduce the energy for the approaching. It seems the [NiFe] hydrogenases combine the advantages of the two mechanisms in the inorganic catalysts.

Conclusions

In summary, H$_2$ evolution from proton and hydride by [NiFe] hydrogenases, involving a maximum hardness − minimum electrophilicity pathway, could be divided into three steps: i) conformational change of the proton position in order to approach to the NiFe active site; ii) the heterolytic proton hydride approaching accompanied by the electron transfer from hydride to proton; and iii) two hydrogen atoms attached to the Ni centre homolytically combine in order to form H$_2$. Moreover, the heterolytic proton hydride approaching is driven by the Coulombic interaction, and stabilised by a decrease of the electronic activity and the electrophilicity of Ni. Contrary to what it is observed in HER catalysed by inorganic catalysts, the redox process by BP86 functional calculations, step ii, (ΔG_{act} = 2.5 kcal mol^{-1}) and approaching process, step iii, (ΔG_{act} = 0.8 kcal mol^{-1}) exhibit very low activation barriers, while the limiting step of this reaction is the conformational change required of the proton (ΔG_{act} = 11.7 kcal mol^{-1}).

Acknowledgements

Notes and references

1   T. He, G. Gao, L. Kou, G. Will, A. Du, *J. Catal.* 2017, **354**, 231-235;
2   J. K. Nørskov, T. Bligaard, A. Logadottir, J. R. Kitchin, J. G. Chen, S. Pandelov, U. Stimming, *J. Electrochem. Soc.* 2005, **152**, J23.
3   C. Madden, M. D. Vaughn, I. Díez-Pérez, K. A. Brown, P. W. King, D. Gust, A. L. Moore, T. A. Moore, *J. Am. Chem. Soc.* 2012, **134**, 1577-1582.
4   P. M. Vignais, B. Billoud, Chem. Rev. 2007, 107, 4206-4272;
5   W. Lubitz, H. Ogata, O. Rudiger, E. Reijerse, *Chem. Rev.* 2014, **114**, 4081-4148.

6   T. Burgdorf, O. Lenz, T. Buhrke, E. van der Linden, A. K. Jones, S. P. J. Albracht, B. Friedrich, *J. Mol. Microbiol. Biotechnol.* 2005, **10**, 181-196;

7   C. Tard, C. J. Pickett, *Chem. Rev.* 2009, **109**, 2245-2274;

8   J. C. Fontecilla-Camps, A. Volbeda, C. Cavazza, Y. Nicolet, *Chem. Rev.* 2007, **107**, 4273-4303.

9   E. Garcin, X. Vernede, E. C. Hatchikian, A. Volbeda, M. Frey, J. C. Fontecilla-Camps, *Structure* 1999, **7**, 557-566.

10 E. Skúlason, V. Tripkovic, M. E. Björketun, S. Gudmundsdóttir, G. Karlberg, J. Rossmeisl, T. Bligaard, H. Jónsson, J. K. Nørskov, *J. Phys. Chem. C* 2010, **114**, 18182-18197.

11 M. Bruschi, M. Tiberti, A. Guerra, L. De Gioia, *J. Am. Chem. Soc.* 2014, **136**, 1803-1814.

12 P. E. M. Siegbahn, J. W. Tye, M. B. Hall, *Chem. Rev.* 2007, **107**, 4414-4435;

13 P. E. M. Siegbahn, Adv. *Inorg. Chem.* 2004, **56**, 101-125.

14 Y. Higuchi, H. Ogata, K. Miki, N. Yasuoka, T. Yagi, *Struct.* 1999, **7**, 549-556;

15 H. Wu, M. B. Hall, *Comptes Rendus Chimie* 2008, 11, 790-804;

16 A. Volbeda, J. C. Fontecilla-Camps, *Dalton Trans.* 2003, 4030-4038;

17 S. Kurkin, S. J. George, R. N. F. Thorneley, S. P. J. Albracht, *Biochemistry* 2004, **43**, 6820-6831;

18 J. Legall, D. V. Dervartanian, E. Spilker, J.-P. Lee, H. D. Peck, *Biochim. Biophys. Acta – Bioenergetics* 1971, **234**, 525-530;

19 B. Bleijlevens, F. A. van Broekhuizen, A. L. De Lacey, W. Roseboom, V. M. Fernandez, S. P. J. Albracht, *J. Biol. Inorg. Chem.* 2004, **9**, 743-752.

20 A. Pardo, A. De Lacey, V. Fernández, H.-J. Fan, Y. Fan, M. Hall, *J. Biol. Inorg. Chem.* 2006, **11**, 286-306.

21 A. Chapman, R. Cammack, C. E. Hatchikian, J. McCracken, J. Peisach, *FEBS Letters* 1988, **242**, 134-138;

22 H. J. Kruger, R. H. Holm, *J. Am. Chem. Soc.* 1990, **112**, 2955-2963;

23 H. J. Krueger, R. H. Holm, *Inorg. Chem.* 1989, **28**, 1148-1155;

24 S. Foerster, M. Stein, M. Brecht, H. Ogata, Y. Higuchi, W. Lubitz, *J. Am. Chem. Soc.* 2003, **125**, 83-93;

25 M. Brecht, M. van Gastel, T. Buhrke, B. Friedrich, W. Lubitz, *J. Am. Chem. Soc.* 2003, **125**, 13075-13083;

26 M. Stein, W. Lubitz, *Phys. Chem. Chem. Phys.* 2001, **3**, 5115-5120.

27 S. Qiu, L. M. Azofra, D. R. MacFarlane, C. Sun, *Phys. Chem. Chem. Phys.* 2016, **18**, 15369-15374.

28 C. Fichtner, C. Laurich, E. Bothe, W. Lubitz, *Biochemistry* 2006, **45**, 9706-9716;

29 A. L. De Lacey, V. M. Fernández, M. Rousset, R. Cammack, *Chem. Rev.* 2007, **107**, 4304-4330;

30 T. Kramer, M. Kampa, W. Lubitz, M. van Gastel, F. Neese, *ChemBioChem* 2013, **14**, 1898-1905;

31 S. J. George, S. Kurkin, R. N. F. Thorneley, S. P. J. Albracht, *Biochemistry* 2004, **43**, 6808-6819;

32 M. R. Linford, P. Fenter, P. M. Eisenberger, C. E. D. Chidsey, *J. Am. Chem. Soc.* 1995, **117**, 3145-3155.

33 A. L. De Lacey, A. Pardo, V. M. Fernandez, S. Dementin, G. Adryanczyk-Perrier, E. C. Hatchikian, M. Rousset, *J. Biol. Inorg. Chem.* 2004, **9**, 636-642.

34 H. Ogata, K. Nishikawa, W. Lubitz, *Nature* 2015, 520, 571-574.

35 J. M. Keith, M. B. Hall, *Inorg. Chem.* 2010, **49**, 6378-6380;

36 S. Qiu, L. M. Azofra, D. R. MacFarlane, C. Sun, *ACS Catal.* 2016, **6**, 5541-5548.

37 R. G. Pearson, *J. Chem. Educ.* 1987, **64**, 561–570

SUPPORTING INFORMATION

Hydrogen Evolution in [NiFe] Hydrogenases accompanied with Heterolytic Proton-Hydride Approaching
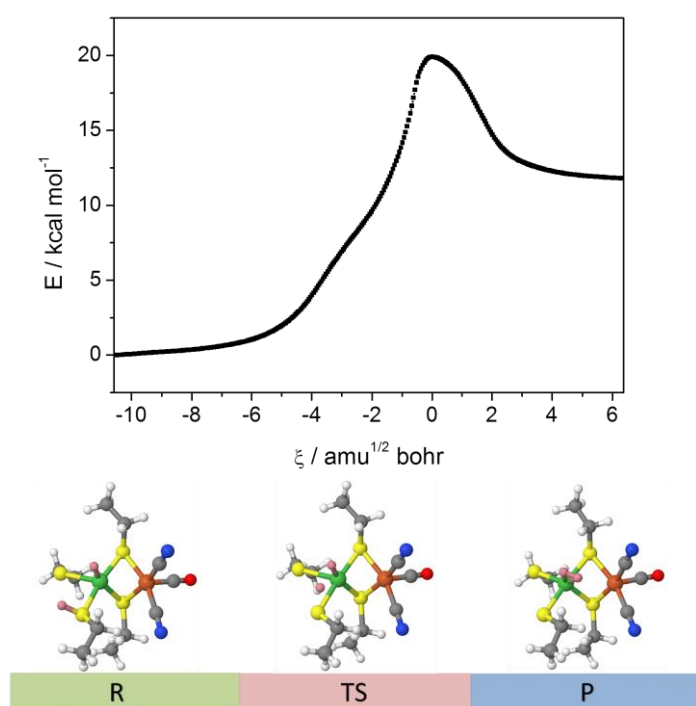
Hybrid Functional Calculation

Fig S1. IRC calculation by M06 hybrid functional over the proton-hydride approaching process.

CHAPTER 5

[FeFe]-hydrogenase-inspired Molecular Catalysts

This chapter investigates the HER on the existing [FeFe]-hydrogenase-inspired molecular catalysts. The [FeFe]-hydrogenase-inspired molecular catalysts have very similar structures with the active site of the [FeFe] hydrogenases. From the free energy calculation on the possible reaction states in the molecular catalysts, the HER pathway could be proposed. Also, a comparison on the HER between the molecular catalysts and [FeFe] hydrogenases could be studied.

This work includes a draft paper 'DFT studies on the [FeFe]-hydrogenases-inspired molecular catalysts'.

By

Siyao Qiu, Douglas R. MacFarlane, Annabella Selloni, and Chenghua Sun.

It could be concluded from this study that:

1. During the HER on the molecular catalysts, the first H^+/e^- injection follows the PT-ET mechanism. The injected proton usually goes to the bridging position between Fe ions and then rotates to the terminal position of a Fe. The largest thermodynamic impediment is mostly the first PT step.
2. In the second H^+/e^- injection, the second proton directly binds to the terminal position of the Fe and form dihydrogen homolytically.
3. Some terminal ligand modifications on the molecular catalyst could change the energy requirement for the PT step, which directly reduce the largest thermodynamic energy. And some other ligand modifications could reduce the largest thermodynamic energy requirement by introducing an intermediate step and providing a proton binding position on the modified ligands.

DFT studies on the [FeFe]-hydrogenases-inspired molecular catalysts

Siyao Qiu,[a] Douglas R. MacFarlane,[a, b, *] Annabella Selloni,[c, *] and ChenghuaSun[d, *]

[a]School of Chemistry, Faculty of Science, Monash University, Clayton, VIC 3800, Australia

[b]ARC Centre of Excellence for Electromaterials Science (ACES), School of Chemistry, Faculty of Science, Monash University, Clayton, VIC 3800, Australia

[c]Department of Chemistry, Princeton University, Princeton, New Jersey 08544, United States

[d]Department of Chemistry and Biotechnology, Faculty of Science, Engineering and Technology, Swinburne University of Technology, Hawthorn, VIC 3122, Australia.

Abstract

The FeFe bio-inspired molecular catalysts mimicking the [FeFe] hydrogenases have been widely synthesized. However, the pathway of the hydrogen evolution reaction (HER) taking place on these catalysts is not very clear. In this work, Density Functional Theory (DFT) calculations on the FeFe molecular catalysts suggested that the two hydrogen atoms would terminally bind to one Fe ion on the catalyst molecule to form H_2, however the bridging binding hydrogens were not able to generate H_2 molecule. Also, the first H^+/e^- injection of the HER on the FeFe molecular catalysts follow the proton transfer followed by electron transfer (PT-ET) mechanism. Moreover, the bridging binding usually requires lower energy than terminal binding for the first proton injection, and the largest thermodynamic impediment is mostly the first proton transfer step. Some terminal ligand modification could obviously change the PT energy. And some bridging ligands modification could reduce the largest thermodynamic energy requirement by introducing an intermediate step by providing a proton binding position by the modified ligands.

Text

CO_2 emission, released from the fossil fuels combustion, is bringing about the worldwide greenhouse gas effect. H_2, as an environmental-friendly energy carrier, is one of the most promising alternatives to our traditional fossil fuels. Therefore, the catalysts for large-scale hydrogen evolution reaction (HER) are grabbing global interest in the researches for years. However the existing high-performance inorganic catalysts for HER are made of expensive materials, like Pt.[1, 2] In nature, a class of enzyme, hydrogenase, has been found to possess impressive catalytic activity, but also consists earth-abundant materials only. [3] Regarding the metal ions at the active site, the hydrogenases could be further classified into the [NiFe], [FeFe] and [Fe] hydrogenases. [4, 5] Among the three, [FeFe] hydrogenases present the highest catalytic efficiency for the hydrogen cleavage

into proton plus electron.[5-8] Hence, the [FeFe]-hydrogenases-inspired molecular catalysts have been synthesized for mimicking the HER on the [FeFe] hydrogenases.

The active site of the [FeFe] hydrogenases, called H-cluster, contains a 'butterfly' Fe_2S_2 group and a Fe_4S_4 cubic. The hydrogen evolution takes place on the butterfly structure, in which the bimetallic Fe centers are bridge ligated by one SCH_2NHCN_2S ligand and one carbonyl. Moreover, one Fe metal (Fe_P) is terminally linked with a $[Fe_4S_4]$ cluster, one carbonyl and one cyanide. And the other Fe (Fe_d) merely bonds to one carbonyl and one cyanide, leaving the binding position vacant for hydrogen. Therefore, different Fe_2S_2 butterfly molecules have been synthesized to resemble the active site of the [FeFe] hydrogenases. [9]

The HER cycle on the active site of [FeFe] hydrogenases has been proposed previously. [10-14] The **Hox** state is the most oxidized active state, being the initial state among the reaction path. The redox state of **Hox** in +1 and +2 for Fep and Fed respectively.[15, 16] The first H^+/e^- added will lead to the **Hred** state, with the proton binding on the bridging azadithiolate (adt) ligand via N and the electron goes to the Fed.[17] Afterwards, the second H^+/e^- injection leads to the **HhydH$^+$** state. Accompanied with the second proton injection, the firstly added proton is transferred to Fed and the second injected proton binds to adt ligand again. [18] Subsequently, the second proton will be delivered to Fe_d, therefore generating H_2 with the hydride and then be released. The Fep atom remains +1 charged along the entire reactive process, and Fe_d experiences a 'charge route' of +2, +1 and +2 along the **Hox**/ **HredH$^+$**/ **HhydH$^+$** steps.[17]

In the molecular catalysts, the HER cycle are slightly different with the [FeFe] hydrogenases.[19] Though a similar 'butterfly' structure could been seen in the molecular catalysts, the redox state of the catalysts are FeIFeI.[20] Previous study indicated the injected proton inclined to form bridging hydride between Fe ions during the HER process. [21] Also, different bridging sulphides and the terminal ligand on Fe have been modified in different molecular synthesis. The performances of the existing molecular catalysts are varied. Felton et al. studied hundreds of the FeFe catalysts and found out the positive correlation between the overpotential and the catalytic efficiency.[22] In this work, the HER process on the FeFe molecular catalysts have been studied to understand HER path on the molecular catalysts. Also, the difference between the molecular catalysts and the FeFe hydrogenases has been investigated.

Density functional theory (DFT) calculations have been done for all models through the Gaussian 09 calculation program. [23, 2425] To find out a relatively good functional for the FeFe molecular calculation, both pure functionals (PBE, BP86, TPSS) and hybrid functionals (PBE0, B3LYP, M062X) were tested for the geometry optimization and redox potential calculations. Def2TZVPP basis set was applied for all models. [26] In all cases, the dispersion of the models has been considered by including the empirical dispersion (GD3) compensation. [27] Also, the Synchronous Transit-

Guided Quasi-Newton (STQN) method (QST3) has been applied to determine the transition state (TS). Polarization Continuum Model has been applied for the calculation, with the acetonitrile solvent condition. [28] To derive the free energy changes, frequency calculations have been conducted. All models were built based on the X-ray crystallographic data of different models.

Test calculations on four different molecular catalysts {$Fe_2(\mu\text{-}SCH_2CH_2)_2O(CO)_6$, ($\mu$-$SCH_2CH_2CH_2S$)-$Fe_2(CO)_5SO(CH_3)_2$, ($\mu$-pdt)$Fe_2(CO)_5P(NC_4H_8)_3$, and [$\mu$-S-2-(4-$FC_6H_4$) $CONHC_6H_4$]$_2Fe_2(CO)_6$} found out that the PBE, PBE0 and TPSS functional give the best result (see Fig. S1). Moreover, the redox potential calculations by pure functionals show better accordance with the experimental data (see ESI). Therefore, PBE has been chosen for the HER energy changes of the molecular catalyst calculations.

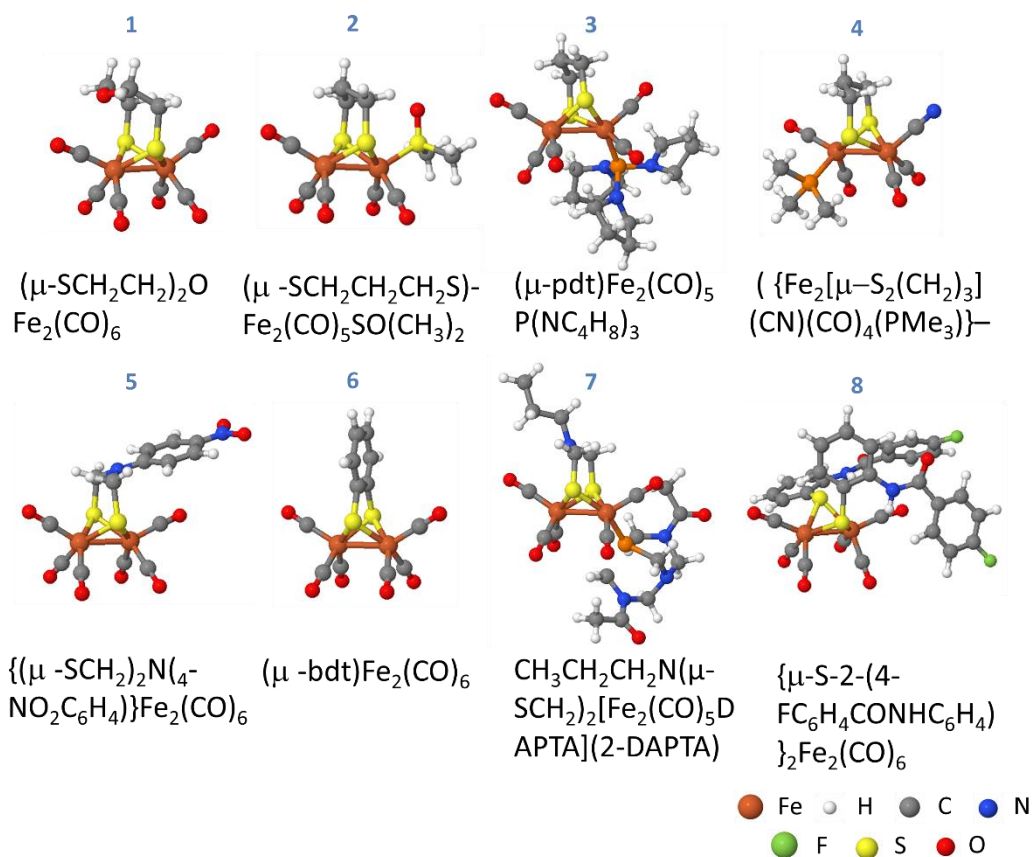Eight different catalysts have been studied in this work (see **Figure 1**).[29-36]

1	2	3	4
(μ-$SCH_2CH_2)_2O$ $Fe_2(CO)_6$	(μ -$SCH_2CH_2CH_2S$)- $Fe_2(CO)_5SO(CH_3)_2$	(μ-pdt)$Fe_2(CO)_5$ $P(NC_4H_8)_3$	({$Fe_2[\mu{-}S_2(CH_2)_3]$ $(CN)(CO)_4(PMe_3)$}–

5	6	7	8
{(μ -$SCH_2)_2N(_4$- $NO_2C_6H_4$)}$Fe_2(CO)_6$	(μ -bdt)$Fe_2(CO)_6$	$CH_3CH_2CH_2N(\mu$- $SCH_2)_2[Fe_2(CO)_5D$ APTA](2-DAPTA)	{μ-S-2-(4- $FC_6H_4CONHC_6H_4$)}$_2Fe_2(CO)_6$

Fe   H   C   N   F   S   O

Figure 1. Modelling the eight FeFe molecular catalysts based on the X-ray Crystallographic data.

The (μ-$SCH_2CH_2)_2O$ Fe_2 $(CO)_6$is the simplest structure among the seven geometries. Test calculations on the possible binding positions for the hydrogen atom have been performed, as shown in **Figure 2**. Three different mechanisms for H^+/e^- injection, concerted proton electron transfer (CPET) proton transfer – electron transfer (PT-ET) and electron transfer – proton transfer (ET-PT), have been studied. The results showed the energy through the PT-ET route is the lowest among the three mechanisms. The largest thermodynamic step is merely 0.61 eV for the PT-ET

mechanism, and the CPET requires 0.71 eV and the ET-PT needs even more energy than the CPET route, being 1.29 eV. The lowest reaction route for HER as shown follows the bold arrows in Figure 1. The proton binds to the bridging position between Fe ions firstly. Afterwards, the second hydrogen atom could not bind to the same Fe, hence the hydrogen molecule could not form at the bridging position. To generate the H_2 molecule, the bridging hydride would rotate to the terminal binding position. The energy barrier for the rotation step is 1.0 eV. After the first H^+/e^- injection, the second hydrogen atom is directly added to the Fe, with an energy demand of 0.12 eV to generate the H_2 molecule and spontaneously releases.
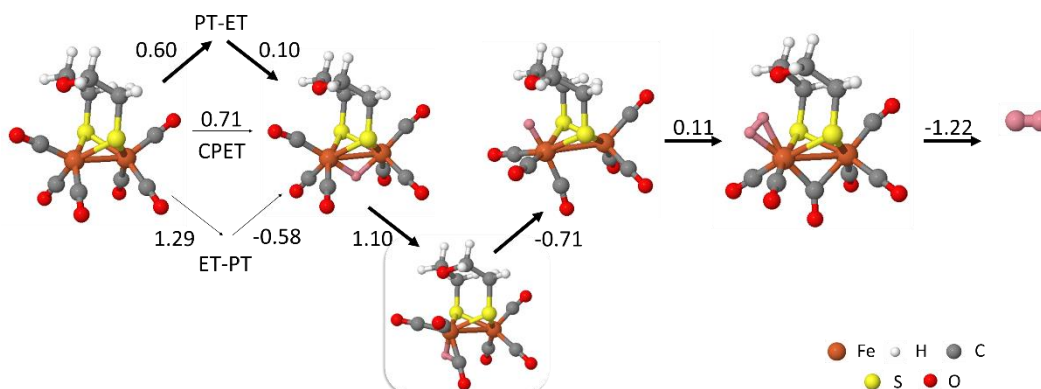
Figure 2. HER pathway followed by the (μ-SCH$_2$CH$_2$)$_2$O Fe$_2$ (CO)$_6$ molecular catalysts. Gibbs free energy differences, in eV, have been shown in figure.

From the calculation of the eight molecules, we found that, except the $\{Fe_2[\mu\text{-}S_2(CH_2)_3](CN)(CO)_4(PMe_3)\}^-$ molecule, the second proton and electron injection only require a small amount of energy, and the first proton/electron injection and proton transformation is the largest thermodynamic and rate-determining step.

The reaction path for the $CH_3CH_2CH_2N(\mu\text{-}SCH_2)_2[Fe_2(CO)_5DAPTA]$ (2-DAPTA) and (μ-bdt)Fe$_2$(CO)$_6$are similar with the (μ-SCH$_2$CH$_2$)$_2$O Fe$_2$ (CO)$_6$ one. The proton initially binds to the bridging position between FeFe, followed with the rotation of the hydrogen atom to the terminal site on single Fe ion. The largest thermodynamic step for the (μ-bdt)Fe$_2$(CO)$_6$ molecule is also the addition of the proton to the bridging position, being 0.67 eV. However the largest impediment could be seen at the electron injection step followed after the first proton injection to the bridging position for the theCH$_3$CH$_2$CH$_2$N(μ-SCH$_2$)$_2$[Fe$_2$(CO)$_5$DAPTA] (2-DAPTA) molecule, which requires 0.47 eV for the ET step and merely requires the 0.19 eV for the PT step. This indicates the terminal ligands modification could justify the PT and ET energy require, but not necessarily change the reaction path for the HER on the molecule catalyst.

Some other calculations on the catalysts showed the modification of the terminal ligands could reduce the energy required for the HER by changing the reaction process. (μ-SCH$_2$CH$_2$CH$_2$S)-Fe$_2$(CO)$_5$SO(CH$_3$)$_2$ molecule has a –SO(CH$_3$)$_2$ terminal ligand terminally links to the Fe ion. The

first proton adding to this ligand to form –SOH(CH$_3$)$_2$ only requires 0.44 eV, which is lower than the H$^+$/e$^-$ concerted injection or the proton to the bridging position between Fe ions, being 0.65 and 0.88 eV respectively. The introduce of the CN$^-$ ligand in the {Fe$_2$[μ-S$_2$(CH$_2$)$_3$](CN)(CO)$_4$(PMe$_3$)}$^-$ molecule helps the proton binding on the CN$^-$ ligand, and this proton binding position is also supported by the experimental research. The proton terminally added onto the Fe ion requires -0.10 eV, and the formation of the bridging binding proton releases for -0.65 eV energy. Therefore, the reaction path of this molecule avoids the formation of the bridging hydride and the rotation to the terminal proton process. Different to the other seven molecules, the second proton inclines to bind to the CN- ligand before the first electron injection, with -0.06 eV energy release. The first electron injection is the largest thermodynamic step, being 0.58 eV.

As for the bridging ligand modification, the { μ-S-2-(4-FC$_6$H$_4$CONHC$_6$H$_4$)}$_2$Fe$_2$(CO)$_6$ and the {(μ-SCH$_2$)$_2$N(4-NO$_2$C$_6$H$_4$)}Fe$_2$(CO)$_6$ suggest the bridging ligands could also provide position for proton binding and therefore reduce the reaction energy for HER. Molecule μ-S-2-(4-FC$_6$H$_4$CONHC$_6$H$_4$)}$_2$Fe$_2$(CO)$_6$ present an overpotential as low as 0.2 eV in the experiment. Calculation on this molecule found out, without consider the bridging sulphide ligand, the first H$^+$/e$^-$ injection required 0.73 eV. However, the first proton injection onto the ketone CO on the sulphide ligand, the injection energy reduced to 0.48 eV. Later, with the 0.26 eV energy injection, the proton transferred to the bridging position between FeFe accompanied with the first electron injection. The first proton adding to the {(μ-SCH$_2$)$_2$N(4-NO$_2$C$_6$H$_4$)}Fe$_2$(CO)$_6$ also binds to –NO$_2$, with the largest impediment of 0.58 eV. Moreover, the review by Felton proposed that 'Actual catalyst may be the product of reduction of the nitrophenyl group'. Therefore, the reduced molecule {(μ-SCH$_2$)$_2$N(4-NO$_2$HC$_6$H$_4$)}Fe$_2$(CO)$_6$ has been calculated, and the largest energy demand for thermodynamic reaction is the first proton injection to the bridging position between FeFe, which is 0.34 eV. However, the reduction energy for the {(μ-SCH$_2$)$_2$N(4-NO$_2$C$_6$H$_4$)}Fe$_2$(CO)$_6$ to {(μ-SCH$_2$)$_2$N(4-NO$_2$HC$_6$H$_4$)}Fe$_2$(CO)$_6$ requires 0.54 eV, hence this step should be the thermodynamic impediment. The experimental overpotential data have been employed to compare with the calculation result. However, the data are not very fitting as shown in **Figure 3**. This could attribute to the different experimental environment and the error exists between the theoretical prediction and experimental result.
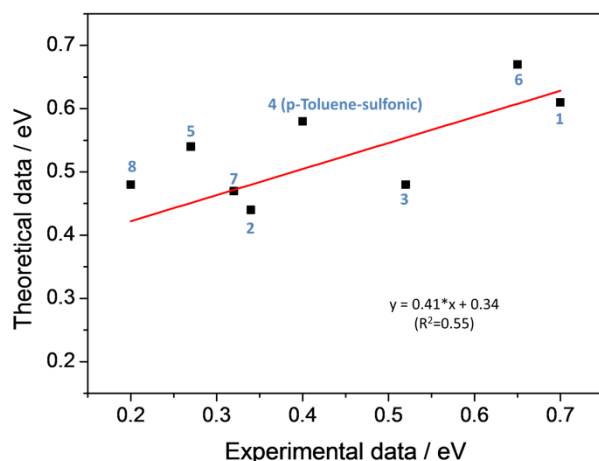
Figure 3. Experimental overpotential[22] versus theoretical overpotential data for the eight molecular catalysts calculations.

In the 'Small' model of the [FeFe] hydrogenases, the terminal proton binding on the active site is spontaneous, releasing –0.11 eV energy for this step. A test calculation by replacing the CO ligand by CN^- in the $(\mu\text{-SCH}_2\text{CH}_2)_2\text{O Fe}_2\text{ (CO)}_6$ found out merely reduced for 0.02 eV, we could see that the number of the CN^- ligands do not result inremarkable changes on the energy required for the hydrogen binding terminally. Also, the redox state of the molecular catalysts is the same, being Fe(I)Fe(I) in all cases, but it is Fe(I)Fe(II) in the [FeFe] hydrogenases. Therefore the redox state between the molecular catalysts and the hydrogenases could be the reason for the energy profile diversity.

In summary, the first H^+/e^- injection of the HER on the FeFe molecular catalysts follows the PT-ET mechanism. The proton is usually been added to the bridging position between Fe ions and then rotate to the terminal position of a single Fe. Then the second hydrogen also binds terminally to the Fe and form dihydrogen homolytically. The largest thermodynamic impediment is mostly the first proton transfer step. While some terminal ligand modification could obviously change the PT energy, and some other ligand modification could reduce the largest thermodynamic energy requirement by introducing an intermediate step by providing a proton binding position by the modified ligands. These findings on the FeFe molecular catalysts might help the design of the bio-inspired molecular catalyst synthesis.

References

1.   B. E. Conway and B. V. Tilak, *Electrochimica Acta*, 2002, **47**, 3571-3594.

2.   J. K. Nørskov, T. Bligaard, A. Logadottir, J. R. Kitchin, J. G. Chen, S. Pandelov and U. Stimming, *Journal of The Electrochemical Society*, 2005, **152**, J23.

3.   C. Madden, M. D. Vaughn, I. Díez-Pérez, K. A. Brown, P. W. King, D. Gust, A. L. Moore and T. A. Moore, *Journal of the American Chemical Society*, 2012, **134**, 1577-1582.

4.   P. M. Vignais and B. Billoud, *Chemical reviews*, 2007, **107**, 4206-4272.

5.   W. Lubitz, H. Ogata, O. Rudiger and E. Reijerse, *Chem. Rev.*, 2014, **114**, 4081-4148.

6.   S. V. Hexter, F. Grey, T. Happe, V. Climent and F. A. Armstrong, *Proceedings of the National Academy of Sciences*, 2012, **109**, 11516-11521.

7.   C. Tard and C. J. Pickett, *Chemical reviews*, 2009, **109**, 2245-2274.

8.   J. C. Fontecilla-Camps, A. Volbeda, C. Cavazza and Y. Nicolet, *Chemical reviews*, 2007, **107**, 4273-4303.

9.   Y. Li and T. B. Rauchfuss, *Chemical reviews*, 2016, **116**, 7043-7077.

10. D. W. Mulder, M. W. Ratzloff, E. M. Shepard, A. S. Byer, S. M. Noone, J. W. Peters, J. B. Broderick and P. W. King, *J. Am. Chem. Soc.*, 2013, **135**, 6921-6929.

11. A. Silakov, C. Kamp, E. Reijerse, T. Happe and W. Lubitz, *Biochemistry*, 2009, **48**, 7780-7786.

12. A. Adamska, A. Silakov, C. Lambertz, O. Rüdiger, T. Happe, E. Reijerse and W. Lubitz, *Angewandte Chemie International Edition*, 2012, **51**, 11458-11462.

13. C. Sbraccia, F. Zipoli, R. Car, M. H. Cohen, G. C. Dismukes and A. Selloni, *The Journal of Physical Chemistry B*, 2008, **112**, 13381-13390.

14. M. Bruschi, G. Zampella, P. Fantucci and L. De Gioia, *Coordination Chemistry Reviews*, 2005, **249**, 1620-1640.

15. W. Roseboom, A. L. De Lacey, V. M. Fernandez, E. C. Hatchikian and S. P. J. Albracht, *J. Biol. Inorg. Chem.*, 2006, **11**, 102-118.

16. A. Silakov, E. J. Reijerse and W. Lubitz, *European Journal of Inorganic Chemistry*, 2011, **2011**, 1056-1066.

17. W. Lubitz, H. Ogata, O. Rudiger and E. Reijerse, *Chemical reviews*, 2014, **114**, 4081-4148.

18. M. Bruschi, C. Greco, M. Kaukonen, P. Fantucci, U. Ryde and L. De Gioia, *Angewandte Chemie International Edition*, 2009, **48**, 3503-3506.

19. F. Gloaguen and T. B. Rauchfuss, *Chemical Society reviews*, 2009, **38**, 100-108.

20. D. Schilter, J. M. Camara, M. T. Huynh, S. Hammes-Schiffer and T. B. Rauchfuss, *Chemical reviews*, 2016, **116**, 8693-8749.

21. S. Tschierlei, S. Ott and R. Lomoth, *Energy & Environmental Science*, 2011, **4**, 2340-2352.

22. G. A. N. Felton, C. A. Mebi, B. J. Petro, A. K. Vannucci, D. H. Evans, R. S. Glass and D. L. Lichtenberger, *Journal of Organometallic Chemistry*, 2009, **694**, 2681-2699.

23. J. P. Perdew, *Phys. Rev. B*, 1986, **33**, 8822-8824.

24. A. D. Becke, *Phys. Rev. A*, 1988, **38**, 3098-3100.

25. M. J. Frisch, G. W. Trucks, H. B. Schlegel, G. E. Scuseria, M. A. Robb, J. R. Cheeseman, G. Scalmani, V. Barone, B. Mennucci, G. A. Petersson, H. Nakatsuji, M. Caricato, X. Li, H. P. Hratchian, A. F. Izmaylov, J. Bloino, G. Zheng, J. L. Sonnenberg, M. Hada, M. Ehara, K. Toyota, R. Fukuda, J. Hasegawa, M. Ishida, T. Nakajima, Y. Honda, O. Kitao, H. Nakai, T. Vreven, J. A. Montgomery Jr., J. E. Peralta, F. Ogliaro, M. Bearpark, J. J. Heyd, E. Brothers, K. N. Kudin, V. N. Staroverov, R. Kobayashi, J. Normand, K. Raghavachari, A. Rendell, J. C. Burant, S. S. Iyengar, J. Tomasi, M. Cossi, N. Rega, N. J. Millam, M. Klene, J. E. Knox, J. B. Cross, V. Bakken, C. Adamo, J. Jaramillo, R. Gomperts, R. E. Stratmann, O. Yazyev, A. J. Austin, R. Cammi, C. Pomelli, J. W. Ochterski, R. L. Martin, K. Morokuma, V. G. Zakrzewski, G. A. Voth, P. Salvador, J. J. Dannenberg, S. Dapprich, A. D. Daniels, Ö. Farkas, J. B. Foresman, J. V. Ortiz, J. Cioslowski and D. J. Fox, Gaussian, Inc., Wallingford CT, Editon edn., 2009.

26. F. Weigend and R. Ahlrichs, *Phys. Chem. Chem. Phys.*, 2005, **7**, 3297-3305.

27. S. Grimme, J. Antony, S. Ehrlich and H. Krieg, *J. Chem. Phys.*, 2010, **132**, 154104.

28. G. Scalmani and M. J. Frisch, *J. Chem. Phys.*, 2010, **132**, 114110.

29. L.-C. Song, J. Gao, H.-T. Wang, Y.-J. Hua, H.-T. Fan, X.-G. Zhang and Q.-M. Hu, *Organometallics*, 2006, **25**, 5724-5729.

30. M.-Q. Hu, C.-B. Ma, Y.-T. Si, C.-N. Chen and Q.-T. Liu, *Journal of inorganic biochemistry*, 2007, **101**, 1370-1375.

31. J. Hou, X. Peng, Z. Zhou, S. Sun, X. Zhao and S. Gao, *Journal of Organometallic Chemistry*, 2006, **691**, 4633-4640.

32. F. Gloaguen, J. D. Lawrence and T. B. Rauchfuss, *Journal of the American Chemical Society*, 2001, **123**, 9476-9477.

33. T. Liu, M. Wang, Z. Shi, H. Cui, W. Dong, J. Chen, B. Åkermark and L. Sun, *Chemistry – A European Journal*, 2004, **10**, 4474-4479.

34. J. A. Cabeza, M. A. Martínez-García, V. Riera, D. Ardura and S. García-Granda, *Organometallics*, 1998, **17**, 1471-1477.

35. Z. Wang, J. Liu, C. He, S. Jiang, B. Åkermark and L. Sun, *Inorganica Chimica Acta*, 2007, **360**, 2411-2419.

36. Z. Yu, M. Wang, P. Li, W. Dong, F. Wang and L. Sun, *Dalton Transactions*, 2008, 2400-2406.

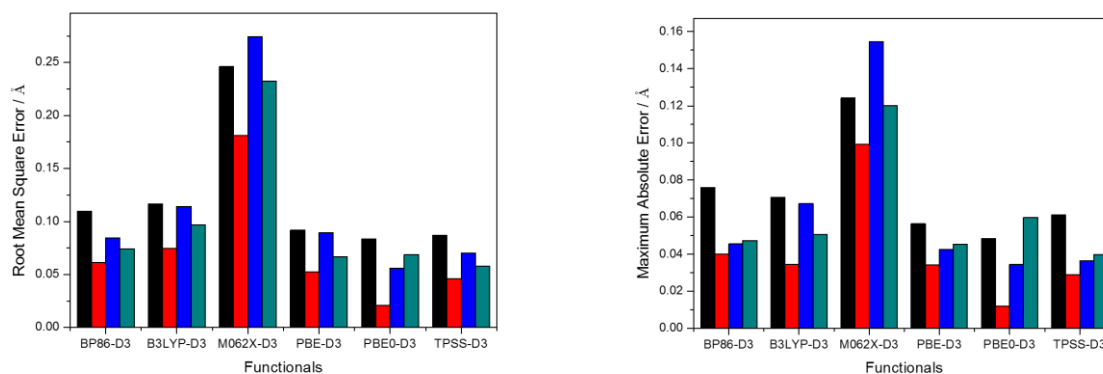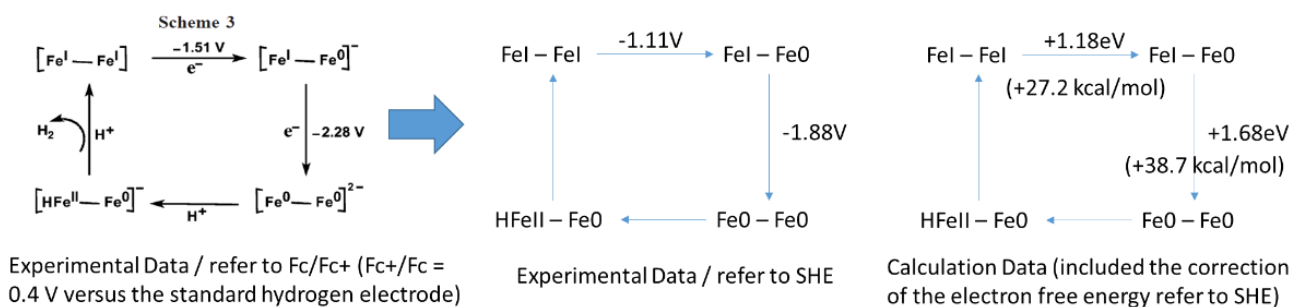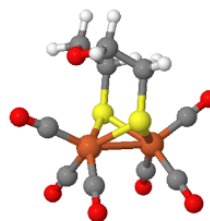# DFT studies on the [FeFe]-hydrogenases-inspired molecular catalysts

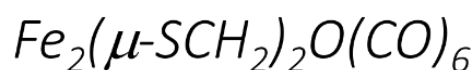**Figure S1.** The root mean square error and maximum absolute error between the X-ray crystallographic data for the four molecular catalysts and the calculated geometries by six different functionals.
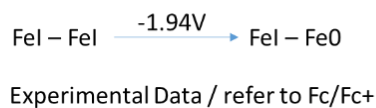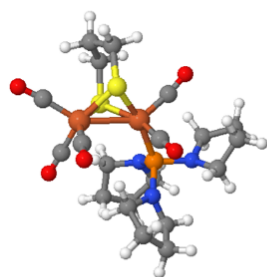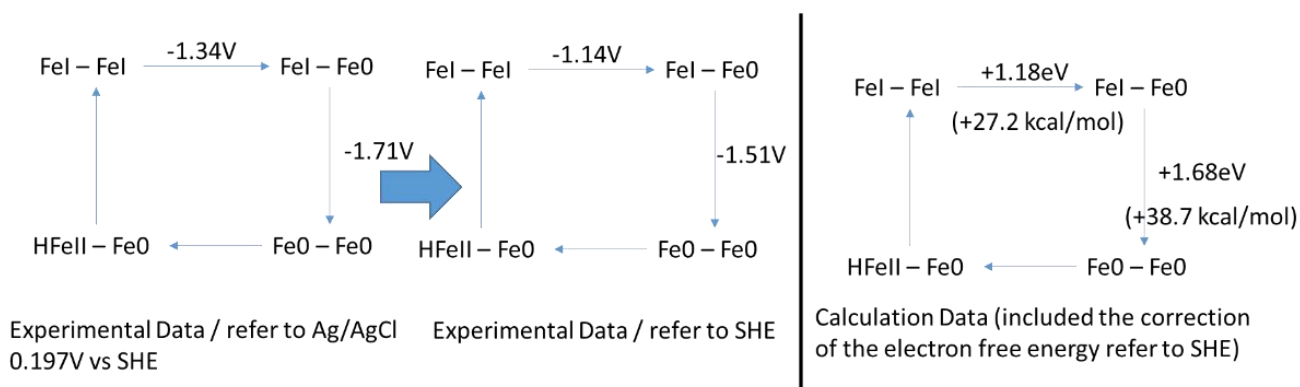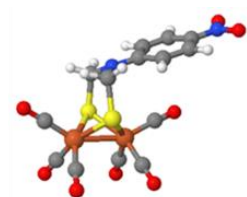
Experimental data of the redox potential compared with the theoretical prediction conducted by PBE

$$Fe_2(\mu\text{-}SCH_2)_2O(CO)_6$$

$(\mu\text{-}pdt)Fe_2(CO)_5P(NC_4H_8)_3$

FeI – FeI $\xrightarrow{-1.94V}$ FeI – Fe0

Experimental Data / refer to Fc/Fc+

FeI – FeI $\xrightarrow{-1.54V}$ FeI – Fe0

Experimental Data / refer to SHE

FeI – FeI $\xrightarrow{+1.42eV}$ FeI – Fe0
$\downarrow$ +2.15eV
HFeII – Fe0 $\leftarrow$ Fe0 – Fe0

Calculation Data (included the correction of the electron free energy refer to SHE)

$\{(\mu\text{-}SCH_2)_2N(4\text{-}NO_2C_6H_4)\}Fe_2(CO)_6$

FeI – FeI $\xrightarrow{-1.34V}$ FeI – Fe0
$\downarrow$ -1.71V
HFeII – Fe0 $\leftarrow$ Fe0 – Fe0

Experimental Data / refer to Ag/AgCl 0.197V vs SHE

FeI – FeI $\xrightarrow{-1.14V}$ FeI – Fe0
$\downarrow$ -1.51V
HFeII – Fe0 $\leftarrow$ Fe0 – Fe0

Experimental Data / refer to SHE

FeI – FeI $\xrightarrow{+1.18eV}$ FeI – Fe0
(+27.2 kcal/mol)
$\downarrow$ +1.68eV
(+38.7 kcal/mol)
HFeII – Fe0 $\leftarrow$ Fe0 – Fe0

Calculation Data (included the correction of the electron free energy refer to SHE)

Anchoring of the molecular catalyst onto the graphene

The periodic calculations on the anchoring model were conducted by the Quantum Espresso (QE) program [Figure S2 (b)]. In the calculations, the first H$^+$/e$^-$ injection and the hydride to proton transformation require total energy of 15.7 and 13.9 kcal/mol, respectively. To compare with the pure FeFe molecular catalyst, the total energies for the first proton injection and transformation on the molecular catalyst have been calculated by QE [the lower numbers in Figure S2 (a)]. As can be seen from the calculations, the anchoring of the molecular catalyst on the graphene does not affect the catalytic performance obviously. And to compare with our previous molecular catalysts

calculations by Gaussian, the total energies for the two step derived by Gaussian program have been shown as the upper numbers in Figure s2 (a), the numbers are similar with the QE results. This indicates the energy results by Gaussian and QE are comparable.
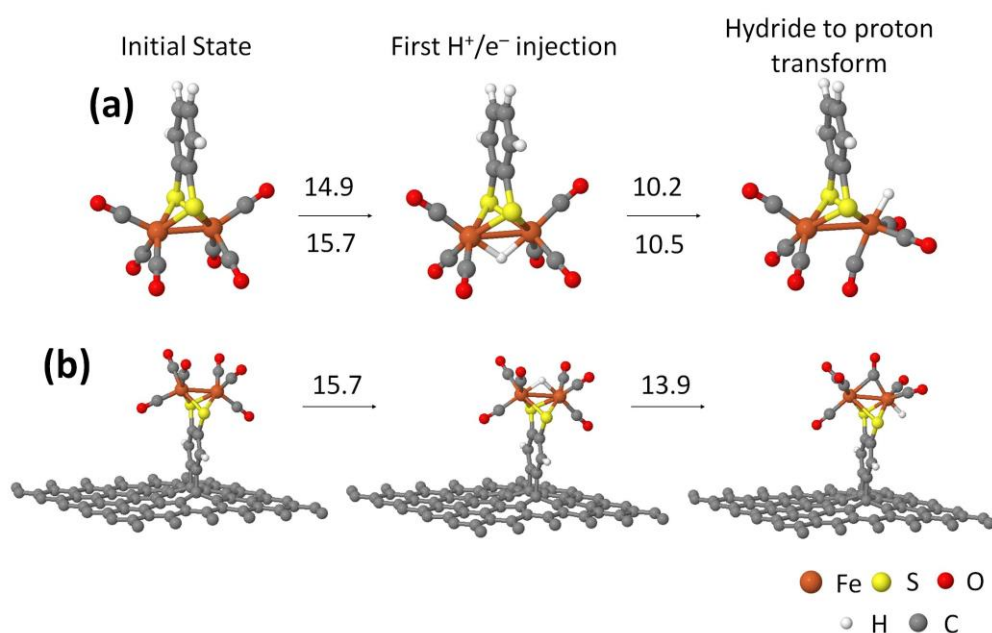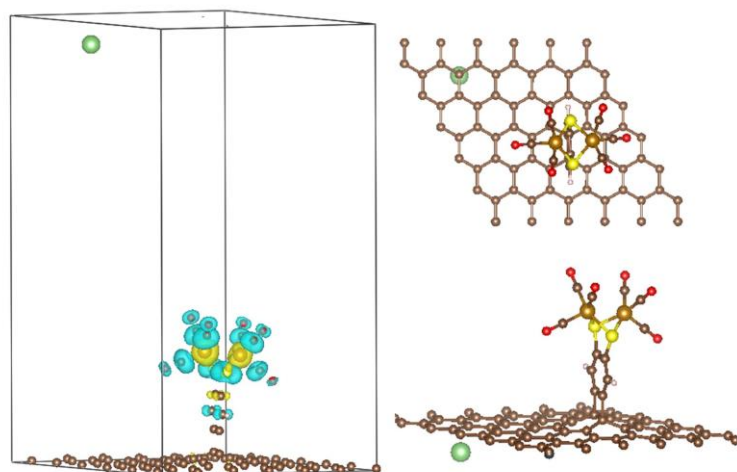

Figure S2. Geometries and total energies (in kcal/mol) for the first H^+/e^- injection and hydride transformation steps during the HER path on the FeFe molecular catalyst and its anchoring model.

And with an electron injected to the grapheme by lithium (Li) doped on the graphene, the electron will spontaneously goes to the molecular catalyst as shown in the spin polarization diagram on the left of the figure, suggesting when anchoring the hybrid structure on the electrode, the electron could be transferred to the catalytic cluster for HER process. The two views on the right of the figure demonstrated how the Li binds to the graphene surface and the bonding of the model.

CHAPTER 6

Conclusion and Future Works

6.1   Conclusion

The aim of this project was to design high-performance catalysts for HER, inspired by the hydrogenase enzyme. A hybrid structure has been proposed for such catalyst design, which anchors a catalytic cluster, derived from the active sites of hydrogenases, onto graphene surface with the aid of computational calculation. Hydrogenases are a class of enzymes that catalyze the reversible HER with almost no overpotential and high turnover frequencies; moreover hydrogenases consist of inexpensive metals.

The synthesis of bio-mimic catalysts is highly inspired by the active sites of hydrogenases; therefore, advanced knowledge of how hydrogenases work in nature is essential. The DFT investigation on the HER of [NiFe] hydrogenases indicates the singlet multiplicity is more stable than triplet and requires less reaction energy for the HER cycle. The largest and limiting rate-determining step is hypothesized for the second H^+/e^- injection step, with 19.7 kcal/mol energy required. Our DFT results also illustrate the role of the ligands attached to the Ni and Fe centers of the active site. The protein ligand confinement on the cysteine residues attached to Ni suggests the protein environment as it is in Nature seems to be more efficient for the catalysis of H_2 production (and cleavage). As for the inorganic ligands on Fe, the replacement of CN^- and CO by each other brings a dramatic energy change on the energy profile. The substitution of CN^- by CO helps the H^+/e^- injection step and inhibits the H^+ to hydride and the H_2 combination steps, while the CO replaced by CN^- shows a contrary energy change.

A variety of bio-inspired catalysts have been synthesized in the literature mimicking the active site of hydrogenases. However, none of the molecular catalysts possesses as impressive performance as the enzyme, highlighting the role of the protein environment around the active site an important question. From our DFT calculation, the energy requirement associated with the rate-determining step in HER decreases by 7.1 kcal/mol when the amino acids present, which is mainly due to the free energy decrease of the H^+/e^- injection steps. By dividing the amino acids into several models, we found that strong hydrogen bonding between the polar amino acids and the active site shows the most significant influence on the energy profile change. Further calculations reveal that geometric distortions caused by the amino acids environment are not the main reason for the energy profile changes observed in this work. Instead, charge redistribution has been identified as the key reason for such energy profile change. Therefore, we assume that, amino acids play a key role through H-bonds in tuning the electron distribution of the active site to improve overall HER performance.

Also, the conceptual DFT method has been applied for the study on the H^+ to hydride and the H_2 combination steps in [NiFe] hydrogenases. In the H^+ transferring to hydride step, two electrons are provided by oxidation of Ni(I) to Ni(III), and are transferred asynchronously. Such transformation is motivated by spontaneous rearrangements of the electron density. During the H_2 combination process, the proton and hydride initially approach to each other heterolytically. Such mechanism is different from the inorganic catalysts under which the two hydrogen atoms usually forms two adatoms and generate H_2 homolytically. Therefore the approach of the proton and electron is driven by the Coulomb force and such force might lower the barrier for HER compared with the inorganic system. Also, similar with the proton to hydride transformation step, the proton and hydride approaching step is motivated by the decrease of electronic activity and electrophilicity index from Ni. While after the charge transfer between proton and hydride, the two hydrogen atoms will anchor onto the Ni ion and form H_2 molecule following the Volmer-Tafel mechanism.

Compared with NiFe bio-mimic molecular catalysts, a larger variety of FeFe molecular catalysts have been synthesized, and they possess similar structure with the active site of [FeFe]

hydrogenases. In this PhD work, 8 different [FeFe] bio-inspired molecular catalysts have been investigated. The calculations demonstrated that the proton and electron are not transferred simultaneously, but follow proton transfer – electron transfer (PT-ET) mechanism. While in hydrogenases, our calculation hypothesized the proton and electron were coupled and transferred to the active site. Also, the proton delivered to the molecular catalysts initially forms a hydride between two Fe metals, and then transforms to a terminal binding proton. While in [FeFe] hydrogenases, only the terminal proton forms during the HER. By anchoring a molecular catalyst onto the graphene, we found the reaction energy for the H^+/e^- injection step is almost unaffected. From the spin polarization analysis, the electron goes onto the molecule cluster after the electron injection to the graphene.

6.2   Future works

1. Chapter 2-4 studied the HER reaction on the [NiFe] hydrogenases. However, the existing molecular catalysts are mostly inspired by the [FeFe] hydrogenases, and in Chapter 5 we also have investigated the HER on the FeFe molecular catalysts. Therefore, the [FeFe] hydrogenases should be studied in the future in order to compare with the molecular catalysts, and have a better understanding on the HER process on these molecular catalysts.

2. In Chapter 5, we have compared the experimental and theoretical overpotential of eight different FeFe molecular catalysts. However the comparison between the experiment and calculation does not show a simple trend. In further work on this topic, more FeFe molecular catalysts should be calculated and studied to achieve a better fitting between the data.

3. When a strong link between the experimental and calculated HER performance can be achieved, modification of the ligands on the molecular catalysts tcan be studied to develop new FeFe molecular catalysts with better HER catalytic performance.

4. Also, some further calculations related to the hybrid catalysts should be done in the future. The anchoring of the different molecular catalysts on different electrode surfaces could also be tested, in order to find a good hybrid catalyst for HER.